THE EFFECTS OF MESO-SCALE TOPOGRAPHY ON THE PERFORMANCE OF ENGINEERED SOIL COVERS

A Thesis Submitted to the

College of Graduate Studies and Research

in Partial Fulfillment of the Requirements

for the Degree of Doctor of Philosophy

in the Department of Civil and Geological Engineering

University of Saskatchewan

Saskatoon

By

Christopher James Kelln

© Copyright Christopher James Kelln, September 2008. All rights reserved.

Permission to Use

In presenting this thesis/dissertation in partial fulfillment of the requirements for a Postgraduate degree from the University of Saskatchewan, I agree that the Libraries of this University may make it freely available for inspection. I further agree that permission for copying of this thesis/dissertation in any manner, in whole or in part, for scholarly purposes may be granted by the professor or professors who supervised my thesis/dissertation work or, in their absence, by the Head of the Department or the Dean of the College in which my thesis work was done. It is understood that any copying or publication or use of this thesis/dissertation or parts thereof for financial gain shall not be allowed without my written permission. It is also understood that due recognition shall be given to me and to the University of Saskatchewan in any scholarly use which may be made of any material in my thesis/dissertation.

Requests for permission to copy or to make other uses of materials in this thesis/dissertation in whole or part should be addressed to:

Head of the Department of Civil Engineering
University of Saskatchewan
Saskatoon, Saskatchewan S7N 5A9
Canada

OR

Dean
College of Graduate Studies and Research
University of Saskatchewan
107 Administration Place
Saskatoon, Saskatchewan S7N 5A2
Canada

Abstract

Understanding the hydrological controls on subsurface flow and transport is of considerable importance in the study of reclaimed landscapes in the oil sands region of Canada. A significant portion of the reclaimed landscape will be comprised of a thin veneer (~ 1 m) of clay-rich reclamation soil overlying saline-sodic shale overburden, which is a waste by-product from the mining process. The global objective of this study was to investigate the first-order controls on soil moisture and salt transport dynamics within clay-rich reclamation covers overlying low permeability waste substrates. The study site is located in a cold, semi-arid climate in the oil sands region of northern Alberta. Preferential flow was the dominant mechanism responsible for the development of perched water table conditions on the cover-waste interface during the spring snow melt. Hydrological and geochemical data indicated that snowmelt infiltration occurs via the macroporosity while the ground is still frozen. An isotope hydrograph separation conducted on water collected in a weeping tile confirmed the presence of fresh snowmelt water at the onset of subsurface flow. This water transitions to a chemical signature that is comprised of approximately 80% connate pore water as a result of chemical equilibration between pore water in the soil matrix and fresh water in the macropores.

Detailed mapping of the spatial distribution of soil moisture and salts within a reclamation cover indicated the lower-slope positions are wetter due to the accumulation surface run-off and frozen ground infiltration in spring. Increased soil moisture conditions in lower-slope positions accelerate salt ingress, while drier conditions in middle and upper-slope positions attenuate salt ingress. The data indicated that fresh snowmelt water is bypassing the soil matrix higher in the cover profile. Subsurface flow and deep percolation are key mechanisms mitigating vertical salt ingress in lower and upper slope positions. The mesotopography of the cover-waste interface imposes a direct control on the depth of perched water and the downslope routing of water. Undulations in the cover-waste interface cause the depth of perched water to vary considerably (± 20

– 60 cm) over short distances (< 5 m), while saturated subsurface flow is routed through the lowest elevations in the cover profile.

A numerical analysis of subsurface flow was able to simulate both the discharge rate and cumulative volume of flow to a weeping tile. Composite hydraulic functions were used in the simulations to account for the increased hydraulic conductivity and drainable porosity created by the macroporosity at near-saturated conditions. The transient Na^+ concentration of discharge water was modelled using the concept of an equivalent porous medium. The good match between measured and modelled data verified the conceptual model, which contends that saturated subsurface flow is dominated by the fracture network and that the concentration of discharge water is function of the depth of perched water. Finally, the results from this study suggest the mesotopography of the cover-waste interface could be used to manage 'excess' water and salts within the landscape.

Acknowledgements

I am deeply grateful for the support and encouragement of my wife Lauria. Together we have faced the joys and challenges of life. Over the last few years, we have been blessed with the birth of our son, Lucas, and the growth of our daughter, Mya. Completing this chapter of my life would have little significance without her at my side.

I owe a debt of gratitude to Lee Barbour. Lee has provided invaluable friendship, encouragement, and mentorship. Lee's amazing words of wisdom helped me grow personally and professionally and inspired me to accomplish more than I believed possible.

Finally, thanks to my brother, Curtis, for his support and friendship. Our many conversations were a constant source of enjoyment and encouragement. Thanks to my mother and father and Lauria's parents for their love, patience, and enduring belief in their children.

Table of Contents

List of Tables

List of Figures

1

Introduction

1.1. Background

Soil cover technology has gained wide-spread acceptance over the last decade in its application to the design of waste containment systems for mine reclamation and landfill closure (e.g., Aubertin et al. 1996; Bussiere et al. 1997; Morris and Stormont 1997; Nicholson et al. 1989; Yanful et al. 1993). Soil covers employing capillary barrier effects have recently been proposed as a potential slope stabilization method for rain-induced landslides (Tami et al. 2004a; Tami et al. 2004b). In general, the primary function of a soil cover is to control the flux of water and/or gas into the underlying substratum. In mine closure and reclamation, soil covers are designed to provide sufficient moisture and nutrients for re-establishing vegetation and sustaining a natural ecosystem.

In the oil sands region of north-central Canada, reclamation will occur on an unprecedented scale. Each mine produces an array of waste streams from the mining and milling processes that will cover areas in excess of a hundred square kilometres. To date, the emphasis of research into the long-term performance of reclamation covers has been on available water holding capacity (Leskiw 1998). That is, the covers must store sufficient water, so that during periods of high evapotranspiration demand, they will not reach levels of water stress that might limit plant growth. Moisture translocation has been considered indirectly in that the majority of instrumented study sites are located on hill slopes with monitoring conducted at various slope positions. The soil moisture and salt transport dynamics due to topographically driven flow; however, have not been systematically investigated. The need for operators to develop diverse ecosites and the recent interest of regulatory agencies in having 'mesotopography' constructed into the

landscape highlights the need to understand the effect of meso-scale topography on the soil moisture and salt regime.

The spatial and temporal distribution of soil moisture imposes a first-order control on the hydrological, geochemical, and biological response of a soil cover. Soil moisture is intrinsically related to hydraulic conductivity and the coefficient of diffusion and therefore influences the flux of water and solutes within the cover. In natural systems and engineered covers, soil moisture also governs a range of hydrological processes including infiltration, evapotranspiration, runoff and surface erosion. Furthermore, soil moisture exerts a strong control on the distribution and dynamics of vegetation growth, which can be pivotal in ecosite development.

The soil moisture regime in a hydrological system is dependent on the complex and dynamic interrelationships between climate, soil properties, vegetation, and topography. Although it is well known that topography (slope angle and surface relief) has a significant impact on moisture distribution and migration within natural landscapes (King et al. 1983), resolving the concomitant impact of each controlling factor is difficult. Dunne (1991) noted that there have been very few studies into the mechanisms of soil moisture movement that have sufficiently detailed topographic surveys to characterize geometry and any trends in the soil moisture distribution. Famiglietti (1998) found that the dominance of topographic control on soil moisture distribution is poorly supported in the literature and there are clear examples where other controls are more important. Yeh et al. (1998) noted that there is no rigorous theory relating the level of soil moisture to the corresponding topographic conditions. The prevalence of the soil moisture variability across natural landscapes is well established, but the mechanisms controlling soil moisture translocation are not well understood.

Topography affects the distribution of soil moisture through a variety of geometric factors including slope angle and aspect, slope curvature, upslope contributing area, and the relative elevation of the land surface (Famiglietti et al. 1998). In general, steeper slopes result in lower average soil moisture values due to increased runoff and lower infiltration rates (e.g. Nyberg 1996). Upslope contributing area affects soil moisture by

controlling the distribution of surface runoff and thus infiltration; hillslope locations with larger upslope contributing areas are more likely to have higher mean soil moisture conditions than those with smaller contributing areas. Aspect influences the net shortwave radiation incident on a soil surface and thus evapotranspiration and soil moisture. For example, Weeks and Wilson (2004) used numerical analysis to demonstrate that actual evaporation from a soil cover on a 1H:1V south facing slope was 75% greater than that from the north facing slope.

Numerous authors have investigated the impact of slope angle on soil moisture movement in the unsaturated zone in both natural hillslopes (e.g. McCord and Stephens 1987; Tsaparas et al. 2003; Zaslavsky and Sinai 1981a; Zaslavsky and Sinai 1981b; Zaslavsky and Sinai 1981c; Zaslavsky and Sinai 1981d) and engineered soil covers (Bussiere et al. 2003; Khire et al. 1997; Khire et al. 2000; Stormont 1995; Stormont 1996). The dominant mechanism affecting the steady-state lateral distribution of soil moisture along a hillslope is topographic forcing. Topographic forcing refers to the total mechanical energy field that is established solely due to elevation gradients (i.e. gravitational potential energy), with hydraulic gradients in the down slope direction approximately proportional to the slope angle.

In general, topography can force a large-scale distribution of soil moisture that reflects the surface elevation. Areas of topographic convergence are favourable for the accumulation of soil moisture while areas of topographic divergence usually experience drier conditions. The upper part of a hillslope will tend to de-saturate more than the lower part under the same climatic conditions (Boldt-Leppin et al. 2000; Bussiere et al. 2003). It is noted that some researchers have found that slope curvature (i.e. concave or convex slopes) has a negligible impact on soil moisture for most hillslope geometries (e.g. Philip 1991a; Philip 1991b).

The mechanism for lateral moisture movement in sloping ground is also related in part to moisture-content heterogeneity that is induced during infiltration and redistribution (Yeh et al. 1985a; Yeh et al. 1985b; Yeh et al. 1985c). As the wetting front moves into the soil, the zone of saturation is sloped due to the topography. As a result, a

sloping region of relatively high hydraulic conductivity is created beneath the slope, which may cause anisotropy in the hydraulic conductivity field. In turn, the path of least resistance to groundwater flow will be downdip, leading to a larger horizontal flow component and possibly the accumulation of water beneath topographic lowlands. Ultimately, this type of anisotropy is directly a function of antecedent moisture conditions.

The effect of topography, and in particular the slope angle, on the spatial distribution of soil moisture is strongly influenced by antecedent moisture conditions (Barling et al. 1994; Grayson et al. 1997b; Ridolfi et al. 2003; Western et al. 2004). Grayson et al. (1997a) theorized that soil water patterns along hillslopes in temperate climates will switch between two different 'preferred states', controlled by different processes. One state occurs in periods when precipitation continually exceeds evapotranspiration. In this case, spatial patterns of soil moisture are dominated by lateral water movement of both surface and subsurface water. Areas of high topographic convergence are wetter than other parts of the watershed because of the concentration of shallow, lateral groundwater flow. In this case, the topography upslope of a given point is the dominant control; denoted as 'non-local control' by Grayson et al. (1997a).

Grayson et al. (1997a) designated situations in which there is no connection between a point in a watershed and its upslope area as 'local control'. This preferred state of soil moisture distribution occurred during periods when evapotranspiration frequently exceeds precipitation. These types of climatic conditions result in a dominance of vertical fluxes (evaporation/transpiration), which attenuate lateral groundwater flow. In this case, moisture patterns primarily reflect soil and vegetation differences, taking on a more random appearance. Only local terrain influences the pattern of soil moisture under dry conditions where areas of high local convergence may cause a temporary elevation of water content following rainfall. The dry pattern is much more random in appearance, with no evidence of redistribution caused by terrain (i.e., there are no non-local controls evident).

The study of Grayson et al. (1997b) highlights a key concept in the hydrology literature: topography (i.e., slope) alone does not govern soil moisture re-distribution, particularly in arid or sub-humid climates. Although the total energy potential (i.e. total head) may be dominated by the elevation potential, the spatial and temporal distribution of soil moisture will be a function of antecedent soil moisture conditions and climate. Downslope moisture translocation will only be operative under 'wet' climatic and high antecedent moisture conditions.

In a very poignant commentary on the rainfall-response of natural hillslopes, McDonnell (2003) also noted that recent research has demonstrated that watersheds display considerable threshold behaviour. This behaviour is partly explained by antecedent moisture conditions, but other processes such as preferential flow are also of considerable importance. Many studies have shown that preferential flow governs infiltration and lateral subsurface flow in natural surficial soils (e.g. Tromp van Meerveld and McDonnell 2006a; Uchida et al. 2004). The general consensus in the literature is that macrostructure is responsible for the rapid transmission of water vertically to depth when the rainfall intensity exceeds the matrix hydraulic conductivity, thereby inducing an overflow of soil water from the matrix into the macrostructure (McIntosh et al. 1999).

Research has also shown that preferential flow can be responsible for rapid lateral flow in hillslopes underlain by a low permeability unit (Freer et al. 2002; Jardine et al. 1990; Newman et al. 2004; Smettem et al. 1991; Tsuboyama et al. 1994). Transient water tables develop at the soil-bedrock interface, and downslope groundwater flow follows the meso-scale topographic relief of the sub-surface impeding layer. Studies have shown that topography of the impeding layer, and not the surface topography, is the most important 'surface' controlling the downslope routing of mobile water (Freer et al. 2002; McDonnell 2003). Naturally, subsurface flow will impose a significant control on the spatial distribution of moisture and salts within the landscape, and is therefore of considerable importance to the performance of reclaimed landscapes. The ability of geotechnical engineers to understand these mechanisms will be fundamental to the design of sustainable mine and landfill closure and reclamation strategies.

1.2. Research Hypothesis

Decades of research into the hydrological response of natural hillslopes has elucidated some of the first-order controls on the spatial distribution of soil moisture. Three of the most significant findings pertinent to this research are the following: (1) preferential flow is a ubiquitous phenomenon in natural soils (Flury et al. 1994); (2) ground surface and 'bedrock' mesotopography may impose a significant control on the spatial distribution of soil moisture in the landscape (Freer et al. 2002); and, (3) moisture translocation due to topographic forcing will be a function of antecedent soil moisture conditions and climate, in which a hillslope may switch between a "wet" and "dry" state (Grayson et al. 1997a).

The literature also suggests that mesotopography can produce a highly complex and transient groundwater flow pattern in the vadose zone. A spatial variation in moisture content implies that the hydrological system is both heterogeneous and anisotropic due to the interdependence of hydraulic conductivity on soil moisture (or matric suction); therefore, infiltration, moisture translocation, and evapotranspiration will also vary spatially. In terms of soil cover performance, spatial variability may lead to a design failure with respect to net percolation, oxygen ingress, or moisture deficiency in reclamation covers. Complex patterns of vegetation may also emerge due to the competing interaction for resources, which may in turn effect moisture translocation, evapotranspiration, and have a significant effect on the transport of solutes within a soil cover.

It is theorized in this research that the moisture dynamics in reclamation covers overlying low hydraulic conductivity waste materials will exhibit the same mechanisms and processes that govern natural landscapes. As such, moisture translocation will be governed by the mesotopography of the cover-waste interface during 'wet' climatic conditions. Preferential flow will have a significant impact on the hydrological response of the covers. It is anticipated that the covers will exhibit large spatial variations in soil moisture during wet periods while showing little variation during dry periods.

In the context of this research, meso-scale topography (i.e. mesotopography) refers to intermediate scale geographic features that are characterized primarily by elevation ('relief') and slope angle. The definition of mesotopography as stated is inherently subjective because there are no dimensional criteria that uniquely identify a feature as being 'intermediate' in scale. As such, mesotopography is uniquely defined herein as a geographic feature having a horizontal dimension of between 1 m and 100 m with amplitude greater than 10 cm. Features less than 1 m in the lateral dimension are typically designated as 'microtopography' in the literature, including potholes or rills (Lissey 1971; Logan and Rudolph 1997; Pal et al. 2003). The upper bound of the lateral dimension (i.e. 100 m) is partially a function of the 'macro-scale' characteristics of the topography. For example, a 100 m long hillslope with a single convex surface would not be considered mesotopography.

The term mesotopography will also be used to designate variations in the thickness of cover material and/or relief of the cover-substratum interface. It is likely that most soil covers are not constructed with a uniform thickness due to lack of construction control during placement with earth moving equipment and/or undulations in the underlying substratum. Covers that are constructed with relatively uniform thickness will eventually develop mesotopography due to geomorphologic processes such as erosion, settlement, deformation, and slope failures or surface sloughing.

1.3. Research Objectives

The global objectives of the proposed research are to understand the mechanisms that govern the spatial and temporal distribution of soil moisture and salts in reclamation covers with mesotopographic relief under the unique climate conditions encountered in the Boreal Plain and to apply this understanding to the development of optimal designs for reconstructed landscapes overlying low permeability substrates. The specific objectives are to:

i. Observe moisture and subsurface flow within reclamation slopes and characterize the mechanisms controlling topographically driven moisture dynamics;

ii. Develop numerical simulations for instrumented site(s) capable of replicating patterns of moisture and salt movement. The numerical modeling will be primarily mechanistic, and as such, will help elucidate the first-order controls on subsurface moisture dynamics; and,

iii. Apply these specific simulations to more general questions of design and moisture regime evaluation (i.e., develop guidelines for incorporating mesotopography into mine reclamation practices).

1.4. Outline of Thesis

This thesis is presented in a manuscript-style format. Chapters two through four are written in a format suitable for submission to a scholarly journal. A preface is included at the beginning of these chapters to discuss the relevance of the manuscript to the overall research objectives. Chapters 5 and 6 provide a summary of the results and recommendations, respectively. Appendix A and B include any data and information pertinent to the thesis. Each manuscript was written exclusively by the author of this thesis. The co-authors listed on each paper were responsible for reviewing and editing prior to submission. It should also be noted that the manuscripts presented herein have been modified from the original versions to ensure consistency throughout the document.

2

Preferential Flow in a Reclamation Cover: Hydrological and Geochemical Response

Preface

Field studies of natural hillslopes, particularly at sites located in humid climates, have shown that preferential flow via macroporosity is a ubiquitous phenomenon that imposes a first-order control on infiltration and lateral groundwater flow. These studies provide a natural analogue from which engineers can glean information on the anticipated behaviour of engineered cover systems. The following manuscript endeavours to understand the hydrological response of clay-rich reclamation covers overlying low permeability waste substrates using techniques borrowed from the hydrology literature. This study is unique in that the site is located in a cold, sub-humid environment, and was constructed on a reclaimed landscape. The findings directly address the global objective of this research: to understand the mechanisms that govern the spatial and temporal distribution of volumetric water content and salts in reclamation covers with mesotopographic relief under the unique climate conditions encountered in the Boreal Plain.

Reference: Kelln, C.J., Barbour, S.L., and Qualizza, C.V., 2007. Preferential flow in a reclamation cover: hydrological and geochemical response. Journal of Geoenvironmental and Geotechnical Engineering, 133(10): 1277-1289.

2.1. Introduction

Preferential groundwater flow is a ubiquitous phenomenon in natural hillslopes (1982; Germann 1990; Wieler and Naef 2003) and is therefore a concern for evapotranspirative (ET) covers employed as a decommissioning and reclamation strategy for waste containment facilities and mine sites (Aubertin et al. 1996; Lutton et al. 1980; Yanful 1993). In most cases, the primary objectives of these covers is to limit oxygen ingress and/or net percolation into the underlying waste (Albright et al. 2004; Fayer and Gee 2006; Khire et al. 1997; Nyhan et al. 1990). In the case of large-scale mining operations, such as the oil-sands developments located in north-central Canada, the fundamental goal of reclamation is to reconstruct landscapes that support the development of natural ecosystems (Elshorbagy et al. 2005; Qualizza et al. 2004). Regardless of the intended design function, the dynamics of soil moisture movement and storage is a primary factor for successful cover performance.

Soil covers are subjected to chemical and bio-physical processes that may alter the saturated hydraulic conductivity and moisture retention characteristics of the soil over time. Processes such as freeze-thaw cycles (Benson and Othman 1993; Benson et al. 1995; Chamberlain et al. 1995), wet-dry cycles (Albrecht and Benson 2001; Daniel and Wu 1993), and root penetration and bioturbation (Wieler and Naef 2003) can lead to the development of macroporosity (Beven and Germann 1982; Germann 1990). Infiltrating waters can therefore bypass the soil matrix and travel along preferential flow paths. Preferential flow will alter the hydrological response of a soil cover and possibly compromise the intended design function. Although some cover systems can include more robust designs to mitigate the effects of bio-physical degradation (e.g., root barrier, protective surface layer), many reclamation soil covers cannot employ these design measures due to the scale of reclamation, the level of construction quality control, the availability of cover materials, and/or economic restraints. These limitations are particularly pertinent to oil sands operations where reclamation will occur on an unprecedented scale (> 80 km^2 for a single mine).

To date, there has been little research on the effect of preferential flow on the performance of ET covers. Melchior (1997) reported unacceptably high leakage rates through a conventional landfill cover due to preferential flow paths caused by desiccation, shrinkage, and root penetration. Albright et al. (2004) reported higher than expected percolation rates in two conventional covers constructed in humid climates. In both cases, percolation was transmitted almost immediately after heavy rainfall, suggesting that either preferential flow or saturated matrix flow was responsible for moisture translocation. Albright et al. (2004) also reported small amounts of percolation through a monolithic ET cover in a sub-humid climate during a heavy rainfall, despite the fact that the cover had sufficient soil water storage.

The objectives of this study are to: (1) investigate the processes that control preferential flow in a reclamation cover in a cold, sub-humid climate; and, (2) evaluate the impact of preferential flow on the hydrological response of the cover. *In situ* hydraulic conductivity data was collected over a period of 5 years to track the change in cover hydraulic properties. Detailed hydrometric and geochemical data were used to study the hydrological response of the cover and develop an understanding of the processes that control preferential flow. Finite element seepage analysis was used to compare measured interflow discharge rates to those expected with macroporosity-dominated groundwater flow. Finally, a commonly employed hydrological technique for studying watersheds, isotope hydrograph separation, was used to analyze the contribution of matrix porosity and macroporosity to interflow.

2.2. Study Site

The study site is located at the Syncrude Canada Mildred Lake mine, north of Fort McMurray, Alberta, Canada (57°2' N, 111°33' W). Three 1 ha prototype test covers were constructed in 1999 on a saline-sodic shale overburden landform, termed the Southwest 30 Hills Overburden Dump (SW30), to track the long-term performance of ET covers constructed for land reclamation. The SW30 was constructed between 1980 and 1996 with approximately 100×10^6 m^3 of shale overburden generated from oil-sands mining. It

is 2 km^2 in area with a plateau elevation rising about 60 m above the surrounding landscape. After construction, the waste dump was contoured into number of discrete watersheds and capped with a 1 m thick soil cover.

The three prototype test covers were constructed on a north facing 5H:1V (~11°) slope with nominal thicknesses of 35, 50, and 100 cm. The thickness of the 100 cm cover, which is the focus of this paper, was mandated by provincial environmental regulations and therefore served as the control plot. The cover was constructed with a 20 cm layer of a peat-glacial soil mixture, overlying approximately 80 cm of glacial soil. Vegetation consists predominantly of trembling aspen (*Populus tremuloides*) and white spruce (*Picea glauca*), although there is an abundance of plant species growing on the covers. The primary hydrological design objective of the cover is to provide sufficient moisture to sustain vegetation during the period of summer moisture deficit. These objectives are achieved through the relatively high hydraulic conductivity and moisture storage of the peat-mineral layer, which promotes the infiltration and storage of high intensity rainfall events. This water is then released more slowly to the lower hydraulic conductivity glacial soil (Barbour et al. 2001).

The climate is classified as sub-humid continental (Koppen Classification, McKnight and Hess 2005) with a mean annual air temperature of 1.5 °C and a mean annual precipitation of 442 mm (1945 to 1995). Monthly mean air temperatures range from 18 °C in July to -20.7 °C in January. On average, the potential evapotranspiration (PET) as estimated by Penman (1948) varies from 433 to 530 mm/yr with a mean of 459 mm/year and daily maximums (~ 7 mm/day) occurring during July and August. Rainfall in summer is associated with thunderstorms and tends to be of short duration but high intensity. Approximately 20% of the annual precipitation occurs as snow during the winter months. Surface run-off is associated with snow melt in the spring and does not typically occur during the summer or autumn. Actual evaporation rates (AET) over the summer growing season range from 212 to 470 mm/yr with an average of 346 mm (Elshorbagy et al. 2005), which leads to frequent net summer moisture deficits of as much as 70 to 80 mm.

2.3. Materials and Methods

2.3.1. Material Characterization

The geotechnical and hydraulic properties of the cover and underlying saline-sodic shale were characterized using field and laboratory testing. Soil cores were collected by manually driving a 50 cm diameter tube into the ground using a drop hammer. Laboratory tests included gravimetric water content (ASTM D2216-05; ASTM 2005a), particle size distribution (ASTM D422-63(2002); ASTM 2002a), and bulk density (ASTM D2937-05; ASTM 2005b). A soil water characteristic curve was developed for the glacial soil using ASTM D6836-02 (ASTM 2002b).

The field saturated hydraulic conductivity (K_s) was measured each year from 2000 to 2005 using a Guelph Permeameter (Reynolds 1993). On average, thirty measurements of K_s were conducted on the cover materials and underlying shale for a given year at upper, middle, and lower slope locations (Meiers et al. 2003; Meiers et al. 2006). Between two and four boreholes were drilled into the shale at each slope location using a hand auger. Two tests were conducted in each borehole at the mid-point of the cover thickness (i.e., on the glacial soil), and two tests were conducted in the shale. In each test, ponded water heights of 5 cm were used initially followed by a second test with a ponded water height of 10 cm. The peat-mineral soil was usually tested between six and twelve times per year.

2.3.2. Hydrometric Data

A soil station (Fig. 2.1) was installed on the cover in 1999 to monitor volumetric water content, temperature, and matric suction throughout the cover profile and into the underlying shale (depths of 5, 20, 30, 55, 90, 115, 125, 145, and 170 cm). Volumetric water content and matric suction were monitored using calibrated time domain reflectometry (TDR) sensors and thermal conductivity suction sensors, respectively. Soil temperature was measured using thermistor sensors. All of the soil instrumentation was connected to a data acquisition system programmed to collect data on an hourly basis. Two meteorological stations were used to collect data on wind speed and direction,

temperature, precipitation, and relative humidity; one station was located on the flat top of the waste dump, while the second was located in the middle of the prototype covers.

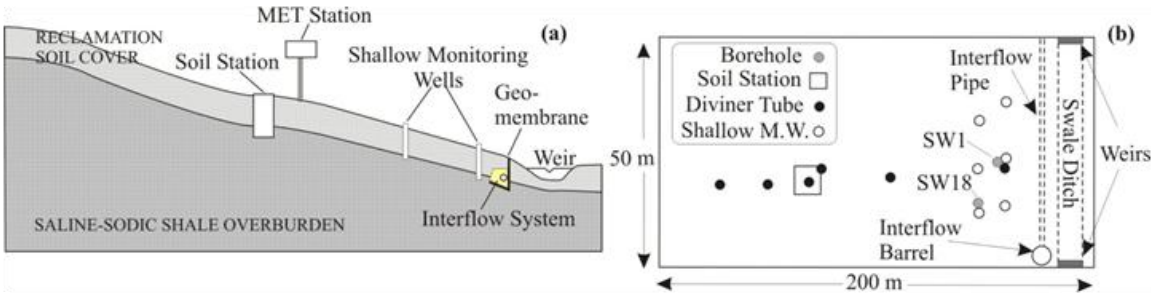

Fig. 2.1 (a) Schematic cross-section of instrumented test section. (b) Plan view of cover.

Lateral saturated groundwater flow (i.e. interflow) along the cover-shale interface was measured using an interflow collection system constructed in June 2000. A shallow trench was excavated into the shale surface about 1 to 2 m upslope of the swale ditch (Fig. 2.1) and was lined with a geo-membrane. A 150 mm diameter perforated pipe (i.e. weeping tile) was installed along the geomembrane and was covered by filter sand. The trench was then backfilled using the appropriate cover layers. The perforated pipe discharges into a large-diameter (~ 1 m) collection well installed to a depth of 1.5 m below the cover-shale interface. An electric bilge pump was used to empty the interflow barrel as required. Flow volumes were measured by recording the pumping time and flow rate on each occasion. Surface runoff was measured using v-notch weirs equipped with sonic sensors and data acquisition systems, installed in the swale ditch upstream and downstream of the cover.

Two rows of shallow monitoring wells were installed approximately 5 and 20 m upslope of the interflow collection system (Fig. 2.1) to monitor the development of a perched water table on the cover-shale interface (Stolte et al. 2000). The monitoring wells were constructed of 50 mm diameter schedule 40 PVC pipe and installed using a hand auger. A hand saw was used to slot the pipe over a length extending 20-30 cm above the measured interface depth.

2.3.3. Water Chemistry

One-dimensional profiles of pore water chemistry were determined at four locations on the cover in 2004. Shallow boreholes (100 to 200 cm deep) were excavated along a north-south transect (i.e. running up the cover) at a spacing of approximately 30 to 40 m. Soil samples were collected every 10-20 cm depth, placed in sealed plastic bags, and refrigerated until the analysis was performed. Pore water from the soil samples collected at a single location was extracted in the laboratory using high-speed centrifugation and analyzed for major anions (Cl^-, NO_3^-, SO_4^{2-}, HCO_3^-) using ion chromatography. The concentrations of soluble salts for the remaining samples were determined using saturated paste extracts (McKeague 1978). Extracts were analyzed for cations (K^{2+}, Mg^{2+}, Ca^{2+}, Na^+) by atomic adsorption spectroscopy and anions (SO_4^{2-} and Cl^-) by ion chromatography.

Interflow water samples were collected for major ion analysis (K^{2+}, Mg^{2+}, Ca^{2+}, Na^+, SO_4^{2-}, HCO_3^- NO_3^- Cl^-) on at least 75 occasions between 2000 and 2005. Sampling frequency varied from daily in the spring to bi-monthly during the summer when flow rates were substantially diminished. Samples were collected from the interflow barrel, which was covered except for sampling, using an electric bilge pump, stored in polypropylene bottles, and refrigerated. Analysis was performed using inductively coupled plasma spectrometry.

2.3.4. Stable Isotopes

Stable isotope analysis ($\delta^{18}O$ and δ^2H) was conducted on seven snow samples, twenty interflow water samples, and four groundwater samples collected during 2005. The snow samples were collected on March 4, 2005 by pushing a snow core (76 mm diameter) through the entire depth of the snow pack (~1-2 m). The samples were placed in polyethylene bags, allowed to melt at room temperature (in the bag), immediately transferred to polypropylene bottles, and stored in a temperature and humidity controlled room until the isotope analysis was performed. A single snow sample was also collected during the snowmelt on April 15, 2005. The twenty interflow samples were collected between April 7, 2005 and September 28, 2005. The four groundwater samples were

collected from the shallow monitoring wells (i.e. perched water table samples) on April 07, 2005.

The 2005 interflow, snow melt, and groundwater samples were analyzed for $\delta^{18}O$ and $\delta^{2}H$ by standard H_2-water and CO_2-water equilibration (Horita and Kendall 2004) with a precision of ± 0.2 ‰ and ± 2 ‰, respectively. All $\delta^{18}O$ and $\delta^{2}H$ values are reported as the difference between $^{18}O/^{16}O$ and $^{2}H/^{1}H$ ratios of the samples and Vienna Standard Mean Ocean Water (VSMOW) in per mil notation (‰).

Soil samples for stable isotope analysis were collected on April 12 (borehole SW18) and April 17 (borehole SW2A) 2005 using a hand auger (Fig. 2.1b). The samples were immediately placed in sealed plastic bags and stored in a refrigerated unit. Stable isotope analysis was performed using direct CO_2-soil water equilibration (Koehler et al. 2000; McConville et al. 1999).

2.4. Results and Discussion

2.4.1. Material Properties

On average, the glacial soil is comprised of 60 to 75% fines (particle diameter less than 0.075 mm, USCS), of which 25 to 40% are clay-size particles (diameter less than 0.002 mm). The cover is heterogeneous as coarser textured lenses containing silty sand are occasionally encountered. The glacial soil is classified as a medium plasticity clay with average plastic and liquid limits of 28% and 44% (n = 12), respectively (Boese 2003). Measured values of bulk dry density ranged from about 1600 kg/m^3 to 1700 kg/m^3 (n = 4). The measured porosity of the glacial soil ranged from 0.40 to 0.43 (n =4).

Fig. 2.2 presents the geometric mean values of *in situ* saturated hydraulic conductivity (K_s) for the shale overburden, glacial soil, and peat-mineral soil. A more detailed analysis of the data is presented by Meiers et al. (2006). The shale overburden K_s increased by about one order of magnitude, from 1×10^{-9} m/s (n = 12) in 2000 to 1×10^{-8} m/s (n = 24) in 2002. The glacial soil experienced the largest increase in mean K_s, from around 1×10^{-8} m/s (n = 12) in 2000 to 6×10^{-6} m/s (n = 12) in 2003. The K_s of the peat-

mineral soil increased by approximately a half an order of magnitude between 2000 and 2002. In all cases, the K_s increased within three to four years after cover placement in 1999. In subsequent years (2004-2005), the values of K_s either remained constant or, in the case of the glacial soil, decreased a half order of magnitude to 2×10^{-6} m/s (n = 12). Although it is speculative at this time, the marginal decrease in K_s after 2003 could be attributed to borehole smearing or operator error. The general increase in K_s over time is consistent with other cover performance studies in which K_s increases are either inferred by increasing drainage rates (e.g., Khire et al. 1997) or measured directly in the field and laboratory (e.g., Albright et al. 2006).

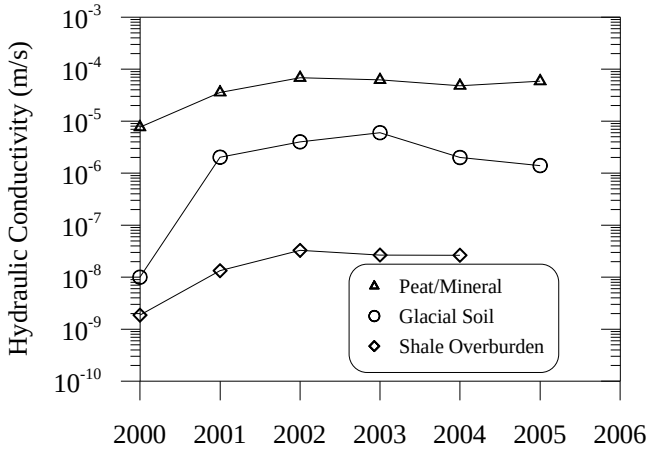

Fig. 2.2. Mean saturated hydraulic conductivity (Meiers, 2006).

Meiers et al. (2003; 2006) suggested that freeze-thaw effects were likely responsible for the development of macroporosity and the corresponding increase in K_s. Numerous laboratory and field studies have demonstrated that freeze-thaw effects have a significant effect on the K_s of clay-rich materials (Benson and Othman 1993; Benson et al. 1995; Chamberlain and Gow 1979; Chamberlain et al. 1990; Chamberlain et al. 1995). These authors report that K_s is increased by two mechanisms: (1) water migration towards the freezing front that induces desiccation cracking below the freezing front; and (2) the formation of ice lenses at the freezing front which alter the structure of the soil (Othman and Benson 1993). The temperature sensors demonstrate that the soil profile freezes to depths greater than 145 cm (Fig. 2.3a and c).

2.4.2. Water Balance

A detailed water balance was not conducted as part of this study; however, the hydrological data collected for this work can provide some general insight into partitioning of precipitation on the covers. As noted above, the snowpack accounts for approximately 20% of the annual precipitation. In general, nearly all of this water reports as runoff during the spring snow melt. Surface runoff during the summer months is essentially non-existent. Subsurface flow distributed over the entire area of the cover accounts for only a small fraction of the overall water balance, ranging from a fraction of a percentage in 2001 to about 1.5% in 2005. Deep percolation would also account for less than a percent of the water budget assuming a flux rate equivalent to the shale hydraulic conductivity (i.e. unit hydraulic gradient), as it would only occur while perched conditions exist in the covers. The combined contribution of deep percolation and subsurface flow would be a maximum of around 2 to 3%. Accordingly, actual evapotranspiration accounts for the majority of the water balance for the covers (~ 80%). Small changes in volumetric water content storage will account for any deficit or excess that occurs due to evapotranspiration.

2.4.3. Hydrological Response

Hydrometric data from 2004 and 2005 are presented the following sections. Data from previous years are not presented for brevity and to avoid redundancy as the same patterns are reflected in each annual record. Table 2.1 summarizes relevant climate and hydrometric data for all years of record.

Ground Temperatures and Snow Melt

Fig. 2.3 presents ground temperatures, cumulative interflow volumes, and daily precipitation for 2004 and 2005, including snow melt run-off. The timing of snowmelt prior to 2004 is indicated by the date of peak weir flow in Table 2.1. Interflow volumes are presented as depth of water (mm) assuming that perched conditions develop in the lower 30 m of the slope (discussed below).

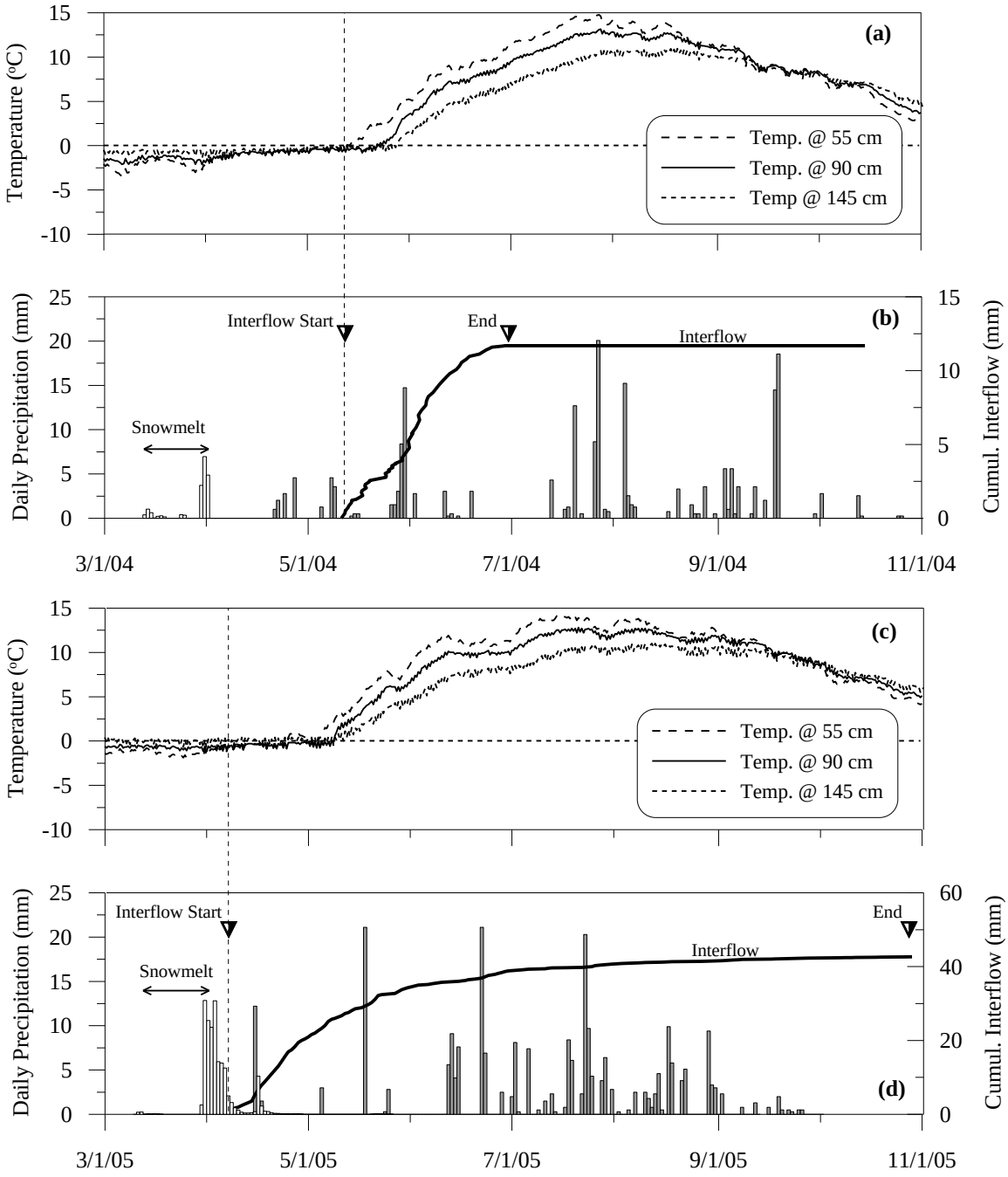

Fig. 2.3. Ground temperature, daily precipitation (bar charts), and cumulative interflow volume (line charts) for 2004 (Fig. 2.3a and Fig. 2.3b) and 2005 (Fig. 2.3c and Fig. 2.3d).

Table 2.1. Summary of annual climate data, peak weir flow, and interflow events.

Year	Rainfall (mm)	Snow Pack Depth (mm SWE)	PET (mm)	Peak Weir Flow	Ground Thaw at ~ 55 cm	Start of Interflow	Total Interflow (Litres)	Duration of Interflow (days)
2001	371	44[a]	530	-	May 15	May 16	965	29
2002	337	77[a]	510	April 10	May 15	May 14	1513	**
2003	308	23	510	April 8	May 9	May 08	12,341	77
2004	326	67	505	March 31	May 13	May 12	17,518	49
2005	341	81	n/a	April 2	April 24	April 7	60,000	**

** Interflow occurred intermittently in the summer of 2002 and throughout the summer and fall of 2005.

[a] Snow pack depth measurements taken adjacent to cover.

In 2004, the ground temperature near the base of the cover (~ 90 cm) increased above freezing and interflow began almost simultaneously (~ May 13). The timing of events is less obvious for 2005 (Fig. 2.3c), as the temperature sensors indicate that the ground was still frozen when interflow began. Interflow was also concurrent with ground thaw in 2001 to 2003 (Table 2.1). In general, the temperature data demonstrate that there is a strong correlation between ground thaw near the cover-shale interface and the initiation of interflow. Small discrepancies in the timing of events, particularly for 2005, are likely explained by differences in ground thaw at the soil station (mid-slope) and interflow pipe. Field borehole logs indicate that the cover is approximately 0.5 m thicker at the soil station than near the toe of the slope.

Snow melt run-off occurs at least one week, and up to 1.5 months, before interflow begins. Snowmelt in 2004 occurred from around March 15 to March 31, while interflow began about 1.5 months later on May 12 (Fig. 2.3a and b). In 2005, snowmelt occurred rapidly at the end of March as daily air temperatures reached 10 to 15°C. Field observations confirmed that snowmelt and runoff were complete by the 1st of April, with the peak weir flow occurring on April 2nd, 2005. These data and observations demonstrate a predictable sequence of annual events: snowmelt and runoff followed later by ground thaw and interflow.

The time-lag between snowmelt/runoff and the initiation of interflow when the ground thaws suggests that vertical preferential flow occurs through frozen soil. Considering that the interflow system is inactive by late autumn, and that the ground is

frozen during snowmelt and runoff, it is most likely that the pathway for infiltrating snowmelt water is via preferential flow paths. Frozen ground conditions generate surface runoff because infiltration capacity is significantly reduced by pore ice (Hayashi et al. 2003; Lauden et al. 2004; e.g., Stähli et al. 1996). Numerous snowmelt infiltration studies have found that fractures can provide vertical preferential pathways in otherwise frozen soil (Baker and Spaans 1997; Derby and Knighton 2001a; Espeby 1990; Sharratt and Goldsmith 1997). Water stored in the preferential flow paths migrates into the soil matrix when the ground thaws, triggering the development of a perched water table on the shale interface if saturated conditions develop. The correlation between ground temperature and the start of interflow is consistent with the findings from these studies.

Monitoring Wells and Matric Suction

Fig. 2.4 and Fig. 2.5 present the monitoring well and matric suction data for 2004 and 2005, respectively. The cessation of interflow in 2004 coincided with a recession of the perched water table and an increase of matric suction in the glacial soil due to drying caused by plant moisture uptake. In contrast, interflow continued intermittently throughout the summer and fall of 2005, a year in which the climate was both cooler and wetter. Accordingly, the matric suction never exceeded 100 kPa at a depth of 55 cm, whereas the suction exceeded 1500 kPa in 2004.

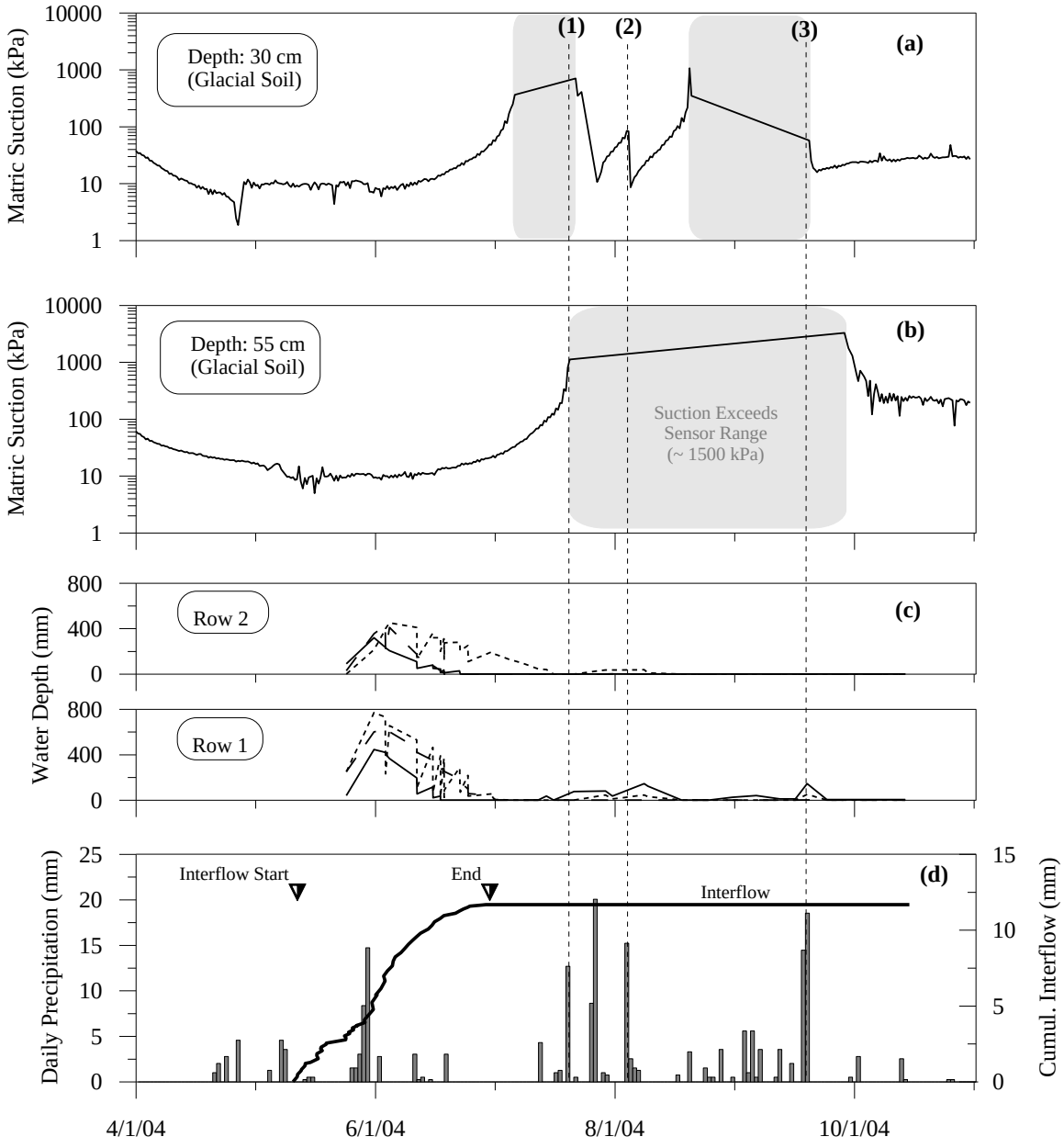

Fig. 2.4. 2004 matric suction and monitoring well data. (a) Matric suction at 30 cm. (b) Matric suction at 55 cm. (c) Water depth in shallow monitoring wells. (d) Cumulative interflow volume (line chart) and daily precipitation (bar chart).

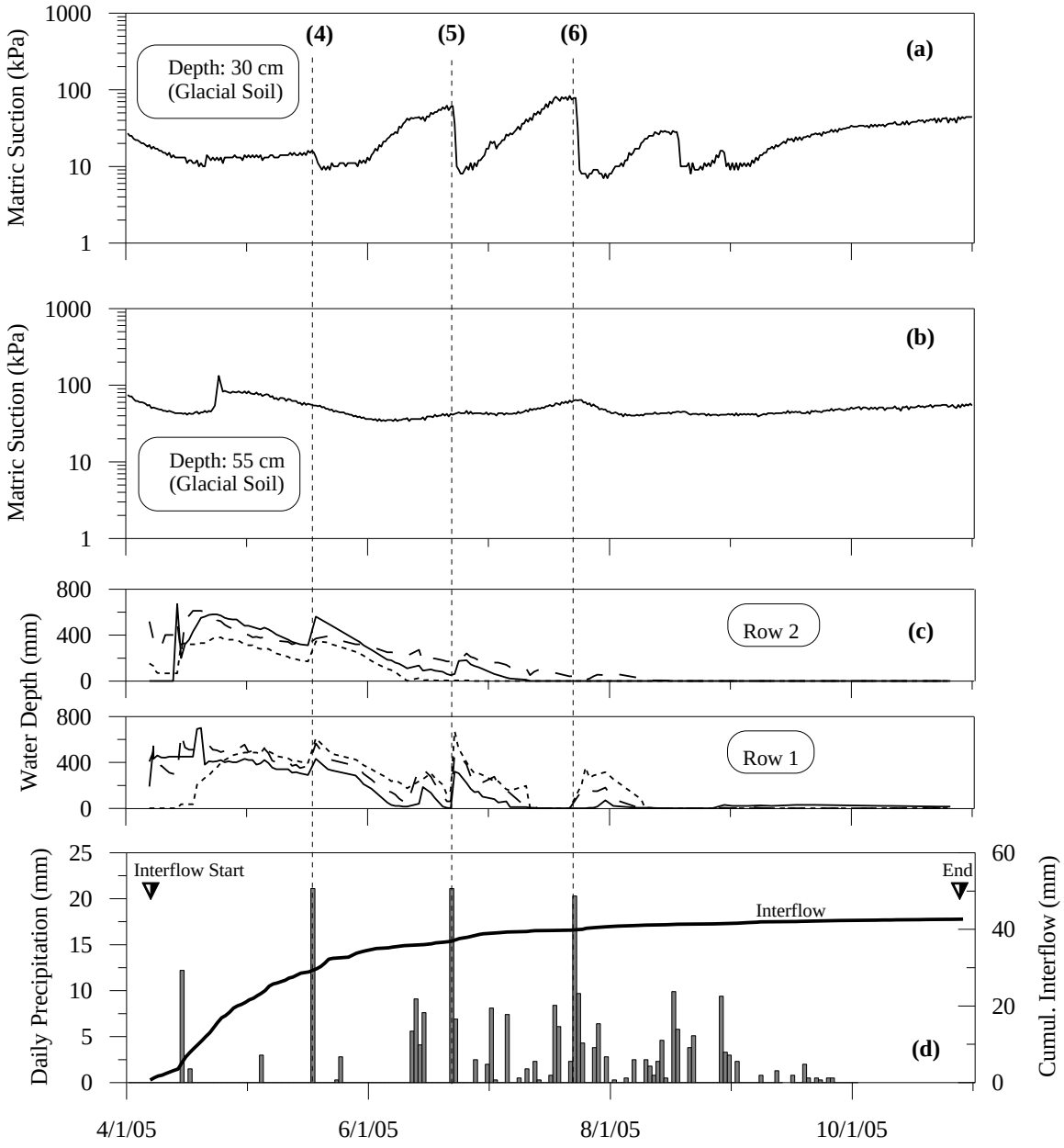

Fig. 2.5. 2005 matric suction and monitoring well data. (a) Matric suction at 30 cm. (b) Matric suction at 55 cm. (c) Water depth in shallow monitoring wells. (d) Cumulative interflow volume (line chart) and daily precipitation (bar chart).

Six climatic events are denoted on these figures to demonstrate the instantaneous response of shallow monitoring wells to high-intensity precipitation events of 10 to 20 mm/day. Perched conditions develop on the interface immediately following rainfall. The suction sensors at 55 cm depth indicate that the cover was not field-saturated and that

a wetting front did not advance through the cover after rainfall (i.e. suction remains nearly constant). This suggests that preferential flow paths contribute to the rapid delivery of infiltration water to the base of the cover. It is also noted that in contrast to 2005, high-intensity rainfall events in 2004 did not generate interflow. This is likely explained by the high matric suctions in 2004 which act to: (1) increase the available storage in the matrix; and, (2) promote flow into the matrix due to large hydraulic gradients, thereby diminishing the contribution of preferential flow paths to the development of perched conditions at the cover-shale interface.

Interflow Volumes

A comparison of K_s and annual interflow data (Fig. 2.2) demonstrates that the increasing volume of interflow water collected annually does not correlate with the measured increase in hydraulic conductivity. Most of the increase in K_s was complete by 2001, but the volume of interflow water continued to increase between 2001 and 2005, despite the relatively constant K_s. Meiers *et al.* (2006) speculated that this offset in interflow volumes from K_s changes may be due to the development of a more interconnected secondary structure.

It is speculated in this paper that it may also be due to: 1) subtle differences in soil moisture conditions prior to freeze-up; and, 2) subtle differences in the thermodynamics during snowmelt. The interflow chemistry (discussed below) demonstrates that pre-event water dominates the spring interflow event; consequently, the volume of water stored in the soil matrix prior to freeze-up (i.e., antecedent moisture) will have a direct impact on the amount of interflow collected in spring. Naturally, perched conditions will only develop if event water stored in the preferential flow paths migrates into the matrix and creates a saturated condition.

The system thermodynamics will also affect the quantity of runoff and the amount of frozen ground infiltration that occurs through preferential pathways. Numerous investigations have shown that infiltration into frozen soil is the result of a complex interaction of the water and heat fluxes (1) at the snow-atmosphere interface, (2) within the snow pack, (3) in the frozen soil layer, and, (4) in the unfrozen soil below the frost

boundary (Flerchinger et al. 1996; Johnsson and Jansson 1991; Stadler et al. 1997a; Stähli et al. 1996; Stähli et al. 1999; Thunholm et al. 1989b). As a result, the rate and timing of snowmelt and ground thaw along with diurnal air temperature fluctuations will affect the volume of interflow collected. A rapid snowmelt followed by warm spring air temperatures (e.g. 2005 spring melt) would facilitate snowmelt infiltration via the preferential flow paths, expedite ground thaw, and allow more time for interflow to proceed before high ET demands begin. Conversely, a slower snowmelt followed by a very cool spring could impede preferential flow due to ice pore blockage caused by re-freezing of infiltration water and limit the time for interflow to occur.

Pore Water and Interflow Chemistry

Fig. 2.6 presents two profiles of pore water sulphate concentrations determined on the centrifuge and saturated paste extracts. The cover-shale interface at both locations is shown on the figure. Sulphate concentrations above the interface varied from approximately 2500 mg/L to 4000 mg/L. The shape of the profile demonstrates that increased salt concentrations in the cover pore water are a result of advective and diffusive transport from the underlying shale.

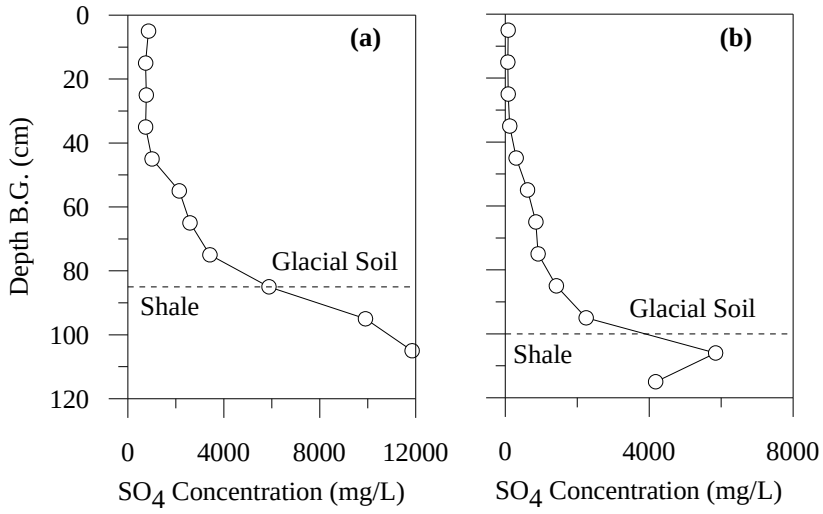

Fig. 2.6. Profiles of pore water sulphate concentration at two locations. (a) Centrifuge extracts. (b) Saturated paste extracts.

Fig. 2.7 presents the sulphate concentration of interflow waters collected between 2002 and 2005. The sulphate concentration increases each year from near 0 mg/L at the start of spring melt to a value equivalent to the pore water concentration near the interface (~2500-3000 mg/L). This transition is partly attributed to preferential flow through macropores. The chemical signature of the interflow waters is consistent with fresh snow melt water at the start of interflow because the ground is still partly frozen and chemical equilibration between the two water reservoirs cannot occur. Once ground thaw is complete, the concentration of the discharge water rises as pore water in the soil matrix equilibrates with fresh water in the macroporosity and the depth of perched water decreases.

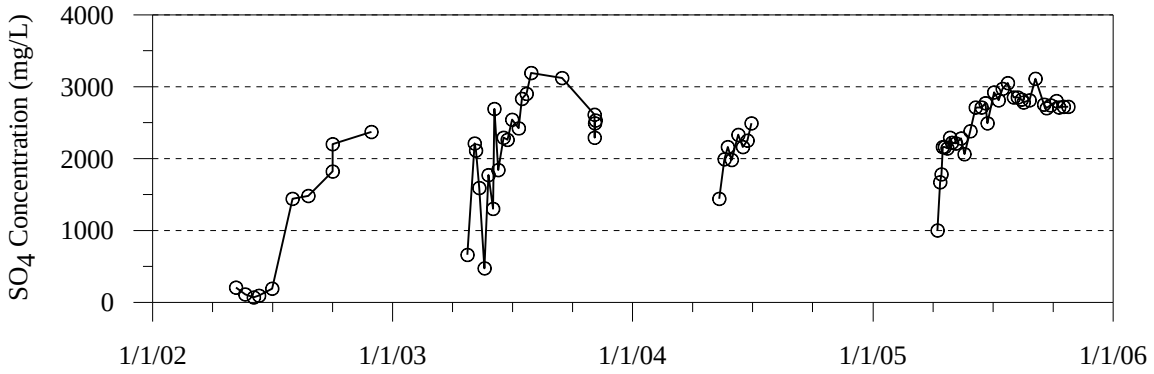

Fig. 2.7. Measured SO_4 concentration of interflow water from 2002 to 2005.

These observations are supported by other studies in the literature where preferential flow generates a transient perched water table at the interface of a lower K_s unit, creating a saturated and highly mobile zone of water that can move laterally down slope (Burns et al. 2001; Hinton et al. 1994; Jardine et al. 1990; Newman et al. 2004; Peters et al. 1995). Macroporosity provides the vertical preferential flow paths that can transmit water rapidly to depth when the precipitation intensity exceeds the infiltration capacity, thereby inducing overflow of soil water from the matrix into the macropores. Uchida *et al.* (2004) and Tromp van Meerveld and McDonnel (2006a) have shown that lateral flow along the interface is highly threshold dependent, controlled by the precipitation amount and the antecedent moisture conditions, and largely via macropores at the soil-impervious layer interface. The chemistry of the water that moves down slope can be predominantly

pre-event from the soil matrix or some mixture of pre-event and event water that is dependent on the relative contribution of lateral preferential flow.

Although the interflow chemistry provides additional evidence for preferential flow, the results are not conclusive because the ion tracers are not conservative. The increasing sulphate concentration in the interflow could be explained, at least qualitatively, by salt release from the underlying shale into the interflow as it travels along the interface; thereby precluding the use of CHS in this study.

2.5. Analysis

2.5.1. Numerical Modelling

Two-dimensional finite element (FEM) seepage modelling was conducted to evaluate the anticipated rate and volume of interflow from the cover with macroporosity-dominated saturated groundwater flow. Modelling results were compared to the 2005 interflow data. The modelling is predicated on the conceptual model for interflow developed in this paper, which states that perched conditions on the cover-shale interface are triggered every spring due to preferential flow through macropores when the ground is frozen. Interflow is initiated when the ground thaws and saturated conditions develop. The discharge rate and volume of interflow should therefore be controlled primarily by the macroporosity of the soil as the slope drains to field capacity. Macroporosity is typically defined as the fraction of soil volume comprised of pores with diameters greater than 1×10^{-3} m (Luxmoore 1981), which corresponds to matric suctions of about –0.3 kPa based on the capillary rise equation (Fredlund and Rahardjo 1993).

The FEM model domain, initial conditions, and boundary conditions are shown in Fig. 2.8. It was constructed as a 1 m thick cover on an 11° slope, extending upslope a horizontal distance of approximately 30 m. The cover was discretized using four noded quadrilateral elements with four-point integration. A potential seepage face boundary condition was used at the 'toe' of the slope to allow groundwater to discharge when positive pore water pressures exist. Mesh refinement was applied near the toe of the slope as high seepage gradients occur during early time steps.

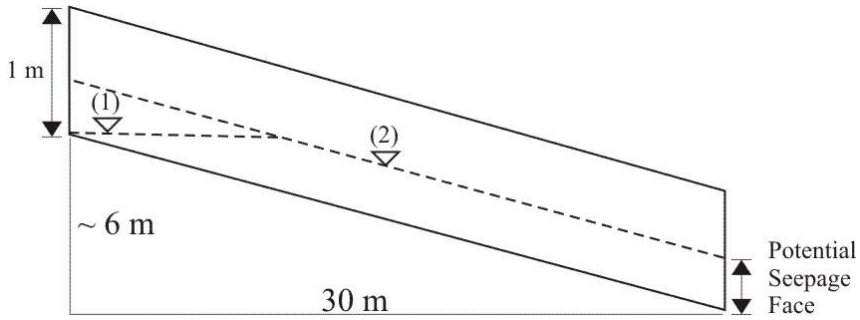

Fig. 2.8. Schematic of FEM model configuration showing two initial water table conditions.

The sensitivity of the model to the geometry of the initial water table was evaluated by using two different initial water table conditions: (1) a 'sloped' water table geometry with a uniform depth of 40 cm between the interflow pipe and a horizontal distance of 20 m, after which it diminished to zero at a horizontal distance of 30 m; and, (2) a uniform water table thickness of 40 cm across the slope (Case (1) and (2); Fig. 2.8). Case 1 is an approximation of conditions measured in 2005, in which water depths in both sets of monitoring wells were equivalent (Fig. 2.5). Water level measurements in ancillary monitoring wells installed in the spring of 2006 suggest that perched conditions diminish at about 30 m upslope of the interflow pipe. Case 2 is presented to evaluate the model sensitivity to the assumed water table geometries.

The sensitivity of the model to available volumetric water content storage was evaluated using two different soil water characteristic curves (SWCC) in the analyses (Fig. 2.9). Each curve was defined over a narrow suction range in order to model drainage from only the macroporosity (n_m). Macroporosity was estimated to range from 2.5 % to 5.0 % of the total soil volume. Reported values of macroporosity typically range from 1 to 8 % of the total soil volume (Germann and Beven 1981; Sollins and Radulovich 1988); ranging from 3 to 5% for clay-rich glacial soils and silty loam soils (Buczko et al. 2006; Jansson et al. 2005). The value of K_s was varied within the measured range of 1×10^{-6} m/s to 6×10^{-6} m/s. It is reasonable to assume that K_s is representative of macroporosity-dominated flow as numerous field studies have shown that water flow rates at near-saturated conditions are dominated by the macroporosity (Waduwawatte and Si 2004; Watson and Luxmoore 1986; Wilson and Luxmoore 1988).

The unsaturated hydraulic conductivity function (Fig. 2.9) was predicted from the laboratory measured SWCC using the method proposed by Fredlund et al. (1994).

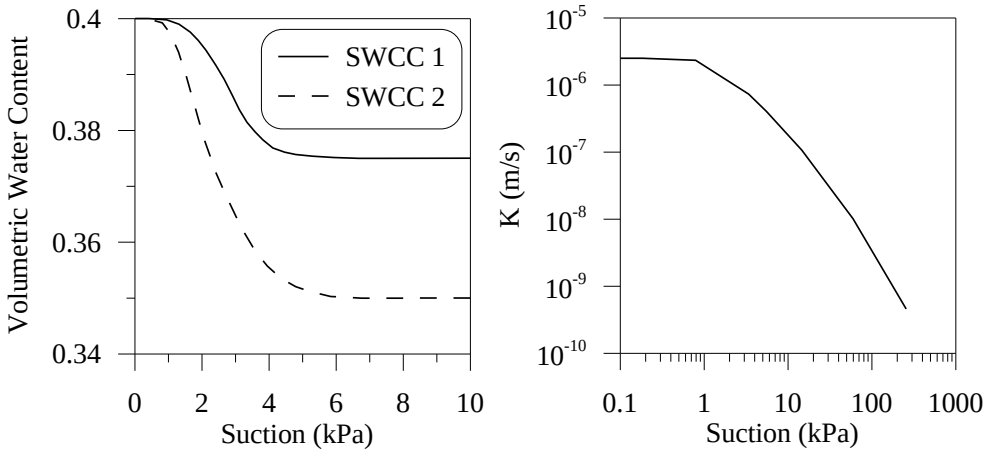

Fig. 2.9. Soil water characteristic curves and hydraulic conductivity function.

Results from the numerical analysis are compared to the 2005 cumulative interflow discharge in Fig. 2.10. A poor match was attained with a n_m of 2.5 % for both initial water table conditions. In contrast, a very good match was attained with a n_m of 5% and a K_s of 2.5×10^{-6} m/s for both the sloping and uniform water table conditions. The discharge rate at early times is controlled almost entirely by the selection of K_s, whereas the cumulative interflow volume is primarily a function of the assumed macroporosity. The simulation results were fairly insensitive to the initial water table geometry. The modelling suggests that interflow is governed by macroporosity-driven groundwater flow. The discharge rate and cumulative interflow are consistent with measured values of K_s, which is representative of preferential flow at near-saturated conditions, and drainage from the macroporosity, respectively.

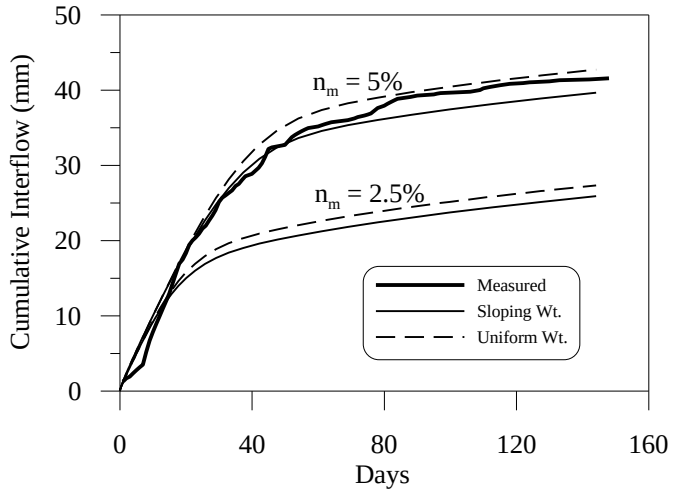

Fig. 2.10. Comparison between modelled and measured interflow volumes.

2.5.2. Isotope Hydrograph Separations

Hydrologists have used isotope hydrograph separation (IHS) and chemical hydrograph separation (CHS) for decades to distinguish the origin and pathway of water flowing in streams. Hydrograph separation techniques are based on the assumption that the chemical or isotope composition of event (i.e. precipitation) and pre-event water (i.e., connate pore water) at a given instant in time are known and that the 'stream' or output water is a mixture of the inputs (Sklash and Farvolden 1979). Pinder and Jones (1969) first used CHS to determine the contribution of groundwater to peak discharge runoff. Dincer et al. (1970) pioneered the IHS technique by using the oxygen and tritium isotope compositions of groundwater, rain, and snow to establish that the majority of river flow in a watershed during spring melt was the result of pre-event water within the soil slope.

In general, conservative isotope tracers ($\delta^{18}O$ and $\delta^{2}H$) are used as indicators of water origin while chemical tracers (e.g. Cl, SiO_2) provide additional information on water flow paths and are used indirectly as indicators of water origin (Kendall et al. 2001). Chemical hydrograph separation is more prone to interpretation error because the chemical signature of the pore water may evolve as it interacts with the soil along the flow path, particularly if the water travels along a soil-bedrock interface (McDonnell 1990). Wels et al. (1991) suggested that IHS provides the upper limit of the groundwater

contribution to stream flow because the event water is less likely to accumulate a dissolved load as it travels through the soil.

The simplest form of an IHS or CHS is a two-component system, where there are two inputs (e.g. precipitation and groundwater) and one output (e.g. stream flow). The composition of the stream water can be expressed as:

$$C_s = f_e C_e + (1 - f_e) C_{pe} \quad [1]$$

where C_s, C_e, and C_{pe} are the concentrations of the stream flow, event water, and pre-event water, respectively, and f_e is the fraction of event water. The fraction of total stream flow due to each component must equal unity (i.e. $f_{pe} + f_e = 1$) so the fraction of event and pre-event water can be written as:

$$f_e = (C_s - C_{pe}) / (C_e - C_{pe}) \quad [2]$$

$$f_{pe} = (C_e - C_s) / (C_e - C_{pe}) \quad [3]$$

There are two fundamental assumptions for the application of hydrograph separations: 1) the event and pre-event waters have distinct compositions; and, 2) the precipitation and groundwater are characterized by constant concentrations during the precipitation event (Sklash and Farvolden 1979). Kendall (2001) notes that these assumptions are often adequate for general characterization of catchment response to major climatic events (e.g., snow melt, spring rain).

A two-component IHS was used to quantify the percentage of macropore water and matrix pore water in the interflow during the spring of 2005. In theory, water that initially flows into the interflow collection system should be water stored in the soil macropores (event water). However, as the drainage pathway increases there will be sufficient time for equilibration of this water with the pre-event water stored within the soil matrix prior to snowmelt infiltration. The fraction of pre-event water in the interflow water was calculated as:

$$f_{pe} = \delta^{18}O_e - \delta^{18}O_I \;/\; \delta^{18}O_e - \delta^{18}O_{pe} \qquad [4]$$

where $\delta^{18}O_I$, $\delta^{18}O_{pe}$, and $\delta^{18}O_e$ are isotopic compositions and the subscripts I, pe, and e refer to interflow water, pre-event water, and event water, respectively.

Isotope hydrograph separations are sensitive to the assumed end-member concentrations. In this study, end-member $\delta^{18}O$ signatures were required for the melt water (event water) and the soil water reservoir (pre-event water). The results of the stable isotope analyses for the interflow water, snow samples, and shallow piezometers are compared to the local meteoric water line (LMWL) for Edmonton, Alberta in Fig. 2.11. All samples plot along on or near the LMWL. Hence, any trends in the isotopic data with time cannot be attributed to fractionation due to post sampling evaporative fluxes caused by storage and handling. Although the interflow water samples plot slightly below the LMWL, the results do not exhibit an evaporative fractionation trend (i.e. shallower slope). The offset from the LMWL is likely due to the differences in the LMWL between Ft. McMurray and Edmonton.

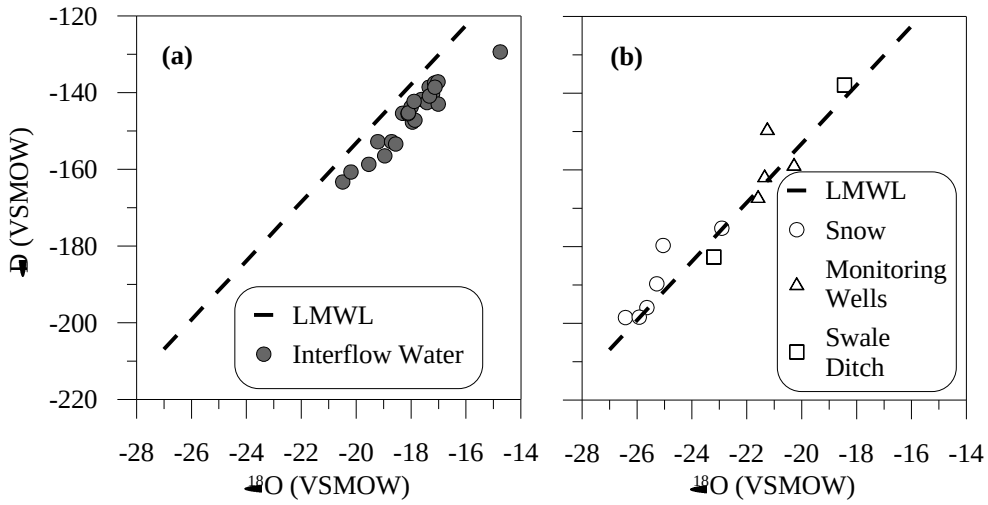

Fig. 2.11. Comparison between δD/$\delta^{18}O$ and the local meteoric water line for Edmonton, Alberta. (a) Interflow water. (b) Snow samples, monitoring wells, and swale ditch water.

Fig. 2.12 presents a time series of $\delta^{18}O$ for water collected from the interflow, monitoring wells, and snow survey. The average $\delta^{18}O$ of water in the shallow monitoring wells on April 7, 2005 (start of interflow) was selected for the event (melt water) end-

member (–21.1 ‰, n = 4). Considering the hydrological data presented above, it is reasonable to assume that water in the monitoring wells at the initiation of interflow is dominated by melt water from the preferential flow paths. The average snow sample signature was not selected as the end-member because fractionation likely occurred during snowmelt due to isotopic exchange between water and ice as the melt water percolates through the snow pack. Taylor (2002) reported the isotopic compositions of melt water samples from four seasonal snow pack studies, and found that on average, the $\delta^{18}O$ increased by about 4 ‰ over the melt period. Coincidentally, the average $\delta^{18}O$ of snow samples collected at the beginning of March, 2005 was –25.2 ‰ (n = 6), which is approximately 4 ‰ more depleted than water from shallow piezometers.

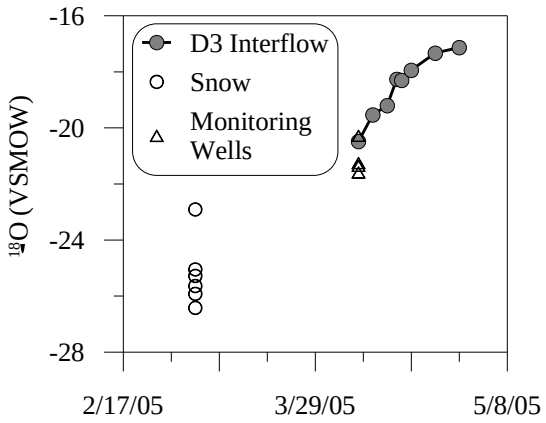

Fig. 2.12. $\delta^{18}O$ signature of interflow water, snow, and shallow monitoring wells during the 2005 spring melt.

Fig. 2.13 presents the depth profiles for pore water $\delta^{18}O$ determined by direct equilibration. Direct equilibration results were not plotted against the LMWL as deuterium results were not available. $\delta^{18}O$ values ranged from –19.5 ‰ in the peat-mineral soil to –15.4 ‰ in the glacial soil. The $\delta^{18}O$ measurements yielded a fairly uniform depth profile for SW2A (sampled on April 17) with an average value of –16.2 ‰ (n = 5). $\delta^{18}O$ values of precipitation measured in autumn 2004 were –16.1 ‰ (Edmonton precipitation; data not presented), which indicates that the soil pore water originated from the previous fall. In contrast to this, a more dynamic depth profile was observed for SW18 (sampled on April 12). The peat-mineral soil had an average $\delta^{18}O$ of –19.25 ‰,

whereas the glacial soil could be subdivided into two distinct regions of $\delta^{18}O$ concentrations. At depths less than about 70 cm the concentrations are more consistent with those of SW2A (~ –16.5 ‰). Below 70 cm, $\delta^{18}O$ concentrations are more depleted (–17.7 ‰).

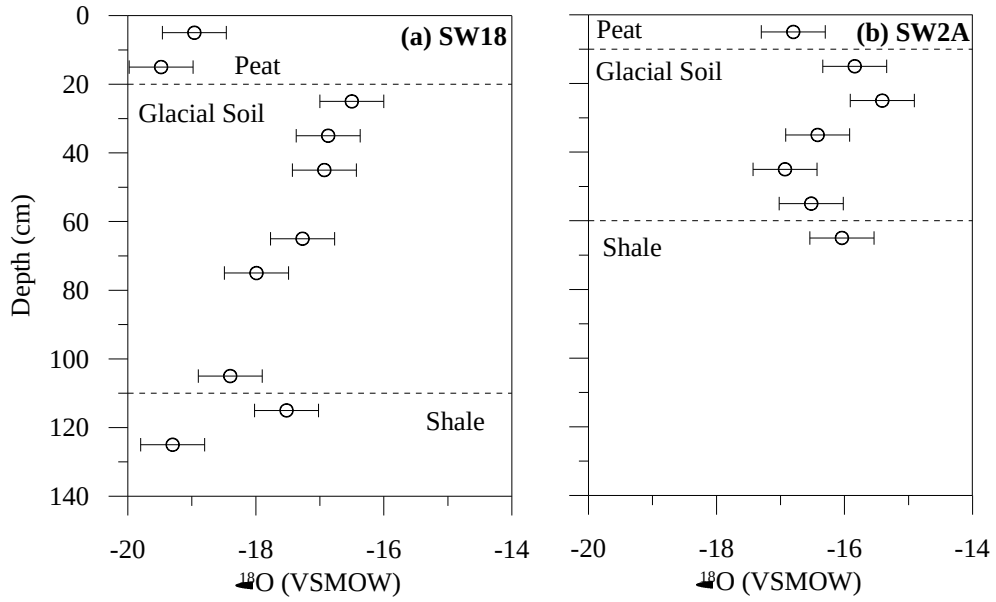

Fig. 2.13. Pore water $\delta^{18}O$ profiles determined by direct soil equilibration.

The depleted $\delta^{18}O$ signature in the peat-mineral soil and lower glacial soil of SW18 suggests that the pore water is a mixture of melt water and pre-event water. The peat-mineral concentration values are not surprising considering the proximity to the surface and given the high porosity of the material. The trend toward a more depleted signature in the lower glacial soil is consistent with the preferential flow mechanism discussed above. Considering that SW18 was sampled five days after the start of interflow, there is a high probability that pre-event matrix water could have mixed with event water in the macroporosity. The different trends in SW2 and SW18 could be explained by sampling locations relative to any preferential flow paths, in that SW2 may have not intersected a macroporosity feature. Based on this discussion, a more enriched $\delta^{18}O$ value for the soil water end-member is justified. Consequently, the average value for SW2 (–16.2 ‰) was used in the analysis.

Fig. 2.14 presents the results of the two-component IHS for the 2005 spring interflow event. The evolution of the isotopic signature confirms that interflow evolves from preferential to matrix pore water. The proportion of pre-event water in the interflow changes from 12 % on April 7, 2005 to over 80 % on April 28, 2005. The similarity between the $\delta^{18}O$ signature of pre-event water and autumn 2004 precipitation indicates that the IHS would be relatively insensitive to the selection of the soil water (pre-event) end-member. Using a value equal to the Edmonton precipitation (–16.1 ‰), would have yielded a pre-event water component of 79 % on April 28. In contrast, the early stages of the interflow event are sensitive to the selection of the melt water signature. If the average snow pack $\delta^{18}O$ value (–25.2 ‰) were used for the analysis, the percent pre-event water would increase from 12% to 52% at the beginning of interflow and from 80% to 90% on April 28.

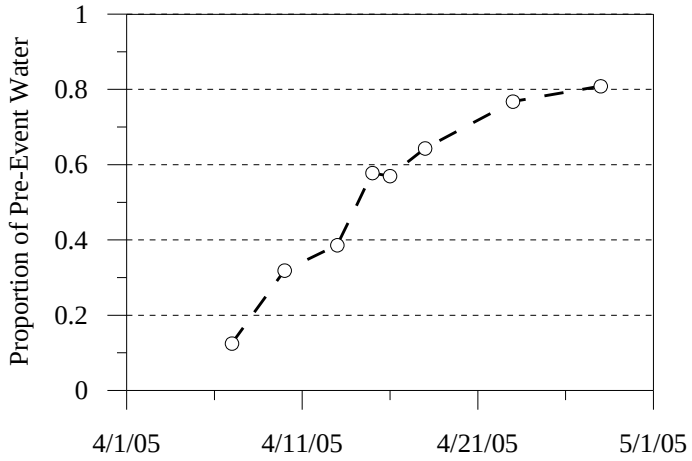

Fig. 2.14. Two-component IHS for spring 2005 interflow event.

In any event, the IHS confirms the interflow mechanism discussed above. Snowmelt water infiltrates into the frozen soil through preferential flow paths and triggers the development of a perched water table as the cover thaws. The chemical signature of water that reports to the interflow system eventually becomes dominated by pre-event water as high solute concentration pore water in the soil matrix equilibrates with fresh water in the macropores. This finding is consistent with the hydrology literature. Buttle

(1994) reports that on average 75% of 'stormflow' reporting to streams is attributed to pre-event water stored in the catchment before the episode.

This result also suggests that flushing of salts from the base of the cover via interflow pathways can still be effective, even though this water infiltrates and flows through preferential flowpaths. As a result, the presence of interflow will act to attenuate the upward diffusion of salts into the cover over time.

2.6. Summary and Conclusions

The hydraulic properties of soil covers used for mine reclamation will evolve over time in response to biophysical and chemical processes. These processes can lead to the development of preferential flow paths that will alter the hydrological response of the cover. Preferential flow within an oil sands reclamation cover overlying saline-sodic shale overburden has been studied using long-term (~ 6 yr) hydrological and geochemical data, a finite element seepage analysis, and the isotope hydrograph separation technique. The cover is on a north-facing 11° slope and comprises 20 cm of peat-mineral soil overlying 80 cm of clay-rich glacial soil.

The *in-situ* hydraulic conductivity of the peat-mineral, glacial soil, and shale overburden increased within three to four years of cover placement. The glacial soil exhibited the largest increase in mean K_s, from around 1×10^{-8} m/s in 2000 to 6×10^{-6} m/s in 2003. The large increase in hydraulic conductivity is attributed to the development of preferential flow paths (i.e., macroporosity) caused primarily by freeze-thaw cycling. Temperature sensors confirm that the cover freezes annually over its entire depth.

Each year snowmelt/runoff occurs while the ground is frozen and the infiltration capacity of the soil matrix is reduced due to pore ice blockage. The initiation of interflow along the cover-shale interface is directly correlated to the onset of ground thaw, and typically occurs after snowmelt is complete. This suggests that infiltration occurs initially along preferential flow paths through frozen soil. As thawing progresses, water stored in the preferential flow paths migrates into the soil matrix, creating a perched water table on the cover-shale interface if saturated conditions develop. In the summer

and autumn months, preferential flow within the cover appears to demonstrate a type of 'threshold' behaviour in which antecedent moisture conditions and precipitation intensity/volume exert considerable control on the relative contribution of preferential and matrix flow to infiltration as well as to the generation of interflow.

Measured sulphate concentrations of the interflow water support the hypothesis that the chemical signature of interflow evolves from preferential (snowmelt) water to pre-event water as chemical equilibration occurs between the two soil-water reservoirs. Numerical analysis of the 2005 interflow event demonstrates that the discharge rate is controlled by the measured *in situ* hydraulic conductivity, which is dominated by macroporosity-driven flow. The cumulative volume of interflow is solely a function of the drainable macroporosity, which is estimated to be 5 % of the total soil volume. An isotope hydrograph separation conducted on the spring 2005 interflow event confirms that interflow becomes dominated by pre-event water. Consequently, the annual spring interflow event will be an important mechanism for attenuating the upwards transport of salts into the cover. Finally, it is noted that the congruence between hydrometric and geochemical data provides a stronger argument for the preferential flow mechanism than the hydrometric data alone.

3

Controls on the Spatial Distribution of Soil Moisture and Salt Transport in a Sloping Reclamation Cover

Preface

Reclaiming shale overburden poses a significant challenge to oil sands operators in north-central Canada. The shale overburden is classified as both saline and sodic, and contains high pore water concentrations of dissolved solids. The upward transport of salts from the underlying shale has the potential to cause salinization of the overlying cover soil, thereby jeopardizing reclamation efforts to re-establish a boreal forest at these sites. This paper addresses the spatial controls on soil moisture and salt transport within sloping reclamation covers overlying low permeability waste substrates. The effect of landscape position, subsurface flow, deep percolation, and upwards advection on salt transport is investigated. Mesotopographic effects on the performance of engineering soil covers (i.e. the global objective of this research) are directly investigated as the distribution of soil moisture, the depth of perched water table conditions, and the direction of subsurface flow are all functions of the meso-scale topography of the cover-waste interface. The second specific objective of this research, which is to develop numerical simulations for instrumented site(s) capable of replicating patterns of moisture and salt movement, is partially achieved through the application of a 'pseudo' one-dimensional finite element analysis. *Reference:* Kelln, C.J., Barbour, S.L., and Qualizza, C.V., 2008. Controls on the Spatial Distribution of Soil Moisture and Salt Transport in a Sloping Reclamation Cover. Canadian Journal of Geotechnical Engineering, **45**: 351-366.

3.1. Introduction

Mine reclamation will occur on an unprecedented scale in the oil sands region of north-central, Canada, over the next 30 to 50 years. There are currently three mining operations in the region that generate saline-sodic shale overburden waste from mining operations. Syncrude Canada Ltd. expects to reclaim approximately 70 km^2 (approximately 1/3 of the final disturbance footprint) of saline-sodic overburden at their Base Mine alone. The levels of soluble salts within these wastes are prohibitive to plant growth, so the placement of natural soil covers on the saline-sodic overburden will be required to return these landscapes to productive ecosystems.

Characterizing the mechanisms that govern soil moisture dynamics and solute transport within these covers is fundamental to the success of these reconstructed landscapes. Soil moisture imparts a control on the key processes of infiltration, evapotranspiration, and nutrient uptake by vegetation and therefore governs the hydrological and biological function of the covers (Elshorbagy et al. 2005; Qualizza et al. 2004). The geochemical function of the cover encompasses the fate and transport of solutes within the system and is inherently linked to soil moisture dynamics through the processes of diffusion and advection. Upward migration of soluble salts from the underlying saline-sodic shale overburden could potentially lead to salinization of these covers and long-term degradation of these reclaimed landscapes.

Determining the controls on the spatial distribution of soil moisture in natural landscapes has received considerable attention in the field of hydrology over the past few decades. Topography has been considered historically to be the dominant control on the distribution of soil moisture and runoff response within a hillslope (Dunne 1978; Kirkby 1978). Recent research, however, has begun to challenge the dominance of topographic controls (Devito et al. 2005; Grayson and Western 2001; McDonnell 2003), particularly in arid and semi-arid climatic regions. Numerous investigations have clearly demonstrated situations where other mechanisms govern the soil moisture dynamics including: the presence of a subsurface impeding layer (Freer et al. 2002; Tromp van Meerveld and McDonnell 2006b); antecedent moisture conditions (Grayson et al. 1997a);

preferential flow paths (Jardine et al. 1990; Tsuboyama et al. 1994; Uchida et al. 2004); vegetation (Rodriguez-Iturbe et al. 1999); soil properties and topography (Famiglietti et al. 1998); or, a combination of these factors.

Down-slope moisture translocation in response to elevation gradients should be expected in evapotranspiration (ET) covers, capillary barriers, and reclamation covers on slopes (Miyazaki 1988). The upper part of a slope will tend to de-saturate more than the lower part of the slope if climatic conditions are equivalent and constant across the slope (i.e. steady-state moisture translocation). Bussiere et al. (2003) demonstrated using physical and numerical models that the volumetric water content in a sloping capillary barrier cover will vary considerably with slope position, with de-saturation of the saturated finer-grained layer occurring near the top of the slope while moisture accumulated in lower slope positions. Other authors have investigated the 'diversion capacity' of engineered covers on slopes, in which the express purpose of the design is to encourage down-slope moisture movement as a means of diverting water away from percolation into underlying waste materials (Nyhan et al. 1990; Ross 1990; Stormont 1995; Stormont 1996).

The objective of this study was to gain insight into the controls on the spatial distribution of soil moisture and salts in a reclamation cover located in a cold, sub-humid climate, in which the moisture dynamics vary considerably over the annual climatic cycle (i.e., transient soil moisture regime). In particular, this study addresses the following: (1) the spatial distribution of soil moisture and salts in the cover; (2) the controls on lateral moisture translocation and subsurface flow; and, (3) the coupling between the hydrological response of the cover and salt transport. Detailed mapping of stratigraphy, soil moisture, and groundwater levels was conducted to determine the relationship between topography and moisture conditions. One-dimensional profiles of *in situ* pore water chemistry were used to glean information on soil moisture dynamics and salt transport. A quasi one-dimensional numerical model was used to explore the mechanisms that control the spatial distribution of solute transport. The implications for

the long-term performance of reclamation covers overlying saline-sodic overburden are briefly discussed.

3.2. Background

3.2.1. Study Site

The study was conducted at the South West 30 (SW30) Overburden Research Site (57°2' N, 111°33' W), located approximately 400 km northeast of Edmonton, Alberta, at the Syncrude Canada Ltd. Mildred Lake mine site. The SW30 is a 2 km^2 saline-sodic shale overburden dump. Reclaimed landscapes developed on saline-sodic overburden will comprise about one-third of Syncrude's reclaimed landscape. Shale overburden is excavated during open-pit mining to gain access to the underlying oil-rich sand. It is then deposited in large waste dumps and re-contoured to resemble a natural Mid-Boreal Upland landscape. Reclamation is achieved by placing a clay-rich ET cover over the shale to provide sufficient moisture and nutrients for the re-establishment of an ecosystem.

Three test covers of varying thickness (35, 50, or 100 cm) were constructed in 1999 on the SW30 to evaluate the optimal cover design for reclaimed saline-sodic shale landscapes (Fig. 3.1). The test covers are 50 m wide by 200 m long and were constructed on a single hillslope, as hillslopes are the basic building block of natural landscapes (Sivapalan 2003). The covers are north facing with a fairly planar slope of 11° (5:1 horizontal to vertical) and are comprised of 15 to 20 cm of a peat-mineral mix overlying clay-rich glacial soil. The thickness of the 100 cm cover, which is the focus of this paper, was mandated by provincial environmental regulations and therefore served as the control plot. Detailed monitoring of these test covers has continued from 1999 to the present.

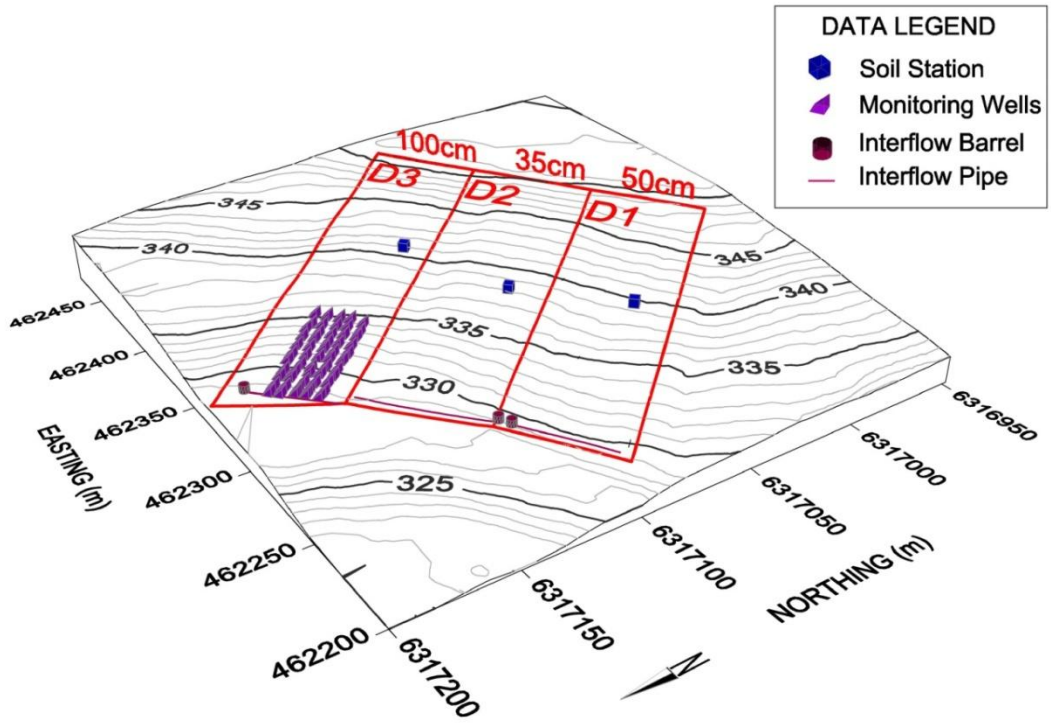

Fig. 3.1. Three-dimensional topography of the study area. Approximate location of interflow pipe is shown.

The climate at SW30 is classified as sub-humid continental, with a mean annual air temperature of 1.5 °C and a mean annual precipitation of 442 mm (1945-1995). The monthly mean air temperature ranges from 18 °C in July to -20.7 °C in January. On average, the potential evaporation as estimated by the Penman (1948) method typically exceeds 500 mm per year with daily maximums of approximately 7 mm/day occurring during July and August. Rainfall in the summer is often associated with thunderstorms and tends to be of short duration but high intensity. Approximately 20% of the annual precipitation occurs as snow during the winter months. Surface run-off is associated with snow melt in the spring and does not typically occur during the summer or autumn. Actual evapotranspiration rates (AET) over the summer growing season are often in

excess of 300 mm, which leads to frequent net summer moisture deficits of as much as 70 to 80 mm (Barbour et al. 2001; Elshorbagy et al. 2005).

3.2.2. Overburden Chemistry

The shale is of marine origin (Cretaceous age) and contains high pore water concentrations of dissolved solids. Saturated paste soil water extracts conducted on over forty samples (Kessler 2007; Nichol et al. 2006) had electrical conductivities greater than 4 dS m^{-1} and exchangeable sodium percentages (ESP) greater than 15, which classifies these soils as both saline and sodic (Richards 1954). Geochemical characterization of the shale overburden (Nichol et al. 2006; Wall 2005) has demonstrated that oxidation of reduced sulphur (pyrite or organic sulphur) within the shale leads to the production of sulphuric acid, which is subsequently neutralized by carbonates to produce elevated concentrations of sulphate (SO_4^{2-}), calcium (Ca^{2+}), and magnesium (Mg^{2+}). Cation exchange with adsorbed Na^+ results in a final pore-fluid solution which is predominately Na^+ and SO_4^{2-}. The shale therefore provides a reservoir of salts that can migrate into the overlying cover via solute transport processes.

3.2.3. Previous Studies

Details of the site instrumentation are provided by Boese (2003) and Shurniak (2003). A soil instrumentation station was installed in 1999 in the middle of the cover to monitor soil moisture, matric suction, and ground temperature at depths of 5, 20, 30, 55, 90, 115, 125, 145, and 170 cm. Vertical profiles of soil moisture were also measured in three neutron and eight capacitance probe access tubes installed along a north-south transect. Two climate stations are located on-site to measure the meteorological data including air temperature, relative humidity, wind speed and direction, and precipitation.

Lateral saturated groundwater flow (i.e. interflow) along the cover-shale interface is measured using an interflow collection system installed in June of 2000 across the entire width of the cover near the toe of the slope (Fig. 3.1). Details of the installation can be found in Kelln et al. (2007b). The interflow collection system is comprised of a perforated pipe that was installed in a geomembrane-lined trench (lined along base and

'downstream' face) and surrounded by a filter-gravel. The clay-rich soil and peat-mineral mix layers were reconstructed above the filter gravel. The perforated pipe discharges into a large-diameter (~ 1 m) collection well. Manual measurements of collection volumes were made from 2001 to 2004. An automated pump system was installed in the spring of 2005. It was comprised of a float-controlled sump-pump wired to a marine battery, which was charged by a low output solar panel. A mechanical flow meter was placed in-line with the pump to measure cumulative pumping volumes.

The long-term hydrological performance of the cover has been investigated by Meiers et al. (2003; 2006) and Kelln et al. (2007b). Meiers et al. (2006) found that the saturated hydraulic conductivity (K_s) of the clay-rich cover soil increased by approximately two orders-of-magnitude within three to four years after cover placement. The large increase in K_s was attributed to the development of macroporosity caused by freeze-thaw cycles (Benson and Othman 1993; Benson et al. 1995; Chamberlain and Gow 1979; Chamberlain et al. 1990; Chamberlain et al. 1995). Kelln et al. (2007b) found that preferential flow paths were responsible for the rapid delivery of 'event' water to the base of the cover during snow melt when the ground is frozen. Lateral saturated groundwater flow was initially dominated by event (snow melt) water, but eventually transitioned into predominately connate water (~ 80%), as fresh water in the preferential flow paths equilibrated with the soil matrix, creating a perched water table on the cover-shale interface. An isotope hydrograph separation performed on the 2005 interflow discharge demonstrated that about 72% of the 64,000 litres collected was connate water.

3.3. Materials and Methods

3.3.1. Field and Laboratory

A concentrated field investigation was conducted within a 25 by 50 m area located on the northeast corner of the 100 cm thick cover (Fig. 3.2). The local slope of the detailed study area is approximately 8°. It is bounded at the toe by a swale ditch used for runoff collection, and at the crest by a slight break in the topography to about a 5° slope. Fifty-five shallow boreholes (< 2 m deep) were excavated on 26 and 27 April 2006 using a

50 mm (2-inch) diameter hand auger and were used to determine the stratigraphy of the cover and collect samples for laboratory testing. The field program was scheduled to coincide with the onset of interflow (i.e. ground thaw). The boreholes were spaced on a 5 by 5 m grid pattern in order to capture meso-scale undulations in the surface and subsurface topography (i.e. the interface). Previous push-probe conductivity studies of the site suggested that the interface exhibited undulations over lateral distances of about 3 to 10 m (Komex International Ltd. 2000). Soil samples were logged in the field, placed in zip-lock bags, and transported to the laboratory for storage in a temperature and humidity controlled room. Material testing included: gravimetric water content (ASTM D2216-05) (ASTM 2005a), particle size distribution (ASTM D 422-63) (ASTM 2002a), and bulk density (ASTM 2937) (ASTM 2005b).

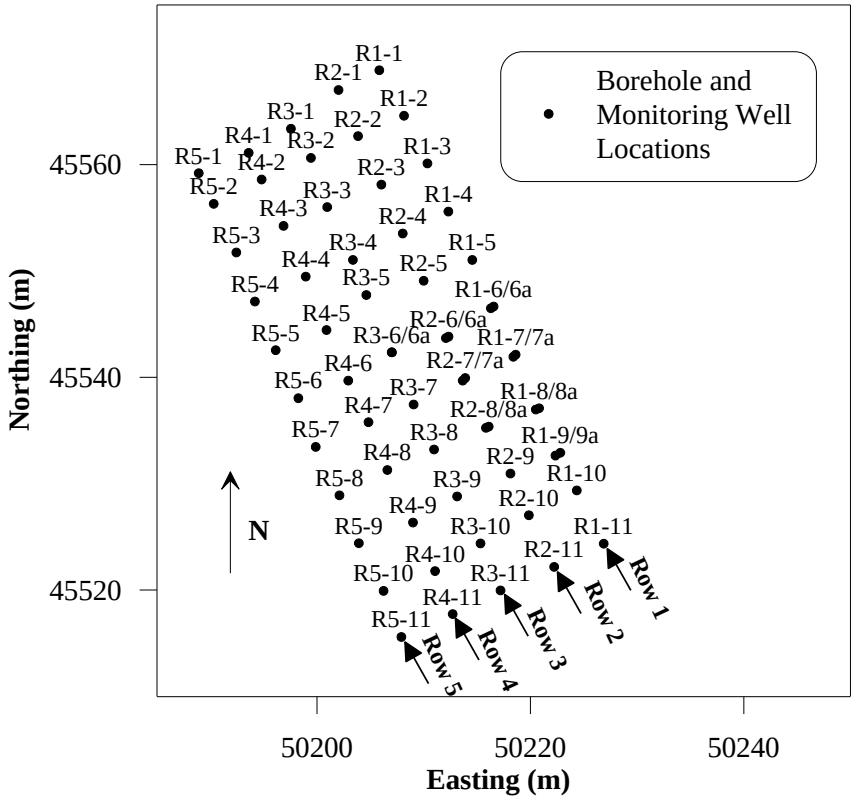

Fig. 3.2. Plan view of borehole and monitoring well locations in detailed study area (Row 1 to Row 5). Some locations have two installations (e.g., R2-7/7a).

Shallow monitoring wells were installed in each of the fifty-five boreholes to measure the dynamic water table response at the cover-shale interface. The wells were

constructed of 50 mm diameter Schedule 40 PVC pipe with 45 cm long #10 slot screens. Unforeseen geological conditions (discussed below) in the field necessitated the installation of eight additional monitoring wells at select locations with the screened zone below the cover-shale interface. These boreholes were excavated until refusal of the cutting bit. Water-level floats were installed in each monitoring well to measure the water depth above the interface or the height of water in the well. Each float was constructed of a ping pong ball (40 mm diameter) attached to a wood dowel that extended above the cap of the monitoring well. The location and elevation (ground/top of pipe) of each installation was surveyed using total station survey.

3.3.2. Water Chemistry

A total of 105 samples of groundwater from monitoring wells, and fourteen interflow samples from the pump discharge, were collected between April and June 2006. The samples were placed in polypropylene bottles, shipped to the laboratory, and stored at 4°C until the analysis was performed. Thirty-one monitoring well samples and six interflow samples were analyzed for major ion chemistry (Na^+, Ca^{2+}, K^+, Mg^{2+}, SO_4^{2-}, Cl^-, HCO_3^-, CO_3^{2-}) using ICP analyses.

Detailed profiles of *in situ* pore water chemistry were determined to study the spatial variability of salt transport in the reclamation cover. High-speed centrifugation was used to extract pore water from 63 soil samples collected from the Row 1, Row 3, and Row 5 installations (Fig. 3.2). Approximately 70 to 80 grams of soil was placed in the centrifuge assembly and rotated at 4000 rpm for 5 to 24 hours. The centrifugate (~ 0.5 to 3 ml) was passed through a 45 μm filter and then diluted to factors ranging from 200 to 2000. Sample dilution was required to produce sufficient volume for the ion analysis (~ 2 ml) while preserving some of the original sample. Chemical analysis for major ion chemistry (Na^+, Ca^{2+}, K^+, Mg^{2+}, SO_4^{2-}, Cl^-, HCO_3^-, CO_3^{2-}) was performed using a Dionex IC25 ion chromatograph. Results are reported with a standard deviation of 5%.

Sodium was selected as the tracer ion for transport modelling in this study because (1) it is naturally present at high concentrations in the shale, (2) it is the dominant pore water cation, and (3) it is of primary concern for the re-establishment of vegetation on the

cover. High pore water sodium concentrations can lead to soil structure degradation, osmotic stress on plant roots, and specific plant toxicity. Sulphate is also present at high concentrations in the shale, but it is produced primarily due to oxidation of pyrite (FeS_2) and is therefore a function of oxygen ingress into the cover, among other factors. Furthermore, SO_4^{2-} can be removed by precipitation of gypsum ($CaSO_4$), which is dependent on Ca^{2+} pore water concentrations, temperature, pH, and alkalinity.

3.3.3. Numerical Modelling

Quasi one-dimensional, finite element, solute transport modelling was conducted with CTRAN/W and SEEP/W (Geo-Slope International Ltd. 2004) to explore the effect of various soil moisture and groundwater flux conditions on vertical sodium (Na^+) transport into the cover from the underlying shale. The modelling is termed 'quasi' one-dimensional because the model domain is one-dimensional, but the boundary conditions for one of the modelling cases are two-dimensional. It is important to note that the modelling is mechanistic in nature; intended to demonstrate the impact of various processes on vertical salt transport. Although a process such as lateral flow is inherently a two-dimensional problem, the overall effect is to remove solutes near the cover-shale interface, thereby reducing the mass available for upward vertical flux into the cover via advection and diffusion.

Four simulation types were conducted: (Case I) diffusion-only with volumetric water contents in the cover ranging from saturated to residual; (Case II) diffusion with downward percolation into the underlying shale; (Case III) diffusion with lateral interflow along the cover-shale interface (percolation not included); and, (Case IV) upward advective-dispersive transport. Case I is predicated on the fact that the effective coefficient of diffusion (D) is a function of volumetric water content (Conca and Wright 1990; Lim et al. 1998). Decreasing volumetric water content increases the tortuosity of the remaining fluid filled pathways, thereby decreasing D. Case II and III simulations were conducted because deep percolation can occur as a result of perched water table conditions that develop on the cover-shale interface, while lateral flux (i.e. interflow) along the cover-shale interface occurs annually during the spring, causing down-slope

flushing of salts. Case IV was conducted to evaluate the effect of upward advective flux in response to hydraulic gradients established as a result of evapotranspiration during the growing season. Results from the modelling were compared to *in-situ* profiles of pore water Na^+ chemistry determined from the centrifuge extracts.

The model was constructed as a one-dimensional column (1 m wide) of elements with 1 m of clay-rich cover soil overlying 5 m of saline-sodic shale overburden. The thin layer of peat-mineral mix (15-20 cm) was not included in the analysis because it does not influence solute transport near the cover-shale interface. The initial pore water Na^+ concentrations in the cover and shale were set to 150 mg/L and 13,500 mg/L, respectively, based on results from this study and previous research (Kessler 2007; Nichol et al. 2006; Wall 2005). The model was run for an elapsed time of 1295 days, equivalent to the number of days in which the cover is unfrozen (~ May 15 to November 15; 185 days/year) over the 7 yrs since cover placement (1999 – 2005) .

Seepage conditions were established using a steady-state SEEP/W analysis. Although moisture conditions in the cover are dynamic due to the transient soil-atmosphere boundary condition, the steady-state analysis is assumed to represent average conditions throughout the year. This was represented by keeping the volumetric water content constant through the soil profile for all model runs, so that groundwater velocity was a function of only the applied surface flux.

For Case I (diffusion-only), the top and bottom boundaries were set to a zero flux condition for both mass and groundwater flow. A downward groundwater flux ranging from 0.01 to 0.05 mm/day (~ 1.85 to 9.25 mm/year for 185 frost free days) was applied to the top of the model for Case II, while the bottom boundary was set to a free-draining condition. The corresponding top and bottom transport boundaries were zero mass flux and a free-exit concentration boundary, respectively.

The volume of net percolation in Case II would be equivalent to the volume of water drained during a drop of a perched water table ranging from 3 to 13 cm, assuming a specific yield of 0.07. Measured depths of ponded water in the spring typically vary from trace amounts (~ 1 cm) to over 40 cm. Although ponded water depth has little control on

the actual percolation rate, the values are noted here to validate the selected boundary flux rates and to recognize the fact that perched conditions drive percolation, not actual infiltration. The model is restrictive in the sense that deep percolation must be modelled through the application of a surface boundary flux. It is assumed that percolation into the underlying shale is averaged over the year, although realistically, it occurs in a series of focused temporal events at a rate controlled by the hydraulic conductivity of the shale. The net percolation rates of 0.01 to 0.05 mm/day would be equivalent to drainage through a material with a hydraulic conductivity of 1 to 5 x 10^{-10} m/s under a gravity gradient of unity.

Lateral flux was modelled in Case III by setting a flux boundary on the left (positive) and right (negative) sides of the model, over a height of 20 cm above the cover-shale interface. The lateral flux was varied from 2 to 8 mm/day, which equates to an annual interflow discharge (over 185 days) ranging from 3.7 m^3 to 14.8 m^3 collected over the width of the cover (50 m). The latter value is in keeping with the average annual interflow volume of 18.5 m^3 collected between 2001 and 2005. The discrepancy between the applied and actual flux is attributed to limitations with modelling the actual 'flushing' mechanism and is discussed below. Finally, a free exit concentration boundary was set on the right side of the model to allow mass to leave the model by both advective and dispersive transport processes.

For Case IV, an upward groundwater flux ranging 0.03 to 0.06 mm/day was applied to both the top and bottom boundaries. A free-exit condition was applied to the top boundary of the transport model, while the lower boundary was set to a zero mass flux condition. These groundwater flux rates are equivalent to upward flux under a unit hydraulic gradient and a hydraulic conductivity ranging from 3.5×10^{-10} to 6.9×10^{-10} m/s. It is noted that, realistically, upward vertical flux would only occur for short temporal periods when excess moisture is available.

Since the objective of the modelling is only to illustrate the relative impact of various mechanisms (i.e. diffusion, advection, deep percolation, interflow) controlling solute transport in the cover, a simple linear function was used for D verses water content. A

value of 1×10^{-10} m^2/s was selected for D at saturation, similar to values reported by other researchers for low-hydraulic conductivity clay-rich soil of glacial origin (Hendry and Wassenaar 2000; Shaw and Hendry 1998). A value of 2×10^{-11} m^2/s was used for D at residual saturation, which corresponds to a volumetric water content of about 0.20 (Shurniak 2003). This decrease in D with saturation is consistent with values reported by Lim et al. (1998) and Conca and Wright (1992). The dispersivity (α) was set to an extremely small value in order to minimize the effect of mechanical dispersion. This is a reasonable assumption considering the scale of the problem (i.e. 1 m thick cover) and the low water velocities.

Sodium adsorption onto clay surfaces in the cover and shale was modelled using an adsorption isotherm determined by Nichol et al. (2006). The isotherm was developed through a comparison between pore water chemistry determined from saturated paste extracts (Kessler 2007) and *in situ* pore water chemistry determined by mineral-phase equilibrium modelling. As a result, the isotherm incorporates the net effect of a number of other processes such as Na^+ exchange with Ca^{2+} in the clay-rich cover soil and the effect of Na^+ dissolution/exchange in the shale triggered by gypsum precipitation and dissolution. The models were also run without the isotherm to ensure that the results were not overly sensitive to the sorption process.

3.4. Results and Discussion

3.4.1. Site Stratigraphy and Material Properties

Cross sections of the study area developed from the shallow borehole logs are presented in Fig. 3.3. It is noted that depth of the interface as estimated from augering could vary by ± 10 cm due to soft ground conditions near the interface, which caused 'over-sampling' in the auger at some locations. The local stratigraphy of the study area consists of the clay-rich cover overlying the saline-sodic shale overburden waste. The cover varied in total thickness from 62 cm to over 120 cm and was comprised of an average particle size distribution (PSD) of 37% sand, 42% silt, and 21% clay size particles (n = 12). Measured bulk density and porosity values ranged from 1600 kg/m^3 to

1700 kg/m^3 (n = 4) and 0.40 to 0.43 (n =4), respectively. These material properties represent the clay-rich cover soils; however, the cover exhibits heterogeneity as lenses of silty-sand and sandy-silt are commonly encountered. Meiers (2003) determined the *in-situ* saturated hydraulic conductivity (K_s) to be approximately 1×10^{-6} m/s ($\sigma \pm 7.7\times10^{-8}$ m/s based on log-normal distribution; n = 12) . The shale overburden is comprised of approximately 16% sand, 51% silt, and 33% clay (primarily illite and montmorillonite; n = 4) and has a K_s of less than 1×10^{-9} m/s (Rutten 2006).

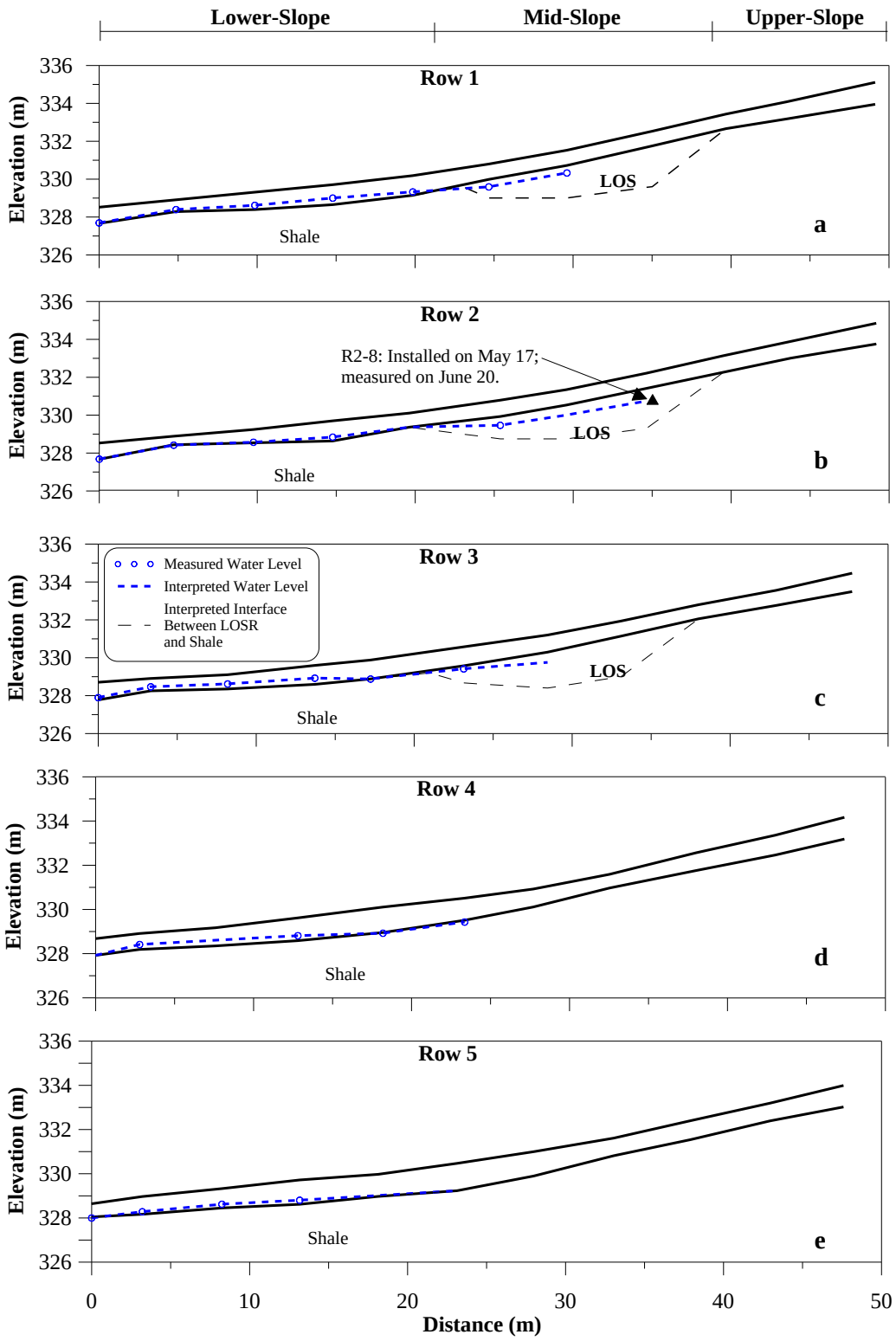

Fig. 3.3. Stratigraphy of the study site and measured/interpreted water levels on May 11, 2006 (Vertical exaggeration ~ 1.4×).

A thick lens of lean oil sand (LOS), a non ore-grade oil sand material typically associated with the overburden stratigraphy, was encountered in the upper part of the slope in Rows 1 to 3 (Fig. 3.3). The lower boundary of the lens could not be defined due to depth limitations with the hand auger. The LOS was un-stratified, unsorted soil, composed of a wide range of material, including fine sand with a hydrocarbon odour and 'pockets' of saline-sodic shale. The average PSD is 48% sand, 32% silt, and 20% clay size particles (n = 7). The estimated *in-situ* K_s would be around 1×10^{-6} m/s based on previous research on tailings sand, which has similar texture and geological origin (Price 2005). The heterogeneity exhibited by the LOS is attributed to its geological origin. LOS is excavated at the contact between the Cretaceous shale and the underlying oil-rich sand deposit and is therefore a mixture of oil sand and shale.

3.4.2. Spatial Volumetric Water Content Measurements

The spatial distribution of volumetric water content on 26 to 27 April 2006 in the top 300 mm of the soil profile and immediately above the cover-shale interface is shown in Fig. 3.4. Gravimetric water contents were converted to volumetric moisture contents using an average measured bulk density of 1690 kg/m^3. The spring snow melt began on March 24, 2006 and was complete by around April 10, 2006. Temperature sensors installed at the soil station indicated that the cover was fully thawed by 25 to 27 April 2006. Interflow started immediately following ground thaw (~ April 26). The timing of the interflow event is consistent with historical trends in which interflow is initiated when snow melt water stored in preferential flow paths migrates into the soil matrix as the ground thaws, creating a perched water table on the cover-shale interface (Kelln et al. 2007b).

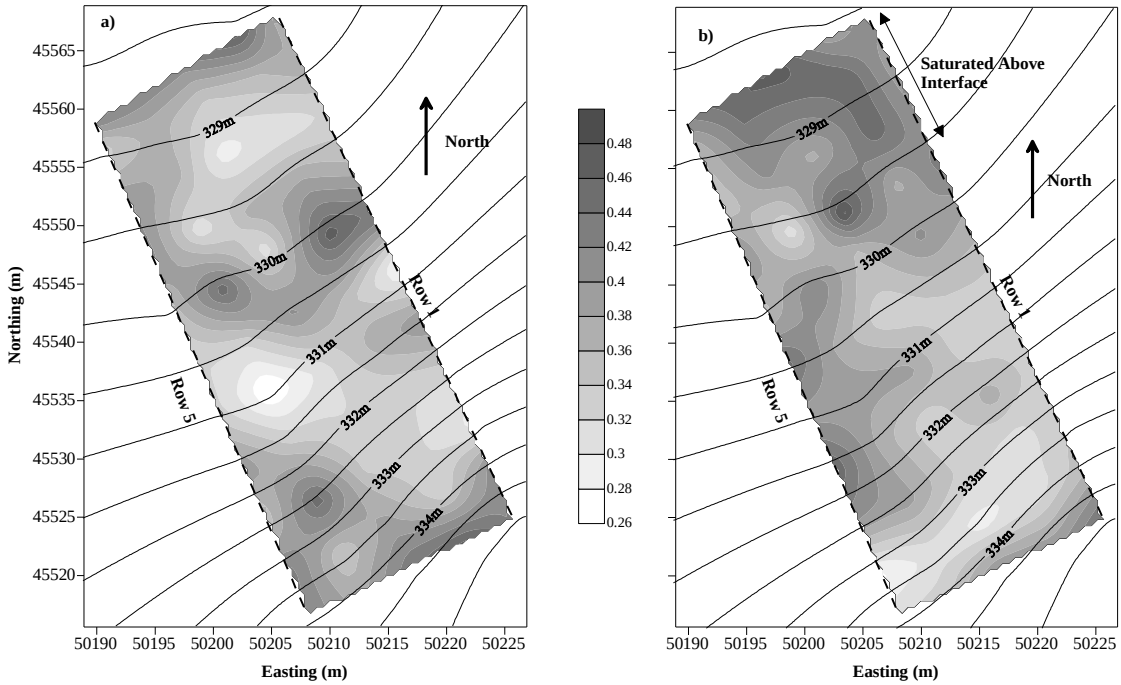

Fig. 3.4. Measured volumetric water content on April 26/27, 2006. (a) Top 300 mm of the cover. (b) Directly above the cover-shale interface.

Moisture patterns in the top 300 mm of the cover do not reflect surface topography (i.e., wetter near the toe of the slope), despite the fact that snow melt and spring rain represent the most significant precipitation event of the year. On average, the snow pack is equivalent to about 80 mm water depth, or 20% of the annual precipitation at site, and usually melts within a week to one month. Runoff during the spring melt is generated due to frozen ground conditions, which restricts infiltration via the matrix and promotes vertical preferential flow to the base of the cover. Surface runoff and preferential flow due to frozen ground conditions are typical in the northern cold region climates of Canada and Europe (Buttle and Turcotte 1999; Hayashi et al. 2003; Jansson et al. 2005; Peters et al. 1995). In temperate climates, shallow volumetric water content patterns may have strong correlations to surface topography during wet climatic conditions (e.g., Grayson et al. 1997a) as matrix infiltration is not restricted by frozen ground conditions and moisture translocation can occur as a result of the elevation gradient.

Volumetric water content patterns at the base of the cover (Fig. 3.4b) appear weakly associated with the interface topography. Although the volumetric water content

generally increases near the toe of the slope, areas known to be saturated (below elevation 329.5 m) exhibit drier spots where the volumetric water content is significantly below the saturated volumetric water content of the cover soil (θ = 0.42). This discrepancy can likely be attributed to textural heterogeneity, which can have a considerable impact on the calculated spatial patterns of volumetric water content (e.g., Famiglietti et al. 1998; Western et al. 2004). For example, a sand and clay-rich glacial soil would have volumetric water contents at saturation of around 0.3 and 0.4, respectively, so a sand lens could manifest itself as a 'dry spot' in a contour map of volumetric water content. The effect of texture is also reflected in vertical profiles of moisture content (data not presented), in which the water content decreases toward the base of the cover in areas known to be saturated. The data do generally indicate, however, that portions of the cover in the upper-slope, and in areas where the cover is underlain by the LOS lens, are drier (above elevation 329.5 m), which suggests that there is spatial variability in the hydrological response of the cover.

3.4.3. Subsurface Flow Dynamics

Monitoring Well Data

Fig. 3.3 presents measured water levels in the monitoring wells on May 11, 2006. A water level was not measured in the LOS lens at distances greater than ~ 30 m from the toe (Fig. 3.3a-c) because three of the eight 'deep' monitoring were terminated above the water table due to refusal being encountered during auguring. The interpreted depth of the LOS lens is speculative; however, the surface area geometry of the lens and the presence of a near-surface perched water table within the lens suggest that the impeding layer (i.e. shale overburden) is not exceedingly deep.

Perched water table conditions and lateral subsurface flow occur in the lower-slope in areas that are underlain by the low hydraulic conductivity shale overburden. Areas underlain by LOS, which has an estimated hydraulic conductivity equal to or greater than the cover material, appear to be under-drained with a water table existing below the cover-shale interface. The measured water levels in the LOS on May 11, 2006 were

329.59 m (R1-6), 330.32 m (R1-7), 329.46 m (R2-6), and 329.41 m (R3-6a), indicating that there is a negligible west-to-east hydraulic gradient within the LOS. The higher water level in R1-7 is consistent with levels measured in R1-8, which was installed on May 20 and measured on June 20, 2006, and suggests that there may be a down-slope gradient in the LOS. However, the anomalously high level may also be due to perched conditions within the LOS, as 'pockets' of saline-sodic shale were encountered during the auguring.

The drier conditions in the upper-slope are consistent with other cover and hillslope studies in which the upper slope positions are drier, while lower slope positions accumulate soil moisture (Bussiere et al. 2001; Bussiere et al. 2003; Grayson and Western 2001; Grayson et al. 1997a). Wetter conditions near the toe of the slope are attributed primarily to the accumulation of surface runoff in lower slope positions during the spring melt. Annual snow surveys have revealed a fairly uniform distribution of snow on the cover, so wetter conditions are not attributed to spatial variability in snow pack depth. Volumetric water content data from capacitance and neutron probes (data not presented) also confirm that the toe of the slope generally remains wetter throughout the summer and fall.

It should be noted that some of the monitoring wells in the upper-slope did collect trace amounts of water (< 5-10 cm), suggesting that at least some water accumulated at the cover-shale interface. As discussed above, Kelln et al. (2007b) reported that preferential flow is responsible for the rapid delivery of snow melt water to the base of the cover during frozen ground conditions. This water migrates into the soil matrix as the ground thaws, creating a transient perched water table above the cover-shale interface if saturated conditions develop. As a result, a perched condition may develop in the upper-slope due to preferential flow, but it will be substantially less significant than at lower slope positions due to a lack of surface run-off and drier antecedent moisture conditions.

In summary, the monitoring well and volumetric water content data demonstrates that: (1) lower-slope positions are wetter primarily due to increased surface runoff accumulation in spring; (2) upper-slope positions are drier due to a lack of up-slope

surface run-off accumulation and possibly down-slope moisture movement; (3) lower antecedent moisture conditions in upper-slope areas mitigate the development of saturated conditions during snow melt infiltration via preferential flow; (4) subsurface flow drains the upper regions of the slope; and, (5) the presence of the LOS promotes drainage of any free water in the cover and likely accentuates sub-surface drainage from upper-slope regions.

Hydrographs

Fig. 3.5 presents hydrographs for five monitoring wells located within the lower slope (Fig. 3.5a) and five wells located within the mid-slope LOS lens (Fig. 3.5b). Hydrographs were not plotted for the upper slope monitoring wells because negligible water depth was recorded throughout 2006. The dynamic response of R1-6 and R2-6 prior to mid-June was likely a result of measurement error. The level-floats proved to be an ineffective method for monitoring the deeper monitoring wells (> 1 m) as they were prone to sinking under the weight of the longer wooden dowels. Most of the measurements taken after mid-June were confirmed using a water-level tape. The rapid water level increase in R2-6 on September 19, 2006 has not been explained at this time, but may be attributed to measurement error or possibly sidewall leakage along the monitoring well during a heavy rainfall event.

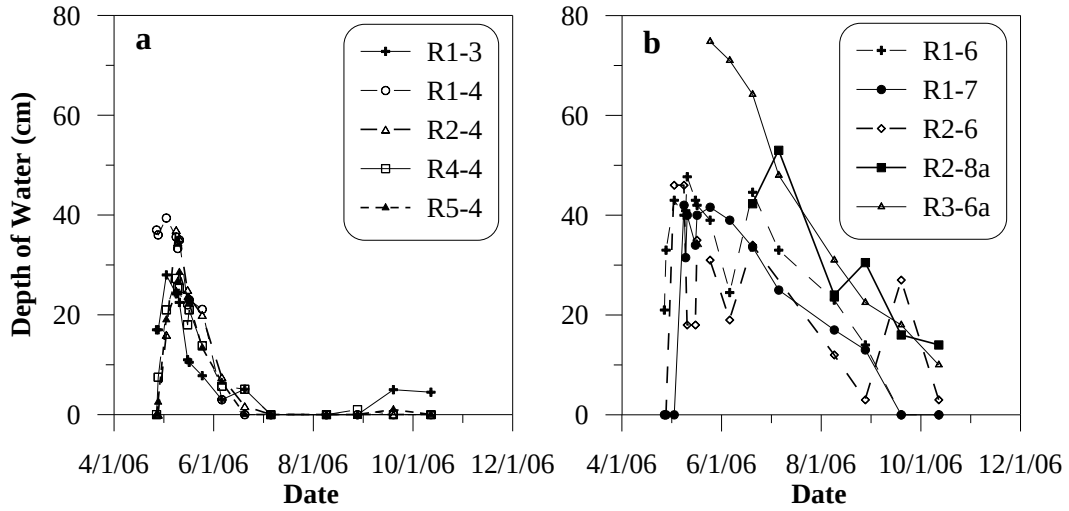

Fig. 3.5. Monitoring well hydrographs. (a) Lower-slope monitoring wells. (b) Mid-slope monitoring wells installed in LOS.

Water levels in the lower-slope monitoring wells (Fig. 3.5a) declined in near unison and correlate with the cessation of interflow that occurred on about June 16, 2006. Considering the contrast in hydraulic conductivity between the cover and underlying shale, it is reasonable to assume that the majority of perched water in the lower-slope drains into the interflow pipe, as opposed to percolating down into the shale. In contrast, the mid-slope monitoring well hydrographs suggest that groundwater in the LOS either does not drain down-slope or is at least partially disconnected from the lower slope. Although the stratigraphic profiles in Fig. 3.3 suggest that some water in the LOS would 'spill' down-slope, the hydrographs show that the lower slope is unsaturated after June 16 (cessation of interflow) while a perched water table still exists in the LOS. The anomalously high water level could be explained by the heterogeneity of the LOS, as perched conditions could develop on 'pockets' of shale within the LOS. Furthermore, the chemistry of interflow and monitoring well water (discussed below) confirms that groundwater in the LOS is at least partially disconnected from the lower slope.

Assuming that groundwater in the LOS is disconnected from the lower-slope after June 16, 2006 and that drainage of the LOS occurs through a lower shale confining layer, it then becomes possible to estimate a net percolation rate into the underlying shale. The water level decreased 54 cm in R3-6a between June 20 and October 12 (114 days). The

calculated net percolation rate is 0.33 mm/day using a measured specific yield of 0.07. Similarly, the water level decrease between June 20 and August 28 (69 days) in R1-6 and R1-7 was 31 and 21 cm, respectively, yielding a net percolation ranging between 0.31 and 0.21 mm/day. The average saturated hydraulic conductivity (K_s) of the underlying shale would then be about 3×10^{-9} m/sec assuming a hydraulic gradient of 1.0, which is in keeping with the measured range of field K_s for deeper overburden shale (Rutten 2006). This observation is significant because it implies that percolation into the shale will occur in areas where interflow does not occur (i.e., benches or relatively flat topography). These rates of net percolation will have an important influence on salt transport in the cover.

Lateral Flow and Subsurface Topography

Fig. 3.3 suggests that lateral saturated groundwater flow (i.e. interflow) appears to be controlled in part by the mesotopography of the interface. A small ridge was observed along transects Row 1 to Row 4 at a distance of approximately 5 m upslope of the interflow pipe (i.e. R1-2, R2-2, R3-2, and R4-2). These monitoring wells dried up sooner than adjacent wells as the perched water table diminished. Lateral flow would therefore be controlled by the development of positive pressures in the small 'depression' upslope of the ridge; lateral flow would be initiated when the perched water table rises above the small ridge and 'spills' over toward the interflow collection pipe. Furthermore, the ridge was less pronounced in Row 5, which implies that subsurface flow may be partly re-directed from higher elevation in Rows 1-4 toward the northwest corner of the cover.

The hydrostratigraphy of the cover demonstrates the importance of the cover-shale interface, which represents the hydrological impeding layer, in controlling the spatial dynamics of lateral subsurface flow. Numerous hillslope hydrology studies have demonstrated the importance of the 'bedrock' surface topography in controlling lateral subsurface flow (Freer et al. 2002; Tromp van Meerveld and McDonnell 2006a; Tromp van Meerveld and McDonnell 2006b; Uchida et al. 2004). Given the spatial distribution in subsurface moisture dynamics, the mechanisms controlling solute transport in the cover should also exhibit spatial variability based on slope position. This hypothesis is

explored below using the salt distribution within the cover as a diagnostic for hydrological conditions.

Interflow Volumes

Fig. 3.6 presents the cumulative interflow volume for 2006. Approximately 14,000 litres of water was collected, which is consistent with the estimated volume of water stored in the lower portion of the slope. The calculated volume of drainable water in the lower-slope area would be around 12,300 litres assuming a drainable porosity of 7%, a contributing area of 17.5 by 50 m (i.e., width of cover), and an average saturated thickness of 20 cm (n=20). Although this rudimentary calculation assumes that the stratigraphy of the study area is uniform across the lower portion of the slope and that the saturated thickness is constant, it does provide some insight into the area of the slope that contributes to interflow. The volume of interflow is equivalent to a depth of water of 16 mm distributed over the contributing area, which is significant in terms of the overall water balance of the cover and will affect the salt balance in the lower-slope positions.

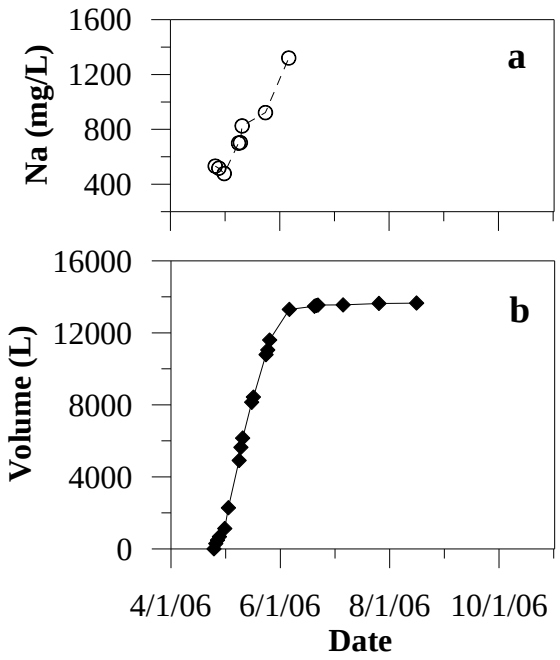

Fig. 3.6. (a) Sodium concentration of the interflow water. (b) Cumulative interflow volume.

3.4.4. Chemistry

Water Chemistry

Fig. 3.6 presents the Na^+ concentration of interflow water collected during 2006 along with the cumulative interflow volume. The Na^+ concentration increases from around 450 to 1300 mg/L. The rising concentrations are again consistent with the preferential flow mechanism as water collected in the interflow pipe transitions from mostly fresh snow melt water stored in the preferential flow paths to predominantly connate pore water. The average Na^+ concentration measured in water collected from fourteen of the monitoring wells on May 9, 2006 in the lower slope was 1290 mg/L (σ = 364 mg/L). The similarity between the peak interflow Na^+ concentration of 1320 mg/L measured on June 6, and Na^+ concentrations measured in the monitoring wells near the beginning of interflow, confirms that the interflow water eventually transitions to the Na^+ enriched water contained in the soil matrix. Sodium is therefore flushed down-slope by interflow. Peak interflow Na^+ concentrations in previous years varied from 650 mg/L in 2002 to 1040 mg/L in 2003; transitioning each year from low to high concentrations.

The average Na^+ concentration in water collected from the mid-slope LOS monitoring wells was 5550 mg/L (σ = 520 mg/L; n = 5). This value is nearly four-fold larger than the peak Na^+ concentration in the interflow water and the average Na^+ of the lower-slope monitoring well water. Water collected immediately down-slope of the LOS did not exhibit higher concentrations than other wells in the lower-slope. For example, the Na^+ concentrations in R1-5 and R2-4 were 1730 and 1320 mg/L, respectively. These observations confirm the assumption presented previously that groundwater in the LOS is mostly disconnected from the lower-slope. Furthermore, the high concentrations within the LOS are consistent with the geologic origin of the material, which is excavated at the contact between the shale overburden and underlying oil sand.

Pore Water Na^+ Profiles

Fig. 3.7 presents the one-dimensional profiles of *in-situ* pore water Na^+ concentrations in the lower-slope, mid-slope, and upper-slope positions determined from

the centrifuge extracts. It should be noted that the scale of the abscissa in Fig. 3.7b is different than that for Fig. 3.7a and Fig. 3.7c as a result of the large range in measured concentrations with depth. Background concentrations were not measured in the saline-sodic shale (i.e. deep samples) as the focus of this investigation was moisture and salt dynamics in the cover. However, previous geochemical investigations found that the background pore water Na^+ concentration of oxidized shale is around 10,000 to 14,000 mg/L (Kessler 2007; Nichol et al. 2006).

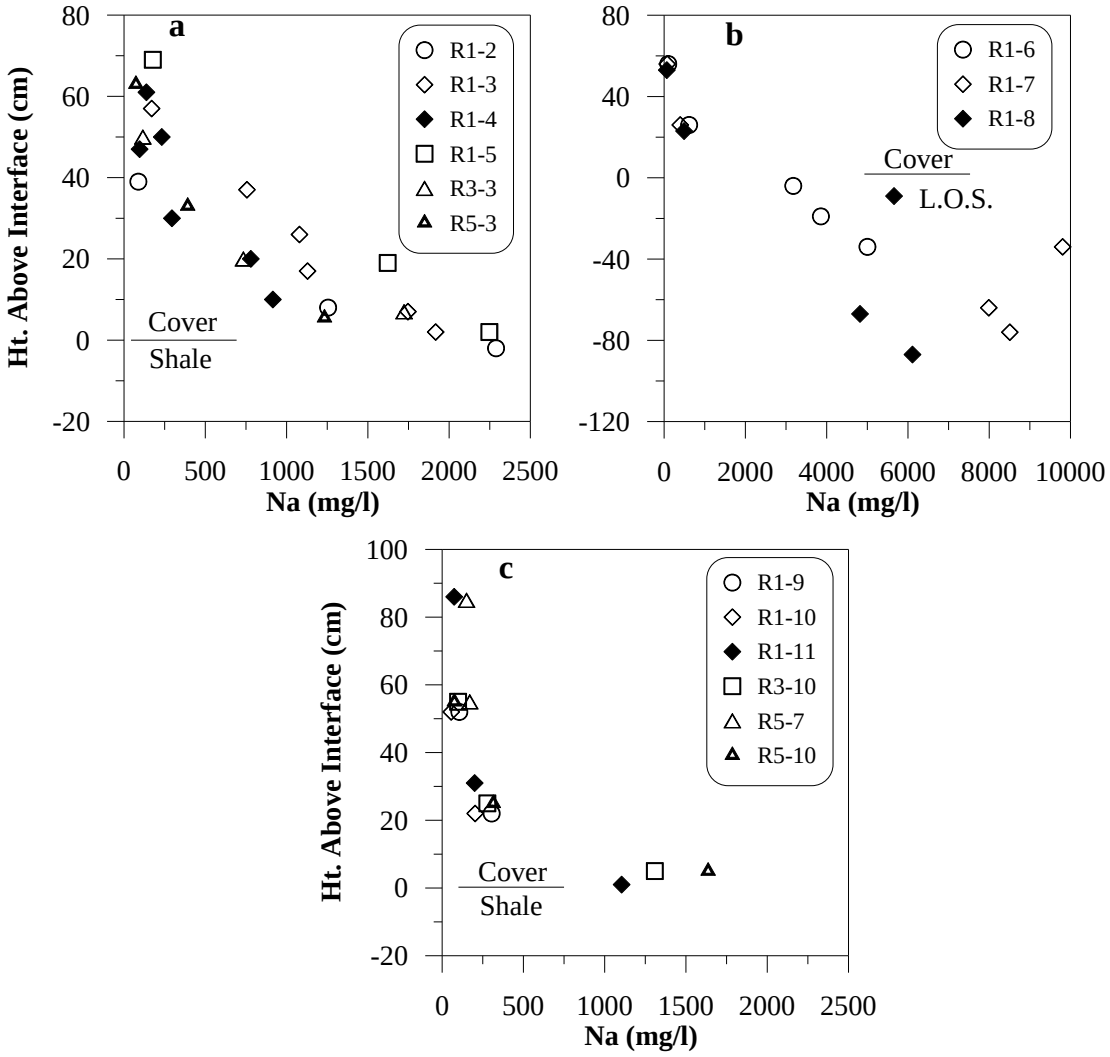

Fig. 3.7. One-dimensional profiles of *in-situ* pore water Na^+ concentration. (a) Lower-slope locations. (b) Mid-slope locations. (c) Upper-slope locations.

In the lower-slope positions (Fig. 3.7a), the profiles suggest that upward salt transport has occurred to about 35 cm above the interface. Sodium concentrations range from 2000 to 2500 mg/L directly above the interface and then decrease to background concentrations (~ 100-200 mg/L) at a height of 35-40 cm above the interface. There is some range in measured Na^+ concentrations with depth at different locations, which is consistent with the spatial variability in volumetric water content and subsurface flow dynamics discussed above. Regardless of this variability, upward salt transport is fairly consistent across the lower slope. The Na^+ concentrations above the interface are also similar to water collected in the shallow monitoring wells.

The profiles of pore water Na^+ concentration in the mid-slope locations (Fig. 3.7b) are more difficult to interpret due to a lack of resolution near the interface. Sodium values in the LOS ranged from around 4000 to 10,000 mg/L, which is slightly less than the shale pore water concentrations, but elevated compared to the cover concentrations. Some of these values are significantly higher than the average concentration measured in the LOS monitoring wells (5090 mg/L). This discrepancy can be explained by the volume of water collected by centrifugation verses the volume of water collected from monitoring wells. The monitoring wells are screened over a 2.5 ft length and therefore collect a bulk water sample while centrifugation was performed on small (~80 g), discrete samples, collected at specific depths. Considering the heterogeneity of the LOS, this implies that centrifugation was performed on a range of LOS materials including fine sand as well as salt-rich shale overburden. Furthermore, infiltration of fresh preferential water during spring melt would dilute the 'bulk' water contained within the LOS.

The mid-slope profiles suggest that upward salt transport into the cover is less advanced than at lower slope positions, despite the lack of resolution above the interface. The average pore water Na^+ concentration at 25 cm above the interface was 500 mg/L, compared to about 1000 mg/L in the lower slope positions. The attenuated salt transport in the mid-slope locations is significant considering the reservoir of salts in the underlying LOS pore water (Fig. 3.7b). It is also consistent with measured soil moisture conditions, which indicated that the mid-slope is under-drained by the LOS and therefore

drier than the lower-slope. Upward salt transport into the cover would therefore be attenuated because the coefficient of diffusion is reduced by unsaturated conditions (Conca and Wright 1990; Lim et al. 1998).

Salt migration occurred less than 20 cm into the cover at the upper-slope positions (Fig. 3.7c). The Na^+ profile is also sharper as compared to profiles observed at lower slope positions. The attenuated salt transport is consistent with the drier conditions, and therefore lower average D, measured in the upper slope-slope positions.

3.4.5. Numerical Modelling

Case I

Fig. 3.8 presents results for the Case I (diffusion-only) analyses. Results are compared to measured *in-situ* pore water Na^+ profiles in the lower and upper-slope positions, but not in the mid-slope locations due to a lack of resolution near the cover-shale interface. In the lower-slope positions, the modelled Na^+ profiles with both D(S=1) and D($S=S_r$) provide a poor match to *in-situ* data. The D(S=1) provides a slightly better match at heights greater than 15 cm above the interface, while D($S=S_r$) yields a slightly better match to data below 15 cm above the interface. A good match was anticipated with D(S=1) as saturated conditions develop in the lower-slope positions. A comparison between modelled and measured profiles, however, demonstrates that three mechanisms control salt transport in the lower slope positions. Firstly, saturated conditions accelerate salt migration into the cover by diffusion, as indicated by the increased concentrations higher in the cover profile (> 15cm). Secondly, the poor match with D(S=1) above 15 cm indicates that another mechanism, likely upward advective transport caused by evapotranspiration during the late spring and summer months (Case IV), is increasing pore water salt concentrations higher in the cover profile. Thirdly, salt transport near the cover-shale interface (~ 0-15 cm) is attenuated by either deep percolation into the shale or lateral interflow (Case III), as indicated by the poor match near the interface with D(S=1).

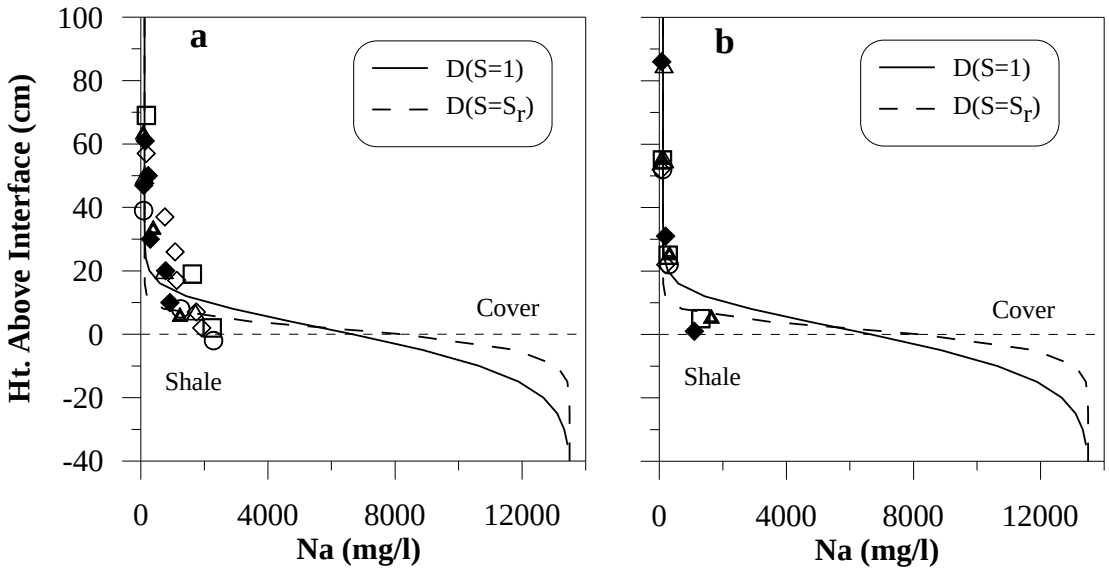

Fig. 3.8. Case I (diffusion-only) modelling results with coefficient of diffusion at saturation (S=1) and residual saturation ($S=S_r$). (a) Lower slope. (b) Upper slope.

In the upper-slope positions, the modelled Na^+ profile with D(S=1) provided a poor match to *in-situ* Na^+ profiles (Fig. 3.8b). A slightly better match was obtained with $D(S=S_r)$, which demonstrates that drier soil moisture conditions in the upper-slope positions attenuate upward salt transport due to the reduced D. Furthermore, the lack of an exact match near the interface (~ 0-10 cm above interface) suggests that other mechanisms are attenuating salt transport.

Case II

Results for the Case II analyses (deep percolation) are presented in Fig. 3.9. A vertical groundwater flux (q_v) ranging from 1.85 to 9.25 mm/yr was modelled with D(S=1). The volumetric water content was constant through the cover profile at 0.40 to account for saturated conditions near the interface. The diffusion-only Na^+ profile (i.e. $q_v = 0$) is presented for comparison. In the lower slope positions, a good match was obtained near the interface (0-15 cm) with $q_v = 9.25$ mm/yr, while diffusion-only still provided a slightly better match at heights of 15 cm above the interface. This result is again consistent with the preferential flow mechanism; infiltration water bypasses the soil matrix during the spring melt and ponds on the cover-shale interface, so only *in-situ* pore water near the interface would mix with fresh preferential flow water and then percolate

into the underlying shale. In general, the results demonstrate that even the slightest amount of downward groundwater flux will have a significant, and positive, impact on the salt balance in the cover.

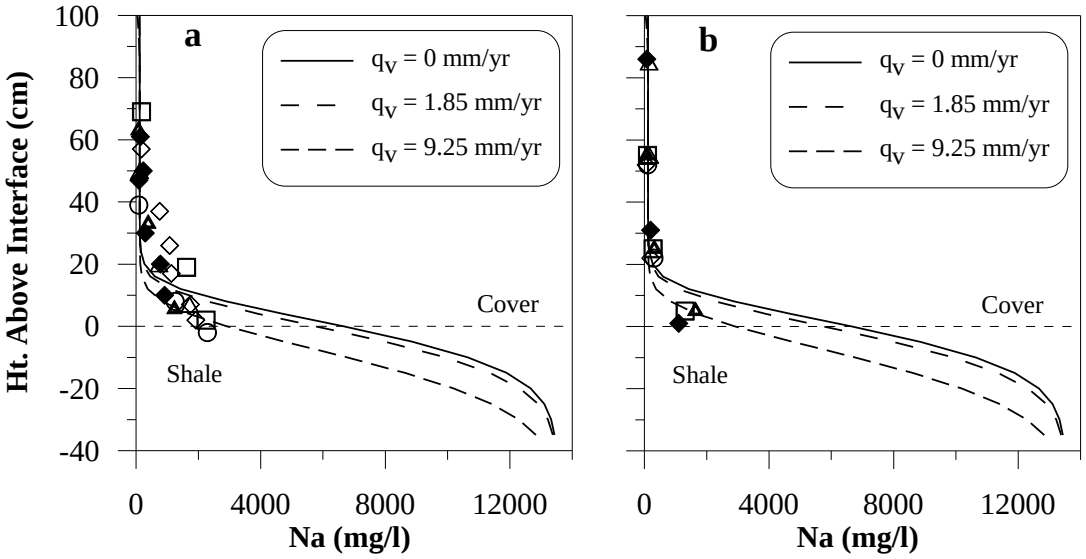

Fig. 3.9. Case II (deeper percolation) modelling results. (a) Lower slope. (b) Upper slope.

A better match was also obtained in the upper-slope positions near the interface with a percolation rate of 9.25 mm/day (Fig. 3.9b), demonstrating that upward salt transport in the upper-slope regions is a function of both soil moisture conditions and possibly deeper percolation. The inclusion of deep percolation yielded a poorer match higher in the cover profile, as it did in lower-slope positions, and is again consistent with preferential flow in the cover (i.e., flushing does not occur higher in the profile).

Case III

Results from the Case III analyses are presented in Fig. 3.10. The lateral flux was varied from 2 to 8 mm/day. In both the lower and upper-slope positions, a good match was obtained near the interface with a lateral flux equal to 8 mm/day. This confirms that the pattern of salt migration near the interface could be due to interflow 'flushing' salt from the system. The lack of a good match above 15 cm is attributed to the one-dimensional model configuration. The model forces mass to be continuously removed from the system, which rapidly reduces the pore water Na^+ concentration above the

interface and therefore reduces vertical diffusion over time. In reality, the perched water table moves down-slope as a saturated plug, providing more time for upward diffusion into the cover.

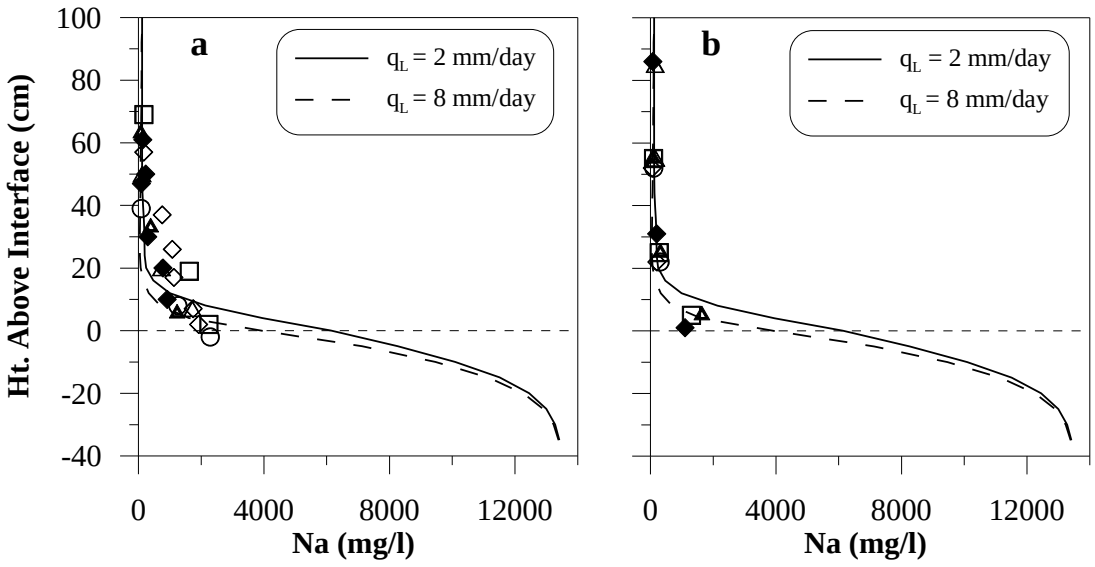

Fig. 3.10. Case III (lateral flushing) modelling results. (a) Lower slope. (b) Upper slope.

Furthermore, the one-dimensional steady-state seepage analysis precludes modelling more than one 'flushing' mechanism at a time. Realistically, the processes of lateral interflow and deep percolation may be occurring simultaneously with upwards advection caused by evapotranspiration. Similarly, the coefficient of diffusion in any given case is likely not constant throughout the soil profile, producing a more dynamic and transient system. Regardless of these deficiencies, the modelling does elucidate some of the mechanisms that control the spatial distribution of salts in the cover.

The term 'flushing' may not be an adequate characterization of the actual mechanism responsible for the attenuated upward Na^+ transport near the interface. It is the process of mixing between the connate pore water and fresh preferential water near the interface that dilutes the *in-situ* pore water concentrations. Once a perched water table develops, interflow is then responsible for the down-slope transport of salts. This interflow may accumulate more solutes as it travels along the cover-shale interface.

Case IV

Results from the Case IV analysis are presented in Fig. 3.11. An upward groundwater flux in the range of 0.03 to 0.06 mm/day produced a good match at heights greater than 15 cm above the interface, particularly for lower-slope positions where the wetter conditions would facilitate transport via advection. Despite some uncertainty associated with selecting a reasonable flux rate, the results demonstrate that upward advection would have a significant impact on the distribution of pore water Na^+ concentration in the cover.

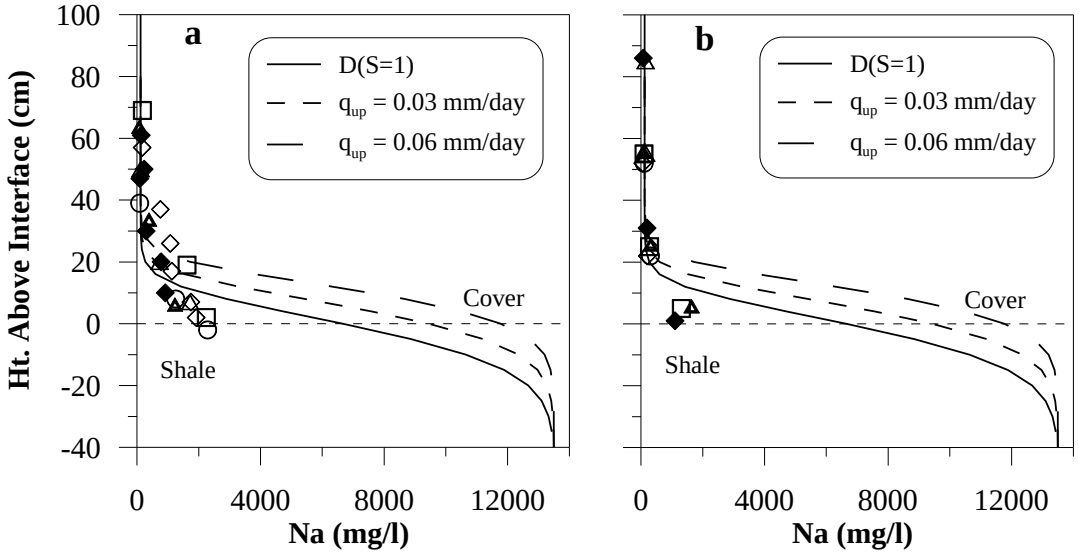

Fig. 3.11. Case IV (upward flux) modelling results. (a) Lower slope. (b) Upper slope.

The modelling results and *in-situ* pore water chemistry demonstrate that salt migration into the cover is attenuated by interflow, deep percolation, and a reduced coefficient of diffusion due to drier conditions. Interflow and deep percolation will be the dominant mechanisms controlling salt transport in the lower-slope positions. In the mid-slope and upper-slope positions, the reduced antecedent moisture conditions, coupled with the slightest amount of either interflow or deep percolation, will act to minimize upward salt migration. As a result, vegetation should not exhibit spatial variability in growth rates as long as there is sufficient soil moisture during the growing season. In lower-slope positions, upward advective flux caused by ET demands is likely accelerating upward salt migration higher into the cover profile. Finally, the results

suggest that deep percolation may attenuate salt transport into the cover in areas where there is minimal topography (i.e. flat benches or topographic lows) during periods when perched conditions exist (i.e. spring and early summer).

3.5. Summary and Conclusions

The spatial distribution of volumetric water content and salts in a reclamation cover overlying saline-sodic shale overburden and located in a cold, sub-humid climate were investigated. Detailed mapping of stratigraphy, volumetric water content, perched water table conditions, and *in-situ* profiles of pore water Na^+ concentrations were used to glean information on the mechanisms that control moisture and salt dynamics. The volumetric water content data suggested that lower-slope positions are wetter in spring due to the accumulation of surface water run-off while the ground is frozen and preferential flow paths are active. The lack of surface run-off water and lower antecedent moisture conditions in upper-slope positions mitigated against the development of a perched water table. The topography of the cover shale interface imposed a primary control on subsurface flow, while the presence of a pocket of LOS created an under-drained condition in the cover at mid-slope positions.

Salt transport from the shale into the overlying cover is directly related to soil moisture conditions and the presence of net percolation and/or lateral groundwater flux. One-dimensional modelling of *in-situ* profiles of pore water Na^+ concentration demonstrated that increased soil moisture in lower-slope positions accelerates salt transport into the cover, while interflow triggered by vertical preferential flow acts to dilute the connate pore water Na^+ concentrations near the interface. The modelling also confirmed that infiltration during the spring melt may be bypassing the soil matrix higher in the cover profile. In contrast, drier conditions in the mid and upper-slope positions decrease D, therefore limiting upward salt movement. The modelling indicated that either a slight amount of interflow or deep percolation is having a positive impact on salt transport in these regions, while upward advective flux may increase salt migration in

lower-slope positions. This study demonstrates that the current reclamation landscape and cover thickness are effective in reducing upward salt transport.

4

Fracture-Dominated Subsurface Flow and Transport in a Reclamation Cover

Preface

One of the principal objectives of this research is to develop numerical models that are capable of replicating the patterns of soil moisture and salt movement within reclaimed landscapes overlying low permeability waste. Numerical modelling is similar to the scientific method in that the analysis is based on the conceptual model used to explain some observed phenomenon. The National Research Council (2001) defines a conceptual model as "an evolving hypothesis identifying the important features, processes, and events controlling fluid flow and contaminant transport of consequence at a specific field site in the context of a recognized problem." This paper uses the findings from Chapters 2 and 3 to refine the conceptual model of flow and transport in sloping reclamation covers comprised of fractured clay-rich soils. A numerical analysis is conducted that is capable of modelling the measured discharge rates, cumulative volumes, and discharge concentrations of subsurface flow from a cover system. The modelling provides independent verification that subsurface flow is controlled by the fracture porosity, while solute transport can be described using the concept of an 'equivalent porous medium' due to the rapid chemical equilibration between water in the fractures and matrix.

Reference: Kelln, C.J., Barbour, S.L., and Qualizza, C.V., 2008. Fracture-dominated subsurface flow and transport in a sloping reclamation cover. Vadose Zone Journal, Submitted.

4.1. Introduction

Understanding the hydrological controls on subsurface flow and transport is of considerable importance in the study of reclaimed landscapes in the oil sands region of north-central Canada. A significant portion of the reclaimed landscape will be comprised of a thin veneer (~ 1 m) of clay-rich reclamation soil overlying saline-sodic shale overburden, which is a waste by-product from the mining process. The upwards transport of salts from the shale via advection and diffusion, and the subsequent re-distribution of these salts by lateral subsurface flow, has the potential to cause salinization of the cover materials (Bailey 2001; Nichol et al. 2006; Oddie and Bailey 1988; Sandoval and Gould 1978). The hydrological behaviour of these systems is analogous to natural hillslopes with thin soil mantles overlying 'bedrock', in which subsurface flow imposes an important control on the delivery of water to streams and the redistribution and flushing of salts and nutrients (Bishop et al. 2004; Weiler and McDonnell 2006).

The generation of subsurface flow depends on a number of complex factors such as surface and 'bedrock' topography, soil layering and properties, climate and vegetation, antecedent moisture conditions, and the presence of macroporosity (Grayson and Western 2001; Grayson et al. 1997a; Tsuboyama et al. 1994; Uchida et al. 2004; Weiler and McDonnell 2006). Numerous studies have shown that the 'transmissivity feedback' mechanism (Weyman 1973), in which the water table rises high enough into the soil profile to interact with near-surface soil of greater hydraulic conductivity, does not explain many of the observed storm flow responses in nature (McDonnell 2003; Weiler and McDonnell 2006).

Decades of research into the hydrological response of hillslopes has demonstrated that preferential flow via macroporosity is the rule rather than the exception (Flury 1996), and is a key process controlling vertical infiltration and lateral subsurface flow in natural surficial soils (e.g., Tromp van Meerveld and McDonnell 2006a; Uchida et al. 2004). Macroporosity can be characterized by animal burrow holes, root and earthworm channels, and fractures or cracks (Beven and Germann 1982). Clay-rich soils, in

particular, are susceptible to cracking when subject to wet/dry or freeze/thaw cycles (Benson and Othman 1993; Benson et al. 1995; Chamberlain and Gow 1979; Chamberlain et al. 1990). Numerous studies have shown that while macroporosity comprises less than 5% of the total porosity of most soils, it can account for almost all (> 80 %) of the water flow at or near saturation (Lin et al. 1996; Waduwawatte and Si 2004; Waduwawatte et al. 2004).

Uchida et al. (2004) noted that there appears to be a general consensus on the mechanism for subsurface flow generation within steep slopes with thin soil mantles: infiltration water moves vertically as matrix and preferential flow, followed by perching and lateral flow above the impeding layer. Depending on the rainfall intensity and antecedent moisture conditions a perched water table can develop at the interface, creating a saturated and highly mobile zone of water than can move laterally down slope (Burns et al. 2001; Hinton et al. 1994; Jardine et al. 1990; Newman et al. 2004; Peters et al. 1995). The topography of the impeding layer or 'bedrock' can impose a significant control on the spatial distribution and path of the subsurface flow (Freer et al. 2002; Tromp van Meerveld and McDonnell 2006a; Tromp van Meerveld and McDonnell 2006b; Uchida et al. 2004).

The importance of preferential flow paths has also been demonstrated in studies of snow melt infiltration into frozen soils (Derby and Knighton 2001b; Stadler et al. 1997b; Stadler et al. 2000; Stähli et al. 1996; Stähli et al. 1999; Thunholm et al. 1989a). Infiltration can occur through frozen soils via the liquid water phase within the soil matrix, that is, between the soil particles and pore ice, but generally occurs as bypass flow in previously air-filled macropores (Johnsson and Lundin 1991). The thermodynamics of frozen ground infiltration is of considerable complexity as it has to account for the thermal and hydraulic interactions between the atmosphere, vegetation, snow pack, and the frozen and unfrozen soil (Stähli et al. 1996).

Preferential flow via fracture porosity can significantly increase solute transport rates through thick saturated aquitards (Hendry 1988; Jørgensen and Fredericia 1992; Ruland et al. 1991; Simpkins and Bradbury 1992) and through near-surface, predominantly

unsaturated, agricultural soils of glacial origin (Köhne and Gerke 2005; Larsson and Jarvis 1999; Villholth and Jensen 1998a; Villholth and Jensen 1998b). Solute transport within aquitard systems is typically characterized by rapid advective transport through fractures, with diffusion into the less mobile pore water in the adjacent matrix (Gerke and Köhne 2004). Diffusive losses to the matrix act to attenuate solute transport by reducing concentrations in the fracture (Grisak and Pickens 1980; Grisak and Pickens 1981; Tang et al. 1981). Similarly, studies of the leaching of surface-applied chemicals have shown that rapid and relatively deep movement of solutes can occur through the unsaturated zone due to preferential flow (Flury 1996; Jarvis 2007).

The objective of this study is to describe a conceptual model for fracture-dominated lateral subsurface flow and transport in a sloping clay-rich reclamation cover immediately following spring snow melt. This conceptual model is supported by field observations and numerical simulations. This study is unique in that the contaminant source, or tracer, is the natural distribution of pore water solutes in the soil matrix. The conceptual model is developed from the observed hydrological response of the cover. A two-dimensional finite element simulation of subsurface flow is conducted assuming that water flow is dominated by the fracture porosity. The Na^+ concentration of discharge water is calculated based on the modelled water flux and the measured *in situ* profile of pore water Na^+ concentrations, assuming that the system behaves as an equivalent porous medium (EPM). Results from the numerical analyses are compared to measured field data, including the discharge rates/volumes and chemistry of lateral subsurface flow discharging to a tile drain installed at the toe of the reclamation cover.

4.2. Study Site

The research site is located in north-central Canada (57°2′ N, 111°33′ W) at the Syncrude Canada Ltd. Mildred Lake oil sands mine site. The climate of the region is classified as sub-humid continental (Koppen Classification, McKnight and Hess, 2005) with a mean annual air temperature of 1.5 °C and a mean annual precipitation of 442 mm (1945-1995). Monthly mean air temperatures range from 18 °C in July to –20.7 °C in

January. Potential evaporation as estimated by the method of Penman (1948) typically exceeds 500 mm per year with daily maximums (~ 7 mm/day) occurring during July and August.

Approximately 100×10^6 m^3 of saline-sodic shale overburden was placed at the site between 1980 and 1996 to create the 'South Hills Overburden Pile', which is 2 km^2 in area with a plateau elevation rising approximately 60 m above the surrounding landscape. The shale was excavated during open-pit mining to gain access to the underlying oil-rich sand. It was deposited in large waste dumps and then re-contoured to create a natural landscape form. The shale is of marine origin (Cretaceous age) and is both saline and sodic. Reclamation is achieved by placing a two-layer cover of thin, organic rich, peat/clay mixture over a thicker layer of clay-rich glacial soil. The clay-rich layer contains 60 to 70% fines (particle diameter < 0.075 mm), of which 25 to 40% are clay-size particles (particle diameter < 0.002 mm), and is classified as a medium plasticity clay.

Four alternative prototype test covers of varying thickness (35, 50, and 100 cm) were constructed in 1999 on a north-facing slope. The covers are designed to provide sufficient moisture and nutrients for vegetation throughout the growing season. The focus of this paper is the 100 cm thick cover, which was constructed of a nominal thickness of 20 cm of the peat-mineral mixture overlying 80 cm of the clay-rich glacial soil. The cover is 50 by 200 m in area and has an overall slope of about 5:1 (~ 11°). Although the landscape is constructed, the study site is analogous to a natural hillslope with a thin mantle of soil overlying a low permeability 'bedrock'.

4.3. Materials and Methods

4.3.1. Field Instrumentation and Testing

Details of the site instrumentation, soil sampling, and testing can be found elsewhere (Barbour et al. 2001; Boese 2003; Elshorbagy and Barbour 2007; Elshorbagy et al. 2005; Kelln et al. 2007b; Kelln et al. 2008). The bulk density and moisture retention curve of the cover soil were determined on 50 cm diameter soil cores according to ASTM D2937-

05 (ASTM 2005a) and ASTM D6836-02 (ASTM 2002a), respectively. A soil monitoring station was installed about 150 m upslope from the slope toe to continuously monitor soil moisture, temperature, and matric suction throughout the cover profile and the upper portion of the underlying shale (depths of 5, 20, 30, 55, 90, 115, 125, 145, and 170 cm). Soil moisture and matric suction were monitored using calibrated time domain reflectometry and thermal conductivity sensors, respectively, while temperature was measured using thermistor sensors. Surface runoff is measured via an instrumented weir located in a swale ditch at the toe of the slope.

Lateral subsurface flow is collected in a tile drain that was installed along the cover-shale interface near the toe of the slope (Fig. 4.1). The tile drain discharges to a large-diameter (~ 1 m) collection well constructed using 45 gallon plastic drums and installed to a depth of approximately 1.5 m. This well was manually pumped in 2004 (May 11 to July 3) and 2005 (April 7 to October 29), and was then pumped using a level-controlled sump pump from 2006 (April 25 to June 22) to 2007 (April 11 to June 20). The pumped water was discharged directly into the swale ditch. Samples of the discharge were collected between 2002 and 2007 and analyzed for Na^+, Ca^{2+}, K^+, Mg^{2+}, SO_4^{2-}, Cl^-, HCO_3^-, CO_3^{2-} using ICP analysis.

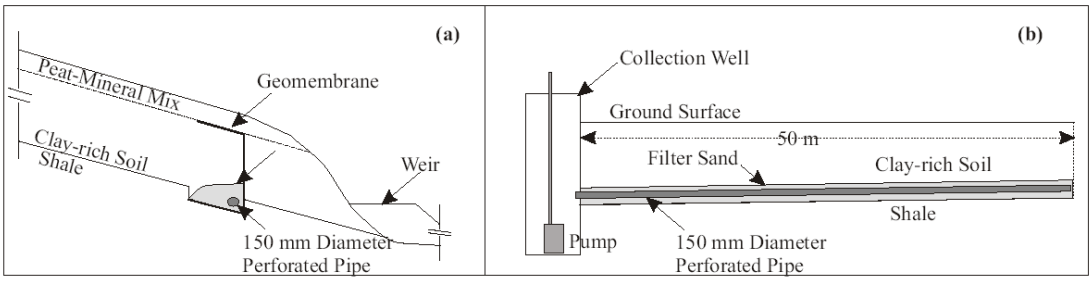

Fig. 4.1. Schematic of subsurface drainage system. (a) North-south profile of cover near toe. (b) East-west profile of cover showing tile drain and collection well.

The depth of perched water on the cover-shale interface was measured in 2004 and 2005 using two sets of three shallow monitoring wells (i.e. six in total) installed across the width of the cover and located 5 m and 20 m upslope of the tile drain. The perched water was measured in 2006 and 2007 using fifty-five shallow monitoring wells installed

on a 5 m by 5 m grid pattern within an area 25 m wide and extending about 50 m upslope from the tile drain (Kelln et al., 2008).

4.4. Conceptual Model

Kelln et al. (Kelln et al. 2007b) described a detailed study of the hydrological response of the cover following snowmelt and noted that snowmelt infiltration into the cover occurs via preferential flow paths when the ground is frozen and the matrix hydraulic conductivity is reduced due to blockage of pores by ice. In general, subsurface flow commences when the ground thaws and fresh snowmelt water stored in the macropores drains and creates a perched water table on the cover-shale interface. In certain years, subsurface flow started when the ground was still frozen or partially frozen. An isotope hydrograph separation performed on three annual drainage events (Kelln et al. 2007a) revealed that in two of the three years, subsurface flow was initially comprised of fresh snowmelt water stored in the macropores, which then transitioned to predominantly 'old water' (> 80%) stored in the soil matrix (2005 and 2007). These observations provided clear evidence of preferential flow through frozen ground.

Based on these observations, a conceptual model for fracture-dominated lateral flow and transport in the reclamation cover was developed as shown schematically in Fig. 4.2. The conceptual model is characterized by: 1) vertical transport of solutes through the matrix from the underlying saline-sodic shale into the overlying reclamation cover via advection and diffusion (Kelln et al. 2008); 2) diffusion of solute from the soil matrix into fresh snowmelt water stored in the macropores; 3) chemical equilibration between water stored in the matrix and macropores; and, 4) macropore-dominated subsurface flow in the reclamation cover. These four processes are discussed below in more detail.

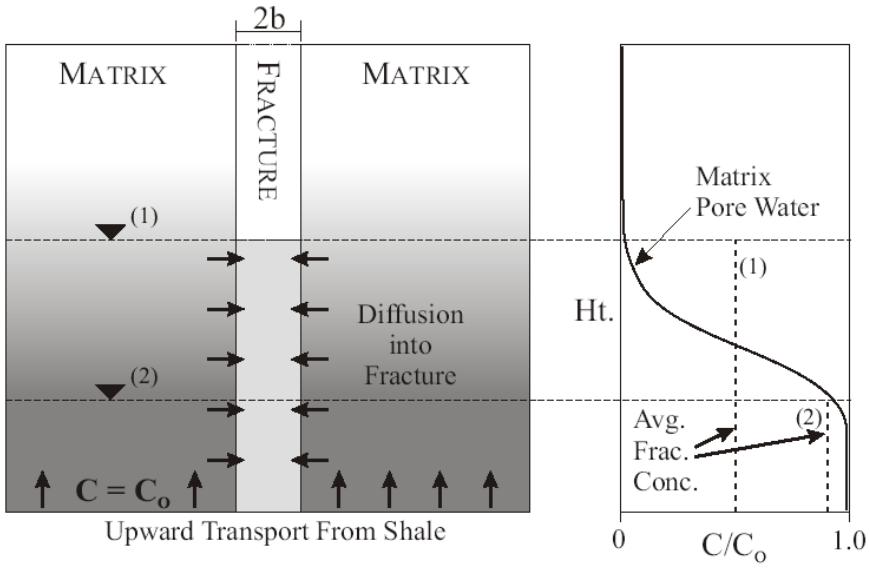

Fig. 4.2. Schematic of transport from the matrix into a fracture of aperture 2b with a constant source input concentration ($C = C_o$) at the bottom boundary. a) The fracture-matrix system showing transport processes and matrix pore water concentrations (shading). b) A profile of matrix pore water concentrations.

Upward transport from the underlying saline-sodic shale due to diffusion and advection results in elevated matrix pore water concentrations in the reclamation cover (Fig. 4.2b) that vary with distance from the shale surface. Kelln et al. (2008) measured vertical pore water solute concentrations on centrifuge extracts from 42 samples collected from thirteen locations and found that pore water Na^+ concentrations range from around 1200 to 2000 mg/L near the cover-shale interface, to background values of around 100 mg/L higher in the cover profile (Fig. 4.3). It was noted that upward vertical transport occurs predominantly within the soil matrix because upward diffusive flux within the macropores requires perched water table conditions, which only occur seasonally (~ spring) and for a relatively short duration (typically 30–60 days).

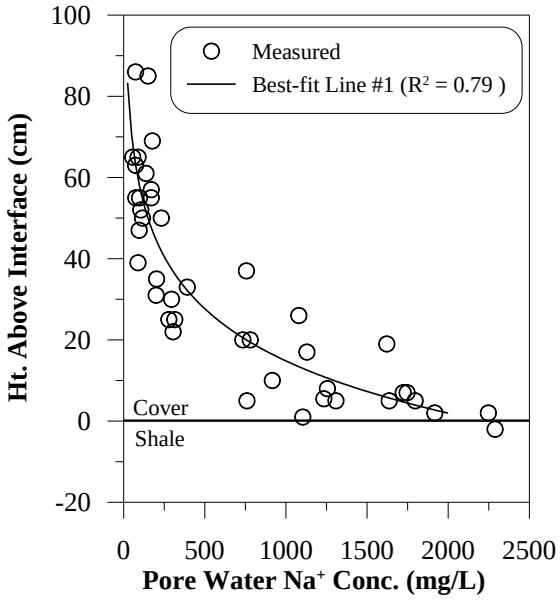

Fig. 4.3. Measured pore water Na^+ concentrations (after Kelln et al, 2008).

Snowmelt infiltration via macropores occurs each spring while the ground is still frozen. Diffusion from the high matrix pore water concentrations into the fresh snowmelt water in the macropores begins following ground thaw. Once the ground is fully thawed, chemical equilibration would occur between water stored in the two reservoirs due to: 1) flow from the saturated fracture into the unsaturated soil matrix; and, 2) diffusion from the high solute concentrations in the matrix pore water into the low concentration water stored in the fracture. The relative importance of the first mechanism would depend on antecedent moisture conditions in the soil matrix and would result in a dilution of *in situ* pore water concentrations. Previous work has shown that the base of the cover is usually near saturation, thus limiting the amount of 'advective mixing' and dilution.

Chemical equilibration between the saturated macropores and matrix by diffusion would be fairly rapid. For a classical fracture-dominated transport model, van der Kamp (1992) noted that the time (t_e) required for solute in fractures to equilibrate with the matrix pore water can be characterized by:

$$t_e = \frac{L^2}{D} \qquad [1]$$

where L is the fracture spacing and D is the coefficient of matrix diffusion. A similar equation can be applied to the fracture-matrix system presented in Fig. 4.2. In this case, the time for solute concentration in the saturated fracture to equilibrate with the high concentration in the matrix would be given by:

$$t_e = \frac{b^2}{D} \qquad [2]$$

where b is the half-width of the fracture aperture. Assuming a coefficient of matrix diffusion of 1×10^{-10} m^2/s and a typical range of fracture apertures for clay-rich soils (~ 10 to 100 μm; (Harrison et al. 1992; McKay et al. 1993a; Sidle et al. 1998)), the time for chemical equilibration would range from 1 to 100 seconds.

The assumption of rapid chemical equilibration between the macropores and the matrix implies that the system would behave as an equivalent porous medium (EPM) (McKay et al. 1997; Schwartz and Smith 1988) in terms of the transport of salts by subsurface lateral flow. This suggests that although lateral subsurface water flow is primarily through the macropores, the concentration of the water would represent soil matrix pore water at any depth. As such, the concentration of discharge water will be a function of the depth of perched water in the slope. Fig. 4.2 shows the average concentration of water in a fracture at two different water table depths. As the water depth increases (e.g., location (1)), the average concentration in the fracture would be weighted toward the lower concentration water ($C/C_o = 0$) contained within the matrix higher in the soil profile. Conversely, the average concentration in the fracture would be weighted toward the concentration within the matrix near the interface ($C = C_o$) if the water table was at location (2).

It is noted that without turbulent mixing, the concentration profile within the fracture would assume a similar shape as the matrix concentration profile, not the average constant profile shown in Fig. 4.2b.

In summary, the conceptual model of fracture-dominated lateral flow and transport in the reclamation cover assumes that the macropores in which water flow is occurring are

in chemical equilibrium with the concentration of the matrix pore-water. The concentration of lateral flow discharging at the toe of the slope is then controlled by the depth of flow through the macropores. This conceptual model is now compared to the interpretation of field observations through the use of numerical simulation.

4.5. Numerical Analysis

4.5.1. Seepage Modelling

A numerical simulation was conducted to illustrate the conceptual model of subsurface flow and transport. The simulation results were compared to the measured drainage data collected from 2004 to 2007. Lateral groundwater flow was simulated using a two-dimensional finite element model (GeoStudio™; (Geo-Slope International 2007)) assuming a single-porosity medium with composite hydraulic functions. This approach is analogous to a very simple dual-porosity flow model in which the Richards equation is combined with a double-hump type composite function for the hydraulic properties (Šimůnek et al. 2003). The composite hydraulic conductivity function includes the increase in hydraulic conductivity near saturation associated with the presence of macropores and the composite moisture retention curve includes the drainable porosity over a low suction range associated with macropores.

Fig. 4.4 presents the composite moisture retention curve and hydraulic conductivity functions used for the clay-rich cover soil. The porosity of the soil matrix is around 0.4 (Boese 2003; Kelln et al. 2008) and the measured volumetric water content data for the soil matrix were fit using the van Genuchten (1980) equation. The drainable fracture porosity (n_f) was varied between 3% and 4 % based on the literature (Buczko et al. 2006; Gärdenäs et al. 2006; Jansson et al. 2005; Jarvis 2007; Lin et al. 1996). The slope of the dual-porosity moisture retention curve was held constant at suctions larger than 10 kPa to minimize any drainage from within the unsaturated soil matrix since this soil matrix is assumed to have come to equilibrium over the winter period. Drainage of the macropores was assumed to occur over a very narrow suction range (~ 1 kPa) to represent the small capillarity generated by larger pores. It is assumed in this analysis that the n_f represents

the meso-scale and macro-scale pores (1×10^{-5} to 1×10^{-3} m in diameter; (Luxmoore 1981)). Based on the capillary rise equation, pores of this size would generate tensions in the range of about 0.3 to 3.5 kPa.

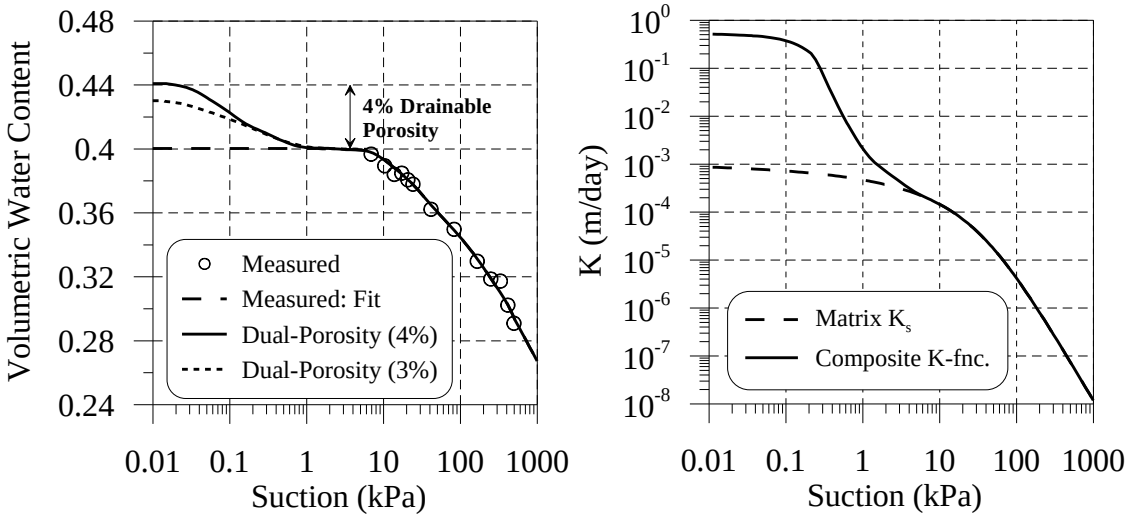

Fig. 4.4. Measured and composite hydraulic functions for the cover soil. a) Moisture retention curve. b) Hydraulic conductivity function.

A measured bulk saturated hydraulic conductivity (K_s) of 6×10^{-6} m/s (0.52 m/day) was assigned to the clay-rich cover soil (Composite K-fnc.; Fig. 4.4b). Meiers et al. (2003; Meiers et al. 2006) found that the K_s of the clay-rich soil increased from around 1×10^{-8} m/s to 6×10^{-6} m/s within four years after cover placement due to the development of macropores associated with freeze/thaw and wet/dry cycling. These values of K_s are similar to the values reported for fractured clay-rich tills (McKay and Fredericia 1995; Sidle et al. 1998). The hydraulic conductivity of the soil matrix is assumed to be 1×10^{-8} m/s (8.64×10^{-4} m/day), which is in keeping with the values measured *insitu* K_s values prior to the development of macroporosity (Meiers et al. 2003; Meiers et al. 2006). The matrix hydraulic conductivity function was predicted from the laboratory measured moisture retention curve using the method of Fredlund et al. (1994). The composite function assumes that the hydraulic conductivity transitions from K_s to the matrix K value over a matric suction of about 1 kPa.

Fig. 4.5 presents the geometry of the two-dimensional finite element model. The model domain extends upslope 50 m – the distance over which saturated conditions were observed (Kelln et al. 2008). The slope angle changes from 4° to 9° at a lateral distance of about 20 m. The cover is assumed to be 1 m thick over the length of the model domain and was discretized using approximately 6500 quadrilateral elements with four-point integration. The average element size was about 0.05 by 0.05 m. All boundaries in the model were assigned as no-flow boundaries. A potential seepage face boundary condition was applied to the left edge of the model to allow discharge under positive pore water pressures (i.e., flux is permitted from the model if pressure is greater than zero).

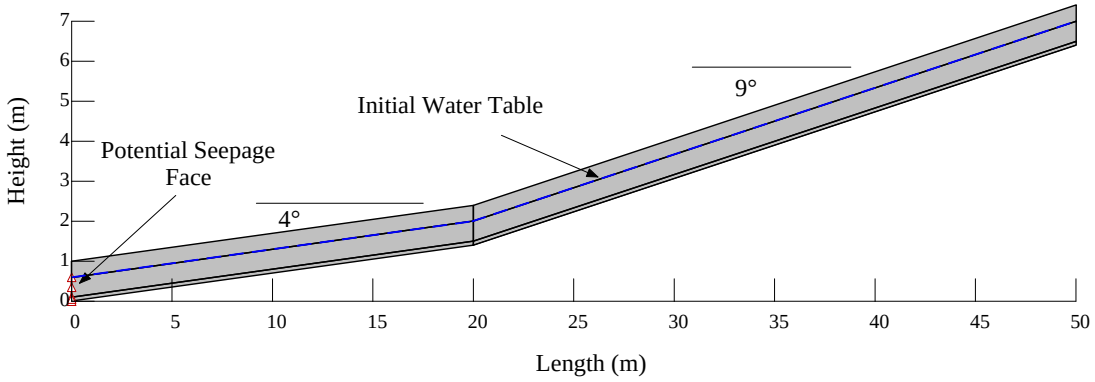

Fig. 4.5. Geometry and boundary conditions for two-dimensional finite element analysis (2× vertical exaggeration). The top, bottom, and left edges of the model domain are assigned a no-flow boundary condition.

Five initial water table geometries were analyzed to represent the range of conditions measured from 2004 to 2007 (Table 4.1). The average depth of water measured in the two rows of monitoring wells in 2004 was about 60 cm (n = 3; σ = 16 cm) and 32 cm (n = 3; σ = 9 cm) at lateral distances of 5 and 20 m, respectively. Accordingly, a sloping initial water table condition was applied with a depth of 60 cm at the left edge of the model, 30 cm at a distance of 20 m, and tapering off to 0 cm depth at a distance of 25 m. For 2005, a constant water depth of 60 cm (n = 6; σ = 120 cm) was modelled over the entire model domain. Although the detailed monitoring well grid was not installed in 2005, measurements in the two rows of monitoring wells were similar to the depth of perched water measured in 2007 at similar locations. The fact that the cumulative

discharge in 2005 was nearly double the amount collected in 2007, suggests that a greater volume of saturated flow in 2005 was derived from upper-slope positions (i.e. beyond a lateral distance of 25 m).

Table 4.1. Water table configurations for numerical analyses.

	Initial Water Table Height (cm)	
Water Table Configuration	From 0 to ~ 25 m	From ~ 25 to 50 m
2004	60 to 32	0
2005	60	60
2006 (1)	20	0
2006 (2)	30	0
2007	60	20

In 2006, perched conditions were confined primarily to the lower-slope (0 to ~ 25 m), with an average depth of about 20 cm (n = 27; σ = 12 cm). This yielded a modelled cumulative discharge that was slightly less than measured (discussed below), so an initial water depth of 30 cm was assumed for the lower-slope. At the onset of drainage in 2007, the average measured depth of water was 60 cm (n = 27; σ = 22 cm) in the 'lower-slope' (0 to ~ 25 m), while it varied dramatically in the 'upper-slope' (25 to 50 m) from around 10 cm to over 60 cm. An average depth of 20 cm in the upper-slope was assumed for the analysis.

Each water table configuration was analyzed for three different possible cover profiles: Cases I and II assumed a homogenous cover with the composite function #1 given in Figure 4b and with n_f values of 4% and 3%, respectively (Fig. 4.4a). Case III assumed that the lower 10 cm of the cover profile was not fractured. Accordingly, the matrix K-function and the laboratory measured moisture retention curve were applied to the bottom 10 cm. A value of n_f equal to 4% was used for the rest of the cover soil. Case III is based on a comparison of the measured pore water Na^+ concentration profile (Fig. 4.3) and the maximum Na^+ concentrations measured in subsurface flow, which suggest that fracture-dominated lateral subsurface flow does not interact with the high pore water concentrations near the cover/shale interface. It is also in keeping with concept of 'transmissivity' feedback, which assumes that hydraulic conductivity and

drainable porosity decline with depth due to changes in soil structure (Weiler and McDonnell 2006).

4.5.2. Transport Analysis

The Na^+ concentration of the discharge water was calculated based on the modelled water flux and the measured Na^+ concentration profile (Fig. 4.3). The calculation is shown schematically in Fig. 4.6. According to the conceptual model, the Na^+ concentration of water in the fractures is in equilibrium with the soil matrix pore water, and consequently the concentration of the discharge water is a function of the depth of perched water. The concentration of the discharge water over any given time step is therefore given as:

$$C_{avg} = \frac{\sum q_n \Delta y C_n}{q_{tot} \Delta y_{tot}} \qquad [3]$$

where q_n is the flux at each node (m/s), Δy is the vertical node spacing (m), C_n is the measured concentration at each corresponding node height (kg/m^3), $q_{tot}\Delta y_{tot}$ is the total discharge per unit width ($m^3/s/m$) over the perched height (Δy_{tot}). The top term represents the mass flux (kg/s/m) per unit width for each time step, while the bottom term represents the cumulative water flux over the same time. The pore water Na^+ concentration profile is assumed constant throughout the duration of drainage and is shown by the best-fit line in Fig. 4.3. As water is focused near the discharge pipe, it mixes, and provides the average discharge concentration. The calculated concentration of the discharge water will be sensitive to the lateral distance at which the nodal fluxes (q_n) are calculated. A sensitivity analysis demonstrated that using the nodal fluxes at a lateral distance of 5 m provided reasonable results for all analyses, particularly for water table configurations 1 and 2 in which the drawdown was fairly significant at early times.

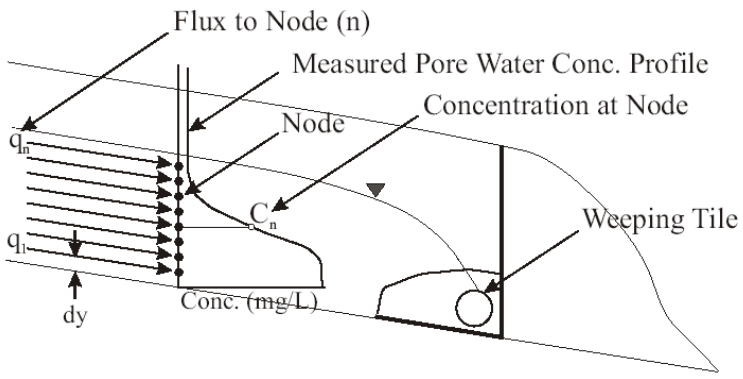

Fig. 4.6. Schematic illustration of groundwater flux to a specific node (q_n) with a constant concentration (C_n).

4.6. Results and Discussion

4.6.1. Subsurface Flow

Case I and II

Fig. 4.7 presents the measured and simulated cumulative discharge (m^3) to the tile drain for Case I and II. For clarity, the results are separated into 'high-flow' years (2005 and 2007; Fig. 4.7a) and 'low-flow' years (2004, and 2006; Fig. 4.7b). In 2005 and 2007, a total of about 60 and 35 m^3 of water was collected, respectively. A cumulative discharge of about 8, 17.5, and 13.5 m^3 was collected in 2003, 2004, and 2006, respectively. The greater cumulative discharge measured in 2005 and 2007 correlates with the larger areal extent and thickness of perched conditions across the slope. The duration of drainage varied from over 120 days in 2005 (data not presented) to around 40 days in 2004 and 2006, when perched conditions were confined to the lower-slope (lateral distance of 0 to 25 m).

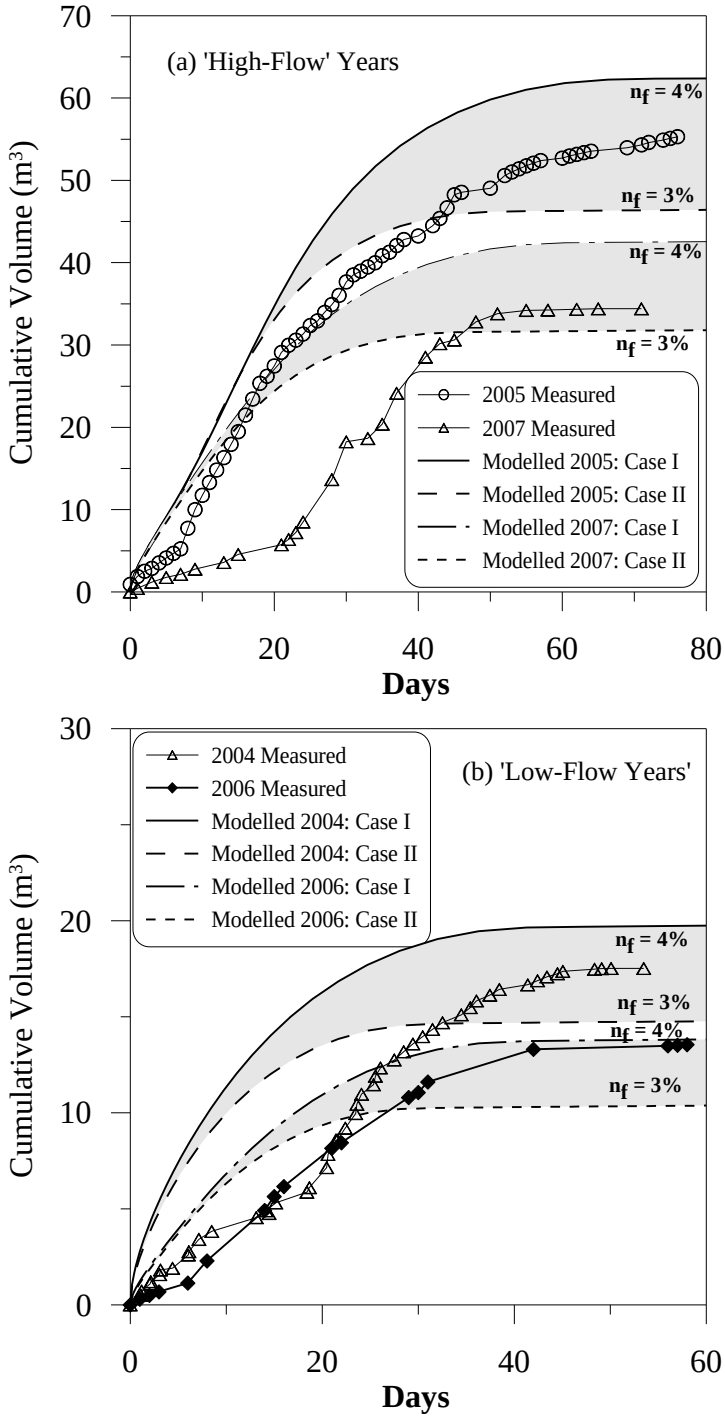

Fig. 4.7. Measured and modelled subsurface flow to the tile drain for Case I (n_f = 4%) and Case II (n_f = 3%). (a) 'High-flow' years of 2005 (76 Days; April 7 to June 17) and 2007 (71 Days; April 11 to June 20). (b) 'Low-flow' years of 2004, (54 Days; May 11 to July 3), and 2006 (58 Days; April 25 to June 22).

The initial measured discharge rate in 2005 (from 0 to ~ 7 days), 2006 (~ 0 to 3 days), and 2007 (from 0 to ~ 20 days) was less than anticipated. Although this observation has not been fully explained at this time, the lower discharge rate could be explained by partially frozen ground conditions and/or the frequency of pumping and problems with the pump. There is considerable evidence (discussed below) that subsurface flow begins in most years while the ground is still partially frozen. It is therefore possible that some of the macroporosity is blocked by pore ice, restricting infiltration and lateral subsurface flow.

The frequency of pumping was also problematic. In 2005, the collection well, which has a storage volume of about 2 m^3, was pumped manually (and only during the day) using a battery-operated bilge pump. Field records show that the system was pumped for about 10 minutes per day from days 1 to 5, and for 20 minutes per day on days 6 and 7 (on two or three occasions throughout the day). After day 7, the system was pumped for at least 30 minutes per day, and up to 90 minutes per day, four to six times per day. The collection well was also pumped manually for the first 20 days in 2007. The sudden increase in the discharge rate correlates to the day when the float-controlled, battery-operated sump-pump with a mechanical flow-meter was installed in the collection well.

In spite of the difficulties with pumping, particularly at early times, the simulated results for Case I and II (Fig. 4.7) capture the discharge rate (i.e. slope of curve) of subsurface flow for both the low-flow and high-flow years. Considering that the measured K_s was at least 2.5 orders-of-magnitude greater than the matrix hydraulic conductivity, the matching discharge rates demonstrate that lateral subsurface flow is dominated by the macropore system. The flux rate is controlled by the saturated hydraulic conductivity and hydraulic gradient. The hydraulic gradient is proportional to the slope angle, which changes from 4° to 9° at a distance of approximately 20m. As a result, the modelled cumulative discharge curves for 2005 and 2007 (Fig. 4.7a) diverge after about 10 days. The discharge rate remains higher in 2005 as water in the upper-slope (25 to 50 m) continues to flow into the lower-slope, thereby maintaining the lateral hydraulic gradient toward the tile drain. In the low-flow years (Fig. 4.7b), the flux rate at

early times is greater in 2004 than 2006 because the initial depth of water at the exit boundary was greater for 2004 (60 cm vs. 30 cm), creating a greater lateral gradient toward the tile drain.

The simulated range of n_f (3 to 4%) yielded cumulative discharge volumes that bracketed the measured volumes in both the high-flow and low-flow years (Fig. 4.7). The good-match between measured and simulated discharge is encouraging considering the simplified planar geometry used in the analysis. In a more detailed study of the cover hydrostratigraphy, Kelln et al. (2008) found that the depth of perched water in the slope exhibited significant spatial variability due to: (i) variations in slope topography and spring surface runoff; (ii) heterogeneity in the underlying saline-sodic shale; and, (iii) the mesotopography of the cover-shale interface. Lower-slope positions naturally collect more surface run-off during the spring snowmelt and therefore develop thicker saturated zones. In addition, the underlying saline-sodic shale was found to contain pockets of lean oil sand, creating an under-drained condition in some parts of the cover. More importantly, undulations in the subsurface topography of the cover-shale interface imposed a significant spatial control on the depth of perched water and the pathway for subsurface flow.

It is therefore conceivable that differences between measured and simulated cumulative discharge volumes are due to variations in the geometry of the initial water table and lower boundary of the model. This is particularly evident for 2006 in which the average measured depth of water was 20 cm with a standard deviation of 12 cm, but an initial water table depth of 30 cm was required to yield a cumulative discharge volume similar to the measured value. Furthermore, the grid of monitoring wells only measured perched conditions over a 25 m width in the middle of the cover. Kelln et al. (2008) found that downslope subsurface flow was re-routed laterally toward the northwest corner of the cover, outside the monitoring grid. It is very likely that the depth of water in this area exceeds the measured average depth within the monitoring grid. However, despite the simplifying assumptions, the simulations capture the character of subsurface flow using fracture porosity typical for clay-rich glacial soils.

Case III

Fig. 4.8 presents results for Case III in which it was assumed that the lower 10 cm of the cover layer was un-fractured. A n_f of 4% was only applied above a height of 10 cm. In the high-flow years, the model captures both the discharge rate and cumulative volume. The presence of the un-fractured soil reduces the cumulative discharge volume, but has little effect on the discharge rate at early times. A similar result was attained for the low-flow years, although the analysis underestimates the cumulative discharge for both 2004 and 2006. The simulation results for the low-flow years are more sensitive to the presence of the un-fractured soil layer because of the smaller initial depths of water. Again, the poorer match between the simulated and observed results can be attributed to the simplified geometry of the numerical model. Irrespective of the assumed initial depth of water and drainable fracture porosity, the finite element analyses captures the character of subsurface drainage to the tile drain for all years of record using hydraulic properties that are characteristic of fractured clay-rich soil.

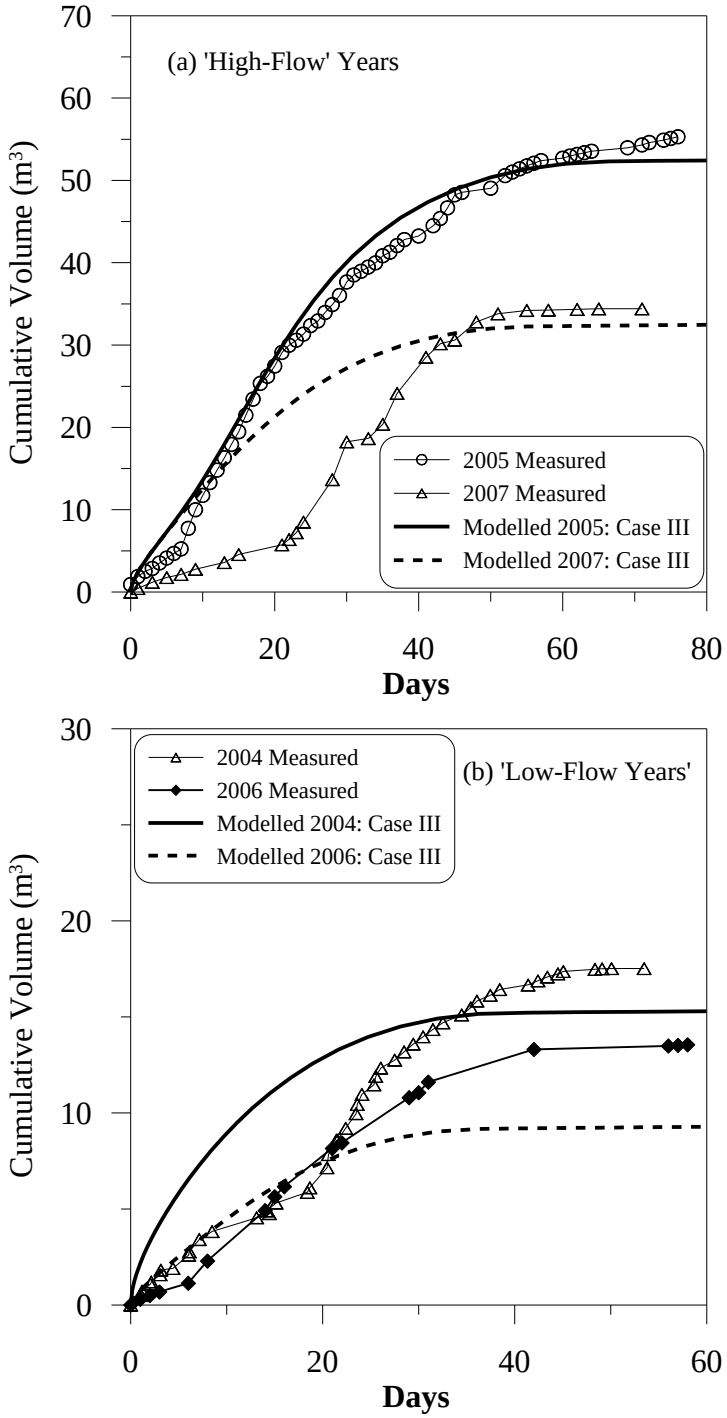

Fig. 4.8. Measured and modelled results for the Case III analyses (two-layer cover). (a) 'High-flow' years (2005 and 2007). (b) 'Low-flow' year (2004, 2006).

4.6.2. Transport Results

Case I and III

Fig. 4.9 presents the measured and calculated Na^+ concentration of water discharging to the tile drain for 'high-flow' years for the Case I and III analyses. Results from Case II (n_f = 3%) analyses are not included because Case I and II are very similar except that the increase in concentration is more rapid for Case II because the depth of water drops more rapidly due to the smaller n_f value. The maximum observed concentration of Na^+ in discharge water was around 1200 to 1300 mg/L (2006 and 2007; Fig. 4.9b and c), substantially lower than the maximum concentrations measured near the cover-shale interface (Fig. 4.3). This indicates that subsurface flow may be restricted deeper in the cover profile near the cover-shale interface, possibly due to decreases in hydraulic conductivity (i.e. less fracturing). Furthermore, Case I brackets the upper-end of the calculated discharge concentration because flow occurs throughout the entire cover profile.

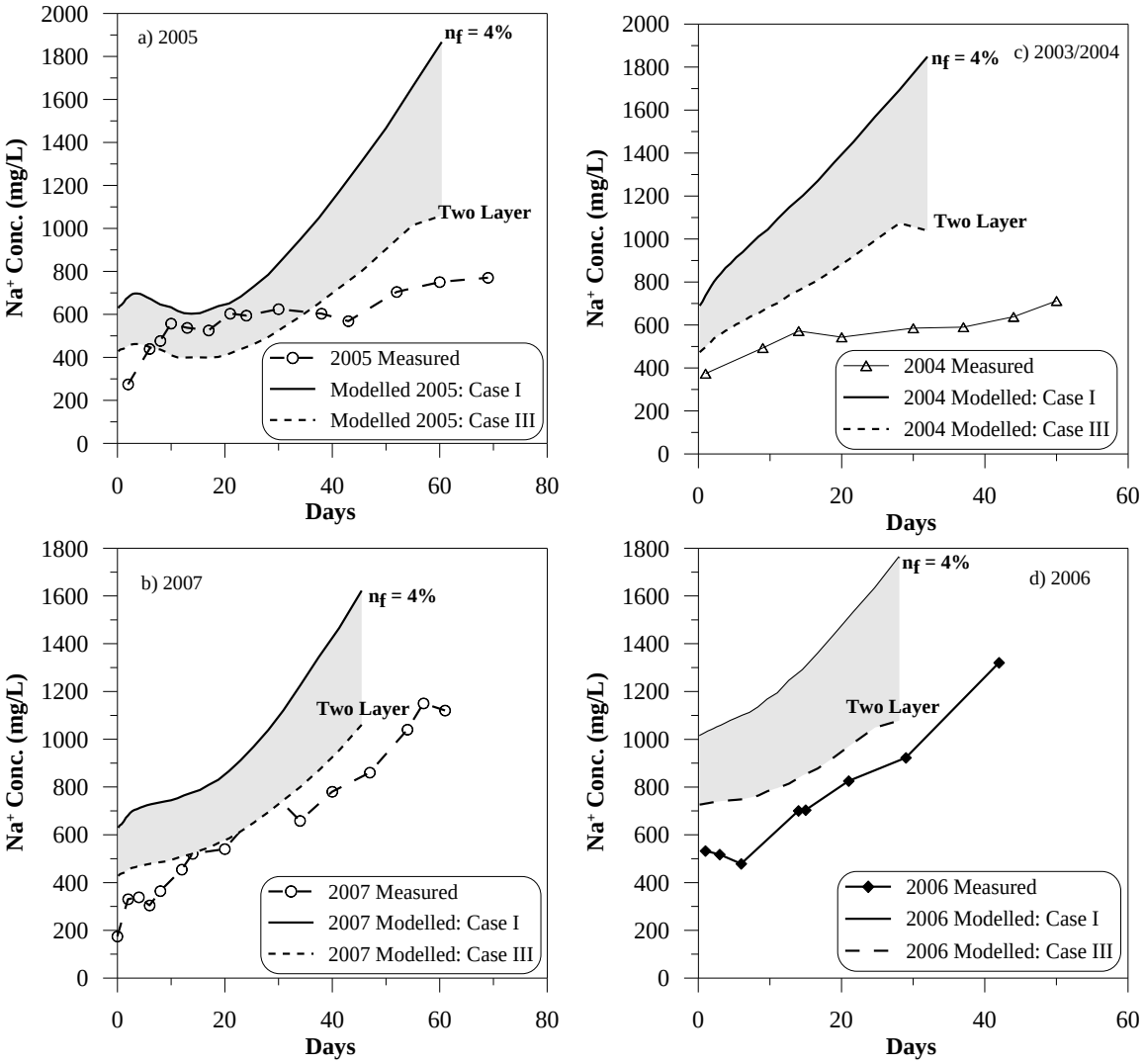

Fig. 4.9. Measured and modelled Na^+ concentration (mg/l) of water discharging to the tile drain (2004-2007).

The simulated results for both Case I (homogenous cover; $n_f = 4\%$) and Case III (two layer cover) capture the trend of increasing Na^+ concentration with time for 2004 – 2007 (Fig. 4.9a to d). The Na^+ concentration increases as the depth of perched water decreases, and lateral subsurface flow through the fractures occurs lower in the cover profile, adjacent to the higher matrix pore water concentrations near the cover-shale interface. In particular, the Case III analysis provides a better match to the measured response over the duration of subsurface flow.

Although the general trend of increasing concentrations in the subsurface discharge is captured, the model appears to over-estimate the concentration of subsurface flow. There are a number of processes that could explain this observation including: 1) greater spatial variability in the profile of pore Na^+ concentrations than used in the analysis; 2) partially frozen ground conditions at the onset of subsurface flow; 3) dilution of pore water in the soil matrix and fractures by spring and summer rains; and, 4) non-equilibrium transport due skin affects and longer than anticipated equilibration times. Naturally, the selection of a single profile of pore water Na^+ concentration shown in Fig. 4.3 may not be valid for all years of record, nor may it fully represent the distribution of salts over the entire area of perched conditions. Furthermore, the maximum modelled concentration could be reduced by a factor of two by simply using the lower bound of the concentration profile shown in Fig. 4.3.

In 2005 and 2007, the Na^+ concentration of discharge water starts at around 200 mg/L and then increases to the anticipated concentration by 10 to 20 days. Temperature sensor data (data not presented) indicated that subsurface flow in 2005 and 2007 started before the ground was fully thawed, indicating that snowmelt was infiltrating through the frozen ground via the macroporosity. An isotope hydrograph separation (IHS) confirmed the presence of fresh snowmelt water in the tile drain at early times for these years (Kelln et al. 2007c). This water transitions to a stable isotope signature representative of matrix pore water (i.e. 'old water') as the ground thaws and the water in the two reservoirs equilibrates. Naturally, fresh snow melt water stored in the fractures would not equilibrate with water in the soil matrix unless the ground was thawed. The stable isotope data indicated that the subsurface flow transitioned from around 10% to over 80 % old water. This observation is in keeping with the 'old water paradox' in hillslope hydrology studies (McDonnell 2003; McDonnell et al. 2007), in which subsurface flow is dominated by preferential flow through macropores, but water emanating from these preferential flow networks comprises water stored in the soil profile prior to the rain event.

The chronology of hydrological events is also consistent with this hypothesis. In 2005, drainage started around April 7. The cover temperature data indicated that the soil had thawed at the 55 cm depth on April 24th, and throughout the cover profile (at ~ 90 cm depth) by around May 1st. Incidentally, the stable isotope signature of discharge water had transitioned to a value more in keeping with the matrix pore water signature by around May 1st (day 23). Similarly, subsurface flow in 2007 started on April 10 while the ground was frozen. The cover was fully thawed by around May 1st to 3rd, which again correlates to the transition to a stable isotope signature more representative of matrix pore water (~ May 1–8). Discrepancies between the timing of events are likely related to the relative location of the soil station (~ 150 m upslope from the tile drain).

These observations are supported by other studies in the literature where preferential water flow occurs through frozen ground (Bayard et al. 2005; Espeby 1990; Thunholm et al. 1989a). In a study of water infiltration and percolation through glacial soils, Johnsson and Lundin (1991) found that discharge to a 1 m deep tile drain started one-month before soil frost had disappeared and when the thawing front had only penetrated 20 cm. Stähli et al. (1996) demonstrated using a one-dimensional coupled heat and mass transfer model that these observations could only be explained by flow through the high-flow domain of the previously air-filled macropores. Similarly, Stadler et al. (1997b) found that the partitioning of snow melt water into lateral runoff and vertical percolation through a sandy-loam was controlled in part by preferential flow through the frozen ground via the macroporosity.

However, partially frozen ground conditions do not fully explain all of the observations. In 2004 and 2006 (Fig. 4.9d), measured Na^+ concentrations were again lower than modelled at the onset of subsurface flow. Hydrological response data and an IHS performed on the 2006 discharge water indicated that the onset of subsurface flow and ground thaw were nearly synchronous (Kelln et al. 2007b). Furthermore, the modelled concentrations are lower than measured at later stages of subsurface flow in all years of record. This may suggest that the system had not fully equilibrated.

It is possible that the equilibration time between the two water reservoirs (Eq. 2) is slower than anticipated due to 1) 'skin' affects (Jarvis 2007); and, 2) diffusion across the matrix blocks. Firstly, Kohne et al. (2002) found that the coefficient of diffusion of surface skins (i.e. clayey and silty coatings on the matrix–fracture interface) can be 30 to 45 times lower for Br^- and Cl^-, respectively. A reduced coefficient of diffusion would reduce the rate of mass transfer between the fractures and matrix, thereby accentuating non-equilibrium transport. However, even if the coefficient of diffusion used in Eq. 2 were 40 times lower, the equilibration time would still be rapid (~ 4000 seconds). However, complete equilibration across the matrix blocks would be governed by Eq. 1. Although it is true that the concentration in the fracture would rapidly equilibrate with pore water in the adjacent matrix, the maximum concentration would not be attained until full equilibration across the soil matrix occurs. Using Eq. 1 with a coefficient of diffusion equal to 1×10^{-10} m^2/s and an average fracture spacing (L) of 2 cm, yields an equilibration time of 4×10^6 seconds (~ 46 days).

Finally, it is noted that spring and summer rain would act to dilute water in both the soil matrix and fractures. For example, the measured concentration does not continue to rise beyond about day 30 in 2005 (Fig. 4.9a). The climate in 2005 was unseasonably wet and cold from spring to fall, causing subsurface flow to continue until freeze-up. A similar trend was observed in 2004.

Sensitivity Analysis

A sensitivity analysis was conducted for the 2006 discharge event to determine the impact of the initial water table geometry on the simulated discharge volume and Na^+ concentrations. As noted above, the depth of water is inversely related to the Na^+ concentrations of discharge water. Consequently, the initial water table geometry will affect the calculated discharge concentration. It has already been noted that the depth of water across the slope may be highly variable due to topographic undulations in the cover-shale interface (Kelln et al. 2008). Monitoring well data (not presented) generally indicate the depth of water increases toward the toe of the slope. It is therefore plausible

that depth of water near the tile drain is much greater than the average depth measured across the slope.

The previous simulations, with the exception of 2004, assumed that the initial water table was parallel to the lower boundary. In 2006, the water depth near the toe was over 40 cm in some monitoring wells. For simplicity, the sensitivity analysis assumed a sloping water table with an initial depth of 40 cm at the exit boundary and the average depth of 30 cm at a distance of 20 m (tapering off to zero at about 25 m). The Case III analysis (two layer cover) was used for the hydraulic properties.

Fig. 4.10a and b presents the results of this simulation. The seepage model once again provides a reasonable simulation of the discharge rate and volume throughout the duration of subsurface flow. The model yielded a slightly closer-match to the cumulative discharge volume than the base case (Fig. 4.8b; 2006). More importantly, the simulated discharge concentrations are closer to the measured values at early time than those from the previous simulation. This is attributed to the greater depth of water near the exit boundary, which increases the amount of water moving through lower concentration matrix soil higher in the cover profile. Although the model is purely speculative, it demonstrates the sensitivity of the analysis to the initial water table geometry.

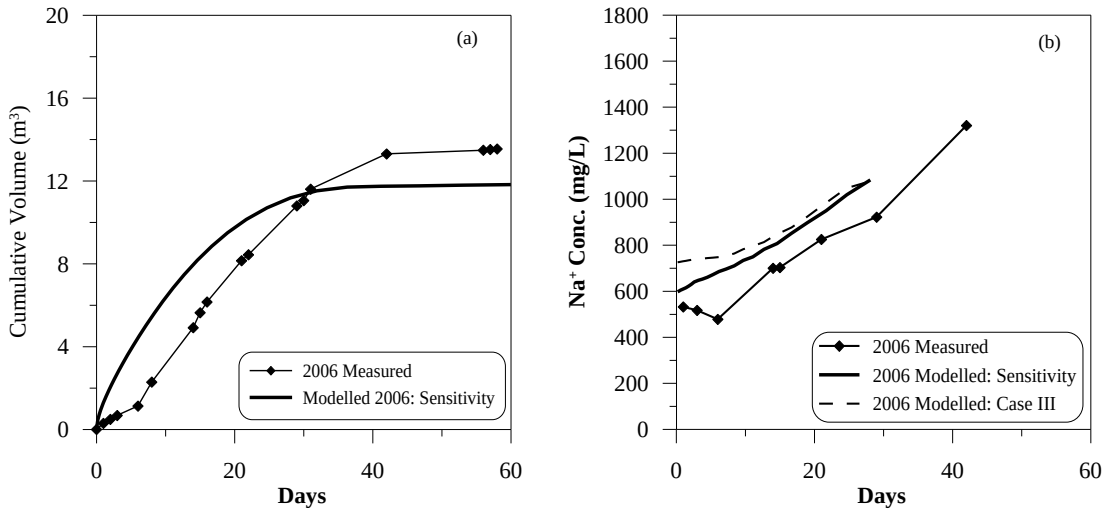

Fig. 4.10. Modelling results from sensitivity analysis. (a) Sub-surface flow. (b) Na^+ concentration of discharge water.

In summary, the seepage and transport simulations capture the general nature (flow and chemistry) of discharge for all years of record. Sampling from a tile drain integrates the effects of spatial variability with respect to flow and transport characteristics within a large soil volume (Villholth and Jensen, 1998b). Consequently, the assumption of a single distribution of pore water Na^+ concentration is a considerable simplification of the physical system. A better match to measured data could have been obtained by using a slightly different profile of pore water Na^+ concentration. Differences between measured and simulated discharge volumes and Na^+ concentrations could also be partly explained by slower than anticipated equilibration due to skin affects and equilibration over the soil matrix blocks. The discharge Na^+ concentration at early times in particular is sensitive to the depth of water near the toe of the slope. Averaging the depth of water across a large area does not capture the nuances of the subsurface flow system caused by the cover-shale topography.

It remains somewhat perplexing as to why snowmelt infiltration reported to the tile drain in 2005 and 2007 while the ground was still frozen, while the melt water infiltration apparently re-froze in the preferential flow paths in 2006. Snowmelt infiltration depends on complex hydraulic and thermal interactions between the atmosphere, snowpack, frozen soil, and unfrozen soil (Stadler, 1997). Antecedent moisture conditions and diurnal temperature fluctuations also impose a significant control on snowmelt infiltration through frozen ground. The snow pack can provide some thermal insulation for the ground, which can protect it from diurnal temperature fluctuations. The snow pack depth in 2005 and 2007 was 81 and 116 mm snow water equivalent (SWE), respectively, compared to only 56 mm SWE measured in 2006. It is therefore conceivable that the thermodynamics of the snow melt in 2005 and 2007 promoted continual infiltration of snow melt water via the fracture network, while this water re-froze after infiltration in 2006.

4.7. Summary and Conclusions

Saline-sodic shale overburden waste in the oil sands region of north-central Canada is reclaimed through the placement of a clay-rich cover soil. The upward transport of salts from the shale into the overlying cover may compromise the long-term sustainability of these reclaimed landscapes. A better understanding of the hydrological controls on subsurface flow and transport is therefore required. The objectives of this study were to develop a conceptual model of fracture-dominated lateral subsurface flow and transport and then to verify this model with field data and numerical simulation. Field data included the measured volume and chemistry of subsurface flow reporting to a tile drain installed at the toe of a sloping reclamation cover over a four-year period (2004–2007).

The results indicate that fracture-dominated subsurface flow could be described assuming a single-porosity medium with composite hydraulic functions. The composite hydraulic functions account for the significant increase in saturated hydraulic conductivity near saturation and an increase in drainable porosity over a low suction range produced by macropores. The simulated results captured the discharge rate of subsurface flow using the measured value of bulk saturated hydraulic conductivity, which is approximately 2.5 orders-of-magnitude greater than the measured matrix hydraulic conductivity. A drainable fracture porosity ranging from 3 to 4% yielded cumulative discharge volumes that bracketed measured volumes for all years of record. A similar result was obtained by assuming a two-layer cover system that included 10 cm of un-fractured soil at the base of the cover overlain by a fractured soil with a drainable fracture porosity of 4%.

A transport analysis was conducted assuming that effective porous medium (EPM) conditions exist. The Na^+ concentration of subsurface flow discharging to the tile drain was calculated using the water fluxes from the seepage simulation and measured profiles of pore water Na^+ concentrations. Despite the simplifying assumption of a single, well-defined, profile of pore water Na^+ concentration, the EPM model was able to capture the character of increasing discharge concentrations with time. Discharge concentrations increase as the depth of perched water decreases, and flow through the fractures occurs

lower in the soil cover profile, that is, adjacent to the higher matrix pore water concentrations near the cover-shale interface. Including the lower 10 cm of un-fractured soil improved the match to field data because it restricted flow near the cover-shale interface (i.e., through matrix of higher pore water concentrations). Modelled results were sensitive to the geometry of the initial water-table configuration. The measured subsurface flow chemistry also suggested that subsurface flow was occurring through frozen ground in certain years. Finally, a comparison between measured and modelled results suggested that the assumption of an EPM may be only partly valid due to longer than anticipated equilibration time and/or frozen ground conditions in certain years.

5

Summary and Conclusions

5.1. General

The oil sands industry is confronted with the challenge of reclaiming hundreds of square kilometres of saline-sodic shale overburden that is derived from the mining process. Successful reclamation of mine landscapes will ultimately be determined by the health, diversity, and sustainability of the re-established ecosystem. Current reclamation strategies prescribe the placement of a clay-rich cover soil over the waste substrate. The cover is designed to provide sufficient moisture throughout the growing season to support re-vegetation efforts. Upward transport of salts from the shale into the overlying cover soil has the potential to compromise the long-term sustainability of these reclaimed landscapes. It is therefore essential to characterize the processes that govern moisture and salt transport dynamics within these reclaimed cover systems.

The global objectives of this study were twofold. Firstly, to identify the processes and parameters that govern moisture dynamics and salt transport in reclamation covers with mesotopographic relief under the climate conditions encountered in the Boreal Plain. Secondly, to apply this understanding to the development of optimal designs for reconstructed landscapes overlying low permeability substrates. The effect of mesotopography on the performance of the cover systems is directly addressed in this research through the study of moisture dynamics, salt transport, and subsurface flow, which are all governed to some extent by the elevation relief and slope of both the land and cover-waste surfaces.

A detailed review of the hydrological and geochemical response from a clay-rich reclamation cover overlying a shale substrate (Chapter 2; Manuscript #1) indicated that

preferential flow imposes a first-order control on infiltration and the development of perched conditions during the spring melt. Snowmelt and surface water runoff begins each year while the ground is frozen and the infiltration capacity of the soil matrix is reduced due to pore ice blockage. The only available pathway for snowmelt infiltration in the frozen cover soil is via the macroporosity. Subsurface flow and ground temperature data revealed that this water can either re-freeze after infiltration or continue to flow through the fractures while the ground is frozen. Once the ground is fully thawed, perched conditions develop on the cover-shale interface and lateral subsurface flow commences. An isotope hydrograph separation performed on the discharge water indicated that this water transitions from fresh snowmelt water stored in the fracture porosity to predominantly connate pore water. This 'evolution' in the chemical signature of the discharge water was attributed to chemical equilibration between the two water reservoirs as the ground thaws (Chapter 4; Manuscript #3). The equilibration time is nearly instantaneous during years in which ground thaw and subsurface flow are synchronous.

The depth of perched conditions during the spring snowmelt was found to be a function of both landscape position and the mesotopography of the cover shale interface (Chapter 3; Manuscript #2). In general, lower-slope positions collect more surface run-off and have greater depths of perched water than middle and upper-slope positions. Measurements of water depths in a grid of shallow monitoring wells demonstrated that perched conditions also develop in upper-slope positions (Chapter 3; Manuscript 2) in some years. The annual variation in the spatial distribution of perched water depths appears to be partially correlated to the depth of snowpack. Naturally, years with greater snowpack depths generate more surface run-off, which increases snowmelt infiltration via the macroporosity, thereby creating a more spatially extensive perched water table.

The mesotopography of the land surface and cover-shale interface varied significantly within the detailed study area. The slope angle changed from about 4° to 9° over a lateral distance of about 25 m. The cover-shale interface exhibited small vertical undulations with an amplitude greater than 10 cm. This subsurface relief imposed a control on the

downslope routing of subsurface flow. A small subsurface ridge in the shale near the toe of the slope re-directed flow laterally toward the edges of the cover. Water depths generally declined in conjunction with diminishing subsurface flow, although the re-routing of water by the cover-waste mesotopography causes some wells along the same isoline of elevation to dry quicker than others.

The texture of the underlying waste material also proved to have a considerable impact on the spatial distribution of perched water conditions. Pockets or lenses of coarse grained soil were present in the shale and created an under-drained condition in which infiltration water that bypasses the cover soil (via the macroporosity) drained directly into the coarse textured soil. Hydrographs from a number of monitoring wells demonstrated that deep percolation into the shale occurs from these pockets at a rate controlled by the shale hydraulic conductivity. This observation has implications for 'mesotopographic design' because it demonstrates that water can be managed within the landscape and that deep percolation could be used to promote the downward flushing of salts.

Salt transport within the landscape is correlated to moisture conditions and the presence of subsurface flow. In general, salt ingress is accelerated in lower-slope positions due to wetter conditions, which increases the coefficient of diffusion and the rate of upwards diffusive transport. Subsurface flow and/or deep percolation appear to cause some flushing of salts in lower-slope positions. Middle and upper-slope positions are generally drier and therefore display attenuated salt ingress. However, profiles of *insitu* pore water chemistry indicated that sub-surface flow and/or deep percolation are acting to reduce salt ingress in upper-slope positions. This observation is in keeping with the conceptual model of water flow in the covers, which contends that perched conditions can develop in upper-slope positions due to preferential flow of snow melt water in spring.

Hydrological response data from the cover indicated that subsurface flow and downslope moisture translocation are insignificant during the drier summer months (Chapters 2 and 3). Downslope moisture translocation would cease after the slope drains

(i.e. subsurface flow ceases) and matric suctions begin to rise in the cover soils due to moisture uptake by plants. Matric suctions near the ground surface and in the middle of the cover reach values in excess of 1000 kPa during the summer months in most years. Moisture dynamics are restricted to vertical movement, as the dominant hydraulic gradient would be toward the drying front, or toward the plant roots. This observation is in keeping with the concept of 'wet' and 'dry' states in natural hillslopes. Downslope moisture movement only occurs when high antecedent moisture conditions or wet climatic conditions persist. It also suggests that 'wet' climatic conditions do exist in the semi-arid climate of the Mid-Boreal Upland region. Although the annual climate is classified as semi-arid or sub-humid, there are temporal periods in which 'wet' conditions exist (i.e., during snow melt).

Finally, the conceptual model for flow and transport in the cover was refined and verified through a numerical analysis of subsurface flow and transport (Chapter 4; Manuscript 3). The key elements of the conceptual model are that: 1) subsurface flow and cumulative discharge volumes are controlled by the fracture porosity; 2) chemical equilibrium between fresh snowmelt water stored in the fractures and connate pore water is nearly instantaneous when the ground is unfrozen; and, 3) the solute concentration of discharge water is a function of the depth of perched water. A two dimensional finite element seepage analysis using composite hydraulic functions was capable of capturing the measured rate and cumulative discharge of subsurface flow. The composite hydraulic functions (i.e. water retention curve and K-function) account for the significant increase in hydraulic conductivity near saturation and the increased drainable porosity over a low suction range caused by the fracture porosity. A drainable fracture porosity ranging from 3 to 4% yielded a modelled cumulative discharge that is consistent with measured values. A pseudo-EPM transport analysis calculated discharge water Na^+ concentrations that were similar to measured values. The analysis demonstrated that the concentration of discharge water increases as fracture-dominated subsurface flow occurs lower in the cover profile, that is, 'adjacent' to high pore water concentrations in the soil matrix.

5.2. Implications for Design

An objective of this research has been to develop guidelines for incorporating mesotopography into the design of reclaimed landscapes. Although this objective has not been entirely realized, there are a number of fundamental concepts that are applicable to 'mesotopographic design' and will guide future research in this area. From a design standpoint, the mesotopography of the cover-waste interface could be used to manage excess water and solutes within the landscape. Naturally, the latter issue is more applicable to situations in which the underlying waste is a source of contaminants (e.g. saline-sodic shale).

It is clear from this study that perched conditions will develop in clay-rich reclamation covers overlying low permeability waste. Perched conditions develop primarily during the spring snow melt as a result of preferential flow through frozen or partially frozen ground. Furthermore, perched conditions develop in middle and upper-slope positions in some years, as well as on benches and gently sloping areas (e.g., flat tops of waste dumps). Although subsurface flow within sloping ground is dominated by the fracture system, this water will inevitably move downslope and collect in topographic lows. Subsurface flow will transport salts from upper-slope to lower-slope positions if the underlying waste contains high solute concentrations. Consequently, there remains a need to manage the excess water and salt that will accumulate.

In general, it is beneficial to have excess water (i.e. saturated conditions) in the landscape at certain times. A preliminary review of tree-growth statistics from the three covers at SW30 (Appendix A) suggested that not only do thicker covers (> 50 cm) have better tree growth rates than thinner covers (~ 35 cm) due to greater available water holding capacity, but that tree growth is better in lower-slope and middle-slope positions due to the availability of excess water. The data also indicated that cover thickness is an important consideration for salt ingress. Salt ingress appeared to limit plant development at lower slope positions in the thinnest cover due to the proximity of the plant root zone to high salinity pore water near the cover-waste interface. This would suggest that there is an optimal thickness that provides excess moisture for plant growth while providing

the necessary 'buffer' between the plant roots and high solute concentrations near the cover-waste interface.

Saturated conditions also promote lateral flushing and deep percolation. The reservoir of salts in the underlying shale is produced primarily due to sulphur oxidation of the shale prior to cover placement. The rate of oxidation is reduced after cover placement because of the reduction of oxygen diffusion rates across the cover thickness and the depletion of the most readily available sulphur within the upper shale (Nichol et al. 2006). Deep percolation and lateral flushing will help to attenuate salt ingress, and may eventually reverse the direction of salt movement (i.e. downward) by overcoming the upwards diffusion gradient, which naturally diminishes with time. However, it should be noted that the development of perched conditions without any lateral drainage (i.e., plateau area) can be detrimental. Previous studies have shown that salt ingress on the plateau of the SW30 waste dump was more rapid than on the slope due to the persistence of near-saturated conditions. The rate of deep percolation is relatively slow (~ 0.1 mm/day), so it is important to have adequate cover thickness and/or subsurface flow (i.e. sloping ground).

That being stated, there are essentially two areas within the landscape that require the most attention: the toe of a slope and gently sloping or flat areas (benches and plateaus). Subsurface flow discharging at the toe of the slope could be collected in drainage swale ditches. This water will be diluted by surface run-off and report to larger collection ponds. These ponds are currently part of the reclamation strategy as they provide natural habitat areas and diversity within the landscape. Based on seven years of performance data, ponds located at the toe of slopes within reclaimed shale landscapes appear to be performing well (Qualizza, personal communication, January 2008).

The greater challenge may be to prevent salinization of benches or gently sloping areas within the landscape. In fact, large plateaus may need to be avoided completely unless cover depths are increased. It should be noted, however, that benches and other mesotopographic features will eventually develop naturally due to geomorphological process such as erosion and subsidence. For example, the SW30 overburden dump was

initially constructed with planar hillslopes. These slopes now display significant mesotopography, with the slope angle and relief varying considerably over short distances. A number of benches have developed along the 200 m long slopes of the study site discussed in this research.

Subsurface flow reporting to benches within a hillslope could conceivably be collected in large swale ditches and conveyed downslope, much like the swale ditches near the toe of the slope. However, the conveyance distance, construction and maintenance issues, and other hydrological concerns would likely make this option unfeasible. It may be more feasible to capture this water within the landscape by sculpting subsurface drainage ditches into the shale interface on benches within the hillslope (i.e., constructing mesotopography). This is conceptually similar to depression focused recharge in prairie pothole environments, except that the 'depression' is within the subsurface. Subsurface flow would collect in the bench area, and then slowly percolate downward into the shale.

The key design issues would therefore be: 1) ensuring adequate storage in the subsurface depression; and, 2) ensuring adequate cover thickness to create a buffer between the high salt concentrations near the cover-shale interface and the plant root zone. The issue of adequate storage would be a function of slope length, the depth of perched water, and drainable porosity. For example, the results from this study suggest that the average perched water depth varies from around 20 to 60 cm and the drainable fracture porosity ranges from about 3 to 4%. Assuming a ponded depth of 60 cm and a drainable porosity of 4%, a slope length of 50 m would yield a volume of 1.2 m^3 per unit length of cover, which would naturally drain into the bench. If the bench were 20 m in length and the soil had a similar drainable porosity, this volume would translate into a ponded depth of about 1.5 m. Conversely, the ponded depth within the bench area would only be 20 cm if the bench were constructed of a 1 m thick clay rich cover overlying a sand pocket with a storage porosity of 30%. The sand pocket would create a large 'reservoir' to collect and store water for deep percolation.

The required cover thickness in these areas would be a function of climate and salt transport. The additional moisture in these areas would likely accelerate salt ingress, as this study has demonstrated (Chapter 3; Manuscript #2). Consequently, the cover soil would have to be sufficiently thick to create a 'buffer' between the plant root zone and the area of high solute concentrations. This optimal thickness could be evaluated using a one-dimensional coupled seepage and transport model with a climate-driven surface boundary condition (see recommendations). This phase of numerical modelling would help to achieve the second global objective of this research: to develop a set of guidelines for incorporating mesotopography into reclaimed landscapes.

5.3. Preliminary Design Evaluation

5.3.1. Modelling Study

A preliminary modelling study was conducted in this section to evaluate some basic slope geometries (i.e. topography) that could potentially be used for the design of reclaimed landscapes. Based on the preceding discussion, the central issue of design is promoting subsurface flow, while ensuring that saturated conditions do not persist over the growing season when evapotranspiration demands are high. Naturally, the slope length, or conveyance distance, will be a function of the slope angle. A greater slope angle is proportional to a greater lateral hydraulic gradient, so the conveyance distance can be increased with increasing slope angle. The inter-slope management areas or benches will be a function of the total discharge volume as discussed above.

Two-dimensional seepage modelling was conducted to determine the maximum slope length for three different slope angles of 4°, 6°, and 8°. The following assumptions were common to each analysis: 1) the initial ponded depth was set to be 60 cm; 2) a drainable fracture porosity of 4 % was assigned to the entire cover profile based on the findings presented in Chapter 4; and 3) the time duration of each analysis was 45 days. The time duration was selected assuming that subsurface flow typically starts around the middle of May (see Chapter 2) and is finished by the end of June (~ 45 days). The objective is to

ensure that perched conditions dissipate prior to July and August, when evapotranspiration demands are much higher (see Chapter 2).

Fig. 5.1 presents the model geometry for a 4° slope that is 30 m long. The left vertical boundary was set to a potential seepage face. The bottom and right vertical boundaries were set to a no-flow boundary condition. The modelled cover thickness was set to 60 cm as the initial water table condition never exceeded this height. For each slope angle, the slope length was increased to find the maximum conveyance distance (i.e. slope length) at which perched conditions would recede within the 45 day time period.

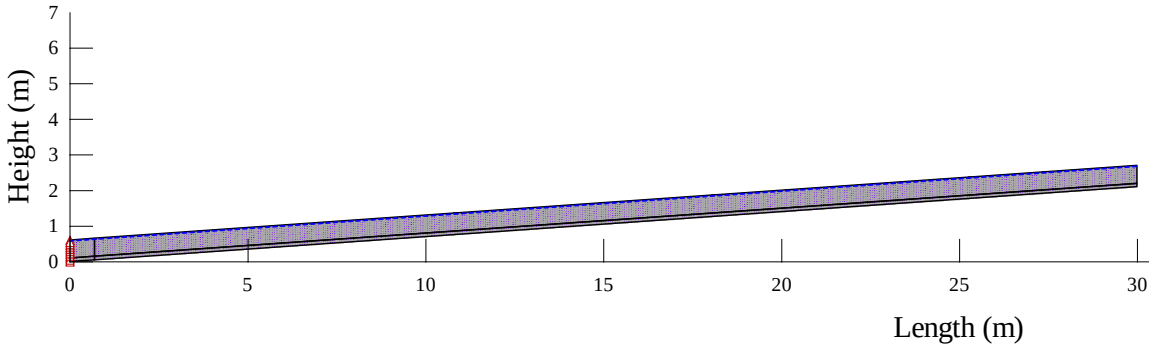

Fig. 5.1. Geometry of finite element model for preliminary modelling.

5.3.2. Results and Recommendations

Fig. 5.2 presents a plot of cumulative discharge verses time for each of the three different slope angles. The horizontal dashed lines represent the target discharge volume, which is calculated as the perched water depth multiplied by the slope length and drainable fracture porosity (i.e. 4%). In other words, this is the total volume of water contained in the fracture porosity. The corresponding maximum slope length for each slope angle is presented in Fig. 5.3. The maximum conveyance distance for slope angles of 4°, 6°, and 8° is 30 m, 40 m, and 60 m. In each case, the fracture porosity is drained by around 45 to 50 days, which is indicated by the cumulative discharge reaching the target discharge volume.

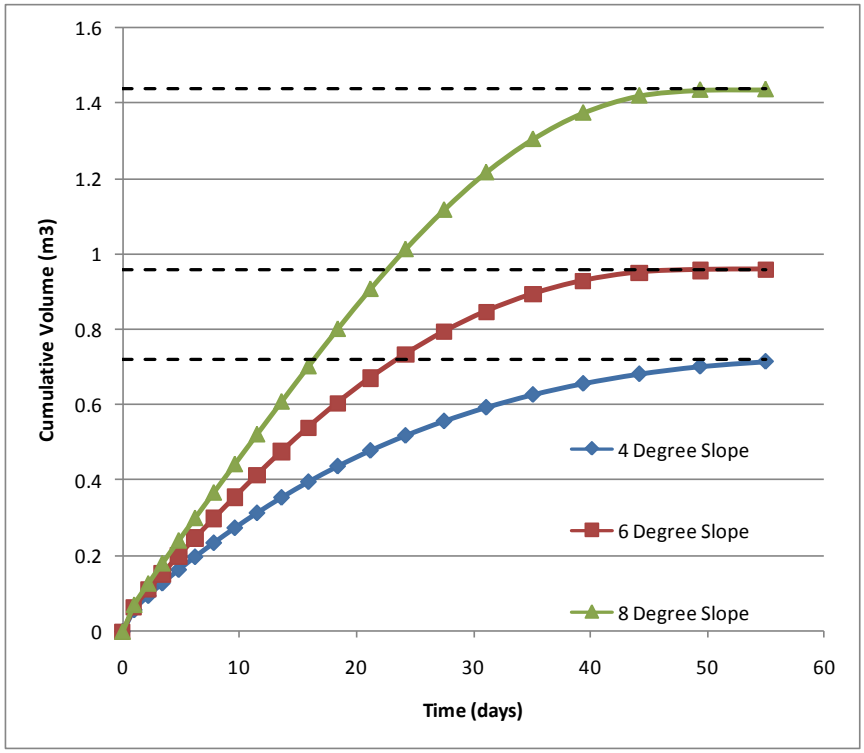

Fig. 5.2. Cumulative discharge verses time for the three slope cases.

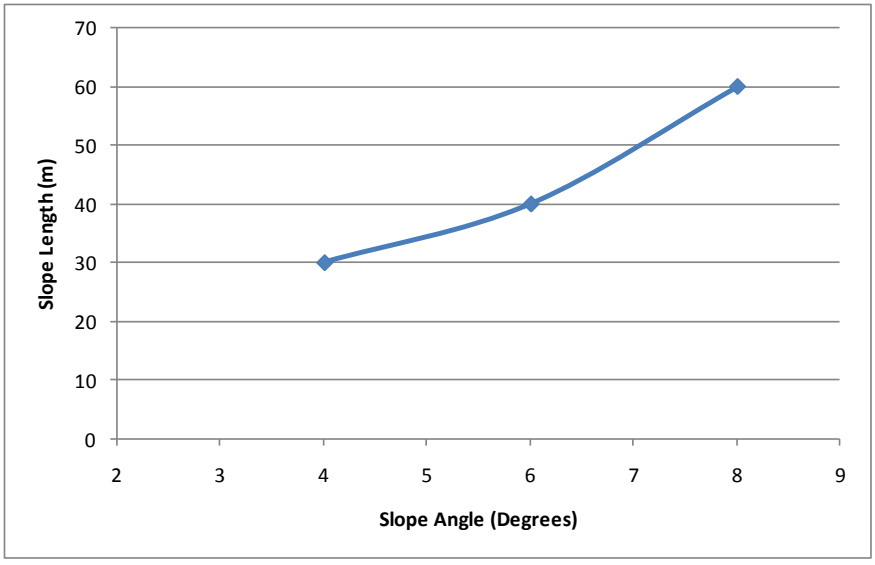

Fig. 5.3. Slope angle verses conveyance distance (i.e. maximum slope length).

In the context of the measured slope geometry (see Chapter 3), the results would suggest that the conveyance distance should be at most 60 m at a slope of 8°. However, the average slope angle at the SW30 overburden site is around 6°, so a more conservative slope length would be around 40 to 50 m. This slope length would yield a typical volume of discharge water around 1 m^3 (per unit width of cover). The slope bench could be designed as discussed above. It would likely be prudent to construct a subsurface collection system comprising a sand in-fill overlain by the cover soil as shown in Fig. 5.4. This configuration would ensure that the overlying cover is under-drained, much like areas within the cover that were underlain by pockets of lean oil sand, and that there is adequate storage in the subsurface soils.

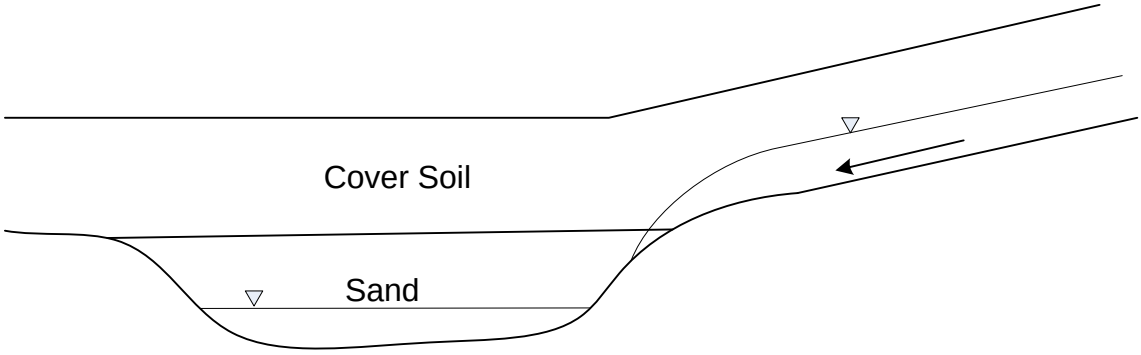

Fig. 5.4. Schematic of subsurface flow collection system.

6

Recommendations

The following recommendations for additional work will aid in the development of guidelines for 'mesotopographic design' in reclaimed landscapes.

6.1. Field and Laboratory

i. The drainable fracture porosity of the clay-rich soil determined in this study was based on a 'calibrated' finite element seepage analysis of subsurface flow. It would be beneficial to independently verify these numbers through field testing. Tension infiltrometer tests are one method that can be used to determine macroporosity (e.g., Waduwawatte and Si 2004). A tension infiltration test is conducted at a pressure head of –0.3 kPa, which is equivalent to a pore diameter of 1×10^{-3} m based on the capillary rise equation. Immediately after the infiltration measurement, a soil core is collected and the volumetric moisture content of the soil is determined using the gravimetric method. The macroporosity is calculated as the difference between the total porosity and volumetric moisture content at the –0.3 kPa pressure head.

ii. Tracer tests are commonly employed to determine the effects of macroporosity on solute transport through clay-rich soils (Gerke and Köhne 2004; Köhne and Gerke 2005; McKay et al. 1993b). Incidentally, a tracer was conducted as part of this research. The data were not presented because the results were inconclusive. A sodium-bromide tracer was added to a line of

three closely-spaced monitoring wells at two locations on the D3 cover. Water samples were collected from monitoring wells installed down-slope of the 'injection' wells at lateral distances of about 20 cm, 50 cm, and 80 cm. The sample wells were constructed of either 0.635 cm (¼ inch) diameter stainless steel pipes with a 15 cm perforated zone (20 and 50 cm locations) or 2.54 cm (1 inch) diameter PVC pipe with a 15 cm long hand-slotted screen (80 cm location). Water was also collected from the injection wells immediately after the tracer was added to determine the initial concentration after dilution with water in the wells.

Unfortunately, the tracer test was conducted before the conceptual model for flow and transport was fully developed. Accordingly, the sampling frequency was not great enough to adequately track concentration with time in a fracture-dominated flow system. Samples were collected from the downslope monitoring wells and injection wells every three to five days. At one location, the tracer was nearly undetectable in one of the injection wells only 30 minutes after the tracer was added. This may suggest that the monitoring well intersected a hydraulically active fracture and was rapidly flushed. However, the ground was still partially frozen during the test, so it is also possible that tracer created a rapid increase in hydraulic gradient (like a 'slug' of water) that quickly drained from the well. At the other location, the bromide concentration in one of the injection wells declined in a near-linear fashion over a period of 30 to 40 days. However, the data are difficult to interpret because only seven water samples were collected over this time. Finally, bromide was detected in very low concentrations at only one of the monitoring wells eight days after the tracer was 'injected'.

The results from this preliminary test suggests the following: 1) samples should be collected from the injection well(s); 2) sampling frequency should be very high at early times; 3) the ground should be fully thawed and water

levels at their maximum before the test begins; (4) very close attention should be paid to the dilution caused by adding the tracer to a certain depth of water in the injection well(s); and, 5) downslope water samples need to be collected from a larger sampling volume (e.g. interflow system) verses 'point' locations within the slope (i.e. monitoring wells). The latter recommendation is due to the irregular flow paths likely created by the fracture system.

iii. Deep percolation into the underlying shale is a key process controlling the vertical flushing of salts. The stable isotopes of water could potentially be used to track the depth of infiltration of modern waters into the underlying shale. This would provide independent verification of percolation rates determined in this study (Chapter 3; Manuscript #2). Cores could be collected from boreholes extending into the shale an analyzed for δD and $\delta^{18}O$ using a direct equilibration technique being developed for samples collected from the vadose zone (Hendry, personal Communication, 2008).

6.2. Analysis and Interpretation

i. This study demonstrated that the spatial distribution of salts is a good surrogate for understanding moisture dynamics within the cover. It would therefore be advantageous to determine profiles of pore water chemistry along numerous transects that traverse larger areas of the reclaimed landscape. In 2007, detailed mapping of pore water chemistry was performed along a number of transects at Syncrude (Peat Pond & Bill's Lake) and Suncor (Waste Area #19 and Dyke 11A). These samples have been analyzed for pore water chemistry; however, the data has not yet been interpreted within the context of this study.

ii. Tracking salt ingress at certain locations over longer time periods would provide useful insight into the long-term hydrological and geochemical

performance of these covers. Kessler (2007) measured salt profiles at various locations on the SW30 waste dump four years after cover placement (i.e. 2003/2004). These locations encapsulated a variety of topographic positions (lower, middle, and upper slope), including the SW30 plateau. In 2007, these locations were re-sampled as part of this research program. Again, these samples have been analyzed for pore water chemistry, but the results have not been interpreted in the context of this research.

iii. A final phase of numerical modelling is required to aide in the development of guidelines for incorporating mesotopography into reclaimed landscapes. As discussed in Chapter 5, this modelling would be mostly mechanistic. A one-dimensional finite element analysis of seepage and transport is recommended to determine the optimal cover thickness under a given set of climatic conditions for various stratigraphic configurations (e.g., cover over sand over shale). An initial water table condition could be applied at the onset of each climatic year. This condition would be representative of a mesotopographic feature (e.g. a 'subsurface' depression) that develops a perched water table due to snowmelt infiltration and lateral subsurface flow. The perched water table could be allowed to drain vertically downward at a rate controlled by the shale hydraulic conductivity. Conceptually, transport could be analyzed assuming an 'equivalent porous medium'. This would be particularly applicable in the subsurface depression areas where lateral subsurface flow would be negligible.

Areas in which lateral subsurface flow occurs (e.g. lower-slope positions) will be more difficult to model. Preliminary modelling conducted as part of this research (Chapter 3; Manuscript #2) demonstrated that it is difficult to capture all of the processes in a quasi one-dimensional model. Although lateral flushing appears to be removing some salts, the efficiency of lateral flushing is reduced due to the fracture-dominated flow system. Modelling transport

without any lateral flushing or deep percolation may provide a good-match higher in the cover profile, but it will discount the flushing near the interface. Regardless, this type of modelling, with a climate-driven surface boundary, may shed some light on the long-term trend in salt ingress. As such, it may be adequate to model deep percolation into the shale as discussed above. Solute transport in the matrix pore water would be governed primarily by vertical moisture dynamics.

7

References

Albrecht, B.A., and Benson, C. 2001. Effect of desiccation on compacted natural clays. Journal of Geotechnical and Geoenvironmental Engineering, **127**(1): 67-75.

Albright, W.H., Benson, C., Gee, G.W., Abichou, T., McDonald, E.V., Tyler, S.W., and Rock, S.A. 2006. Field performance of a compacted clay landfill final cover at a humid site. Journal of Geotechnical and Geoenvironmental Engineering, **132**(11): 1393-1403.

Albright, W.H., Benson, C., Gee, G.W., Roesler, A.C., Abichou, T., Apiwantragoon, P., Lyles, B.F., and Rock, S.A. 2004. Field water balance of landfill final covers. Journal of Environmental Quality, **33**(6): 2317-2332.

ASTM 2002a. D422-63 Standard test method for particle-size analysis of soils. *In* Annual Book of Standards. ASTM International, West Conshohocken, PA.

ASTM 2002b. D6836-02 Standard test methods for determination of the soil water characterestic curve. *In* Annual Book of Standards. ASTM International, West Conshohocken, PA.

ASTM 2005a. D2216-05 Standard test methods for laboratory determination of water (moisture) content of soil and rock by mass. *In* Annual Book of Standards. ASTM International, West Conshohocken, PA.

ASTM 2005b. D2937-04 Standard test method for density of soil in place by the drive-cylinder method. *In* Annual Book of Standards. ASTM International, West Conshohocken, PA.

Aubertin, M., Bussiere, B., Chapuis, R.P., and Barbera, J. 1996. Construction of Experimental Cells with Covers on Acid Producing Tailings. *In* Proceedings of the 49th Annual Canadian Geotechnical Conference, St. John's, Newfoundland, pp. 655-662.

Bailey, D.L.H. 2001. Properties of soil profiles over sodic mine spoil 16 years after construction. M.Sc. Thesis, University of Alberta, Edmonton.

Baker, J.M., and Spaans, E.J.A. 1997. Mechanics of meltwater movement above and within frozen soil. *In* International Symposium on Physics, Chemistry, and Ecology of Seasonally Frozen Soils, US Army Cold Regions Research Engineering Laboratory, Fairbanks, AK, pp. 31-36.

Barbour, S.L., Boese, C., and Stolte, B. 2001. Water balance for reclamation covers on oilsands mining overburden piles. *In* 54th Canadian Geotechnical Conference: An Earth Odyssey, Calgary, AB, pp. 313-319.

Barling, R.D., Moore, I.D., and Grayson, R.B. 1994. A quasi-dynamic wetness index for characterizing the spatial distribution of zones of surface saturation and soil water content. Water Resources Research, **30**: 1029-1044.

Bayard, D., Stähli, M., Parriaux, A., and Flühler, H. 2005. The influence of seasonally frozen soil on the snowmelt runoff at two Alpine sites in northern Switzerland. Journal of Hydrology, **309**: 66-84.

Benson, C., and Othman, M. 1993. Hydraulic conductivity of compacted clay frozen and thawed insitu. Journal of Geotechnical and Geoenvironmental Engineering, **119**(2): 276-294.

Benson, C., Abichou, T., Olson, M., and Bosscher, P.J. 1995. Winter effects on the hydraulic conductivity of a compacted clay. Journal of Geotechnical Engineering, **121**(1): 69-79.

Beven, K., and Germann, P. 1982. Macropores and water flow in soils. Water Resources Research, **18**(5): 1311-1325.

Bishop, K., Seibert, J., Köhler, S., and Laudon, H. 2004. Resolving the double paradox of rapidly mobilized old water with highly variable responses in runoff chemistry. Hydrological Processes, **18**(1): 185-189.

Boese, C.D. 2003. The Design and Installation of a Field Instrumentation Program for the Evaluation of Soil-Atmosphere Water Fluxes in a Vegetated Cover over Saline/Sodic Shale Overburden. M.Sc. Thesis, University of Saskatchewan, Saskatoon, SK.

Boldt-Leppin, B., O'Kane, M., and Haug, M.D. 2000. Soil covers for sloped surfaces of mine waste rock and tailings. *In* Proceedings of the Seventh International Conference on Tailings and Mine Waste. Fort Collins, Colorado, USA.

Buczko, U., Bens, O., and Hüttl, R.F. 2006. Tillage effects on hydraulic properties and macroporosity in silty and sandy soils. Soil Science Society of America Journal, **70**(6): 1998-2007, DOI: 1910.2136/sssaj2006.0046.

Burns, D.A., McDonnell, J.J., Hooper, R.P., Peters, N.E., Freer, J.E., Kendall, C., and Beven, K.J. 2001. Quantifying contributions to storm runoff through end-member mixing analysis and hydrologic measurements at the Panola Mountain Research Watershed, Georgia, USA. Hydrological Processes, **15**(10): 1903-1924.

Bussiere, B., Aubertin, M., and Chapuis, R.P. 2001. Unsaturated flow in layered cover systems: a comparison between numerical and field results. *In* 54th Canadian Geotechnical Conference: An Earth Odyssey, Calgary, AB, pp. 1612-1619.

Bussiere, B., Aubertin, M., and Chapuis, R.P. 2003. The behavior of inclined covers used as oxygen barriers. Canadian Geotechnical Journal, **40**: 512-435.

Bussiere, B., Nicholson, R.V., Aubertin, M., and Benzaazoua, M. 1997. Evaluation of the effectiveness of covers built with desulfurized tailings for preventing acid mine drainage. *In* Proceedings of the 50th Annual Canadian Geotechnical Conference, Ottawa, Ontario, pp. 17-25.

Buttle, J.M. 1994. Isotope hydrograph separations and rapid delivery of pre-event water from drainage basins. Progress in Physical Geography, **18**(1): 16-41.

Buttle, J.M., and Turcotte, D.S. 1999. Runoff processes on a forested slope on the Canadian Shield. Nordic Hydrology, **30**: 1-20.

Chamberlain, E., and Gow, A. 1979. Effect of freezing and thawing on the permeability and structure of soils. Engineering Geology, **13**(1-4): 73-92.

Chamberlain, E., Iskander, I., and Hunsiker, S. 1990. Effect of freeze-thaw on the permeability and macrostructure of soils. *In* International Symposium on Frozen Soil Impacts on Agricultural, Range, and Forest Lands. U.S. Army Corps of Engineers, Hanover, N.H., pp. 145-155.

Chamberlain, E., Erickson, A., and Benson, C. 1995. Effects of frost action on compacted clay barriers. *In* Geoenvironment 2000. ASCE, New York. pp. 702-717.

Conca, J.L., and Wright, J. 1990. Diffusion coefficients in gravel under unsaturated conditions. Water Resources Research, **26**(5): 1055-1066.

Conca, J.L., and Wright, J. 1992. Diffusion and flow in gravel, soil, and whole rock. Applied Hydrogeology, **1**(1): 5-24.

Daniel, D.E., and Wu, Y.-K. 1993. Compacted clay liners and covers for arid sites. Journal of Geotechnical Engineering, **119**(2): 223-237.

Derby, N.E., and Knighton, R.E. 2001a. Field-scale preferential transport of water and chloride tracer by depression-focussed recharge. Journal of Environmental Quality, **30**(1): 194-199.

Derby, N.E., and Knighton, R.E. 2001b. Field-scale preferential transport of water and chloride tracer by depression-focussed recharge. Journal of Environmental Quality, **30**: 194-199.

Devito, K., Creed, I., Gan, T., Mendoza, C., Petrone, R., Silins, U., and Smeardon, B. 2005. A framework for broad-scale classification of hydrologic response units on the Boreal Plain: is topography the last thing to consider? Hydrological Processes, **19**: 1705-1714.

Dincer, T.B., Payne, B.R., Florkowski, T., Martinec, J., and Tongiorgi, E. 1970. Snowmelt runoff from measurements of tritium and oxygen-18. Water Resources Research, **6**(1): 110-124.

Dunne, T. 1978. Field studies of hillslope flow processes. *In* Hillslope Hydrology. John Wiley, New York. pp. 227-293.

Elshorbagy, A., and Barbour, S.L. 2007. A probabilistic approach for design and hydrologic performance assessment of reconstructed watersheds. Journal of Geotechnical and Geoenvironmental Engineering, **133**(9): 1110-1118.

Elshorbagy, A., Jutla, A., Barbour, S.L., and Kells, J. 2005. System dynamics approach to assess the sustainability of reclamation of disturbed watersheds. Canadian Journal of Civil Engineering, **35**(1): 144-158.

Espeby, B. 1990. Tracing the origin of natural waters in a glacial till slope during snowmelt. Journal of Hydrology, **118**(1-4): 107-127.

Famiglietti, J.S., Rudnicki, J.W., and Rodell, M. 1998. Variability in surface moisture content along a hillslope transect: Rattlesnake Hill, Texas. Journal of Hydrology, **210**: 259-281.

Fayer, M.J., and Gee, G.W. 2006. Multiple-year water balance of soil covers in a semiarid setting. Journal of Environmental Quality, **35**(1): 366-377.

Flerchinger, G.N., Baker, J.M., and Spaans, E.J.A. 1996. A test of the radiative energy balance of the SHAW model for snowcover. Hydrological Processes, **10**(10): 1359-1367.

Flury, M. 1996. Experimental evidence of transport of pesticides through field soils - a review. Journal of Environmental Quality, **25**: 25-45.

Flury, M., Flühler, H., Jury, W.A., and Leuenberger, J. 1994. Susceptibility of soils to preferential flow of water: A field study. Water Resources Research, **30**(7): 1945-1954.

Fredlund, D.G., and Rahardjo, H. 1993. Soil Mechanics for Unsaturated Soils. Wiley, New York.

Fredlund, D.G., Xing, A., and Huang, S. 1994. Predicting the permeability function for unsaturated soils using the soil-water characterestic curve. Canadian Geotechnical Journal, **31**(4): 533-546.

Freer, J., McDonnell, J., Beven, K.J., Peters, N.E., Burns, D.A., Hooper, R.P., Aulenbach, B., and Kendall, C. 2002. The role of bedrock topography on subsurface storm flow. Water Resources Research, **38**(12): 1269.

Gärdenäs, A., Šimůnek, J., Jarvis, N.J., and van Genuchten, M.T. 2006. Two-dimensional modelling of preferential water flow and pesticide transport from a tile-drained field. Journal of Hydrology, **329**: 647-660.

Geo-Slope International 2007. GeoStudio 2007, Calgary, Alberta, Canada.

Geo-Slope International Ltd. 2004. Geo-Studio 2004, Calgary, Alberta, Canada.

Gerke, H.H., and Köhne, J.M. 2004. Dual-permeability modeling of preferential bromide leaching from a tile-drained glacial till agricultural field. Journal of Hydrology, **289**: 239-257.

Germann, P.F. 1990. Macropores and hydrologic hillslope processes. *In* Process Studies in Hillslope Hydrology. John Wiley & Sons, New York. p. 539.

Germann, P.F., and Beven, K.J. 1981. Water flow in soil macropores I. An experimental approach. European Journal of Soil Science, **32**(1): 1-13.

Grayson, R., and Western, A. 2001. Terrain and the distribution of soil moisture. Hydrological Processes, **15**: 2689-2690.

Grayson, R.B., Western, A.W., and Chiew, F.H.W. 1997a. Preferred states in spatial soil moisture patterns: local and non-local controls. Water Resources Research, **33**(12): 2897-2908.

Grayson, R.B., Western, A.W., and Chiew, F.H.W. 1997b. Preferred states in spatial soil moisture patterns: Local and nonlocal controls. Water Resources Research, **33**(12): 2897-2908.

Grisak, G.E., and Pickens, J.F. 1980. Solute transport through fractured media; 1. The effect of matrix diffusion. Water Resources Research, **16**(4): 719-730.

Grisak, G.E., and Pickens, J.F. 1981. An analytical solution for solute transport through fractured media with matrix diffusion. Journal of Hydrology, **52**: 47-57.

Harrison, B., Sudicky, E.A., and Cherry, J.A. 1992. Numerical analysis of solute migration through fractured clayey deposits into underlying aquifers. Water Resources Research, **28**(2): 515-526.

Hayashi, M., van der Kamp, G., and Schmidt, R. 2003. Focused infiltration of snowmelt water in partially forzen soil under small depressions. Journal of Hydrology, **270**(3-4): 214-229.

Hendry, M.J. 1988. Hydrogeology of clay till in a prairie region of Canada. Ground Water, **26**(5): 607-614.

Hendry, M.J., and Wassenaar, L.I. 2000. Controls on the distribution of major ions in pore waters of a thick surficial aquitard. Water Resources Research, **36**(2): 503-513.

Hinton, M.J., Schiff, S.L., and English, M.C. 1994. Examining the contributions of glacial till water to storm runoff using two- and three-component hydrograph separations. Water Resources Research, **30**(4): 983-993.

Horita, J., and Kendall, C. 2004. Stable isotope analysis of water and aqeous solutions by conventional dual inlet mass spectrometry. *In* Handbook of Stable Isotope Analytical Techniques. Elsevier, Amsterdam. pp. 1-37.

Jansson, C., Espeby, B., and Jansson, P.-E. 2005. Preferential water flow in a glacial till soil. Nordic Hydrology, **36**(1): 1-11.

Jardine, P.M., Wilson, G.W., and Luxmoore, R.J. 1990. Unsaturated solute transport through a forest soil during rain storm events. Geoderma, **46**(1-3): 103-118.

Jarvis, N.J. 2007. A review of non-equilibrium water flow and solute transport in soil macropores: principles, controlling factors and consequences for water quality. European Journal of Soil Science, **58**: 523-546.

Johnsson, H., and Jansson, P.-E. 1991. Water balance and soil moisture dynamics of field plots with barley and grass ley. Journal of Hydrology, **129**(1): 149-173.

Johnsson, H., and Lundin, L.-C. 1991. Surface runoff and soil water percolation as affected by snow and soil frost. Journal of Hydrology, **122**: 141-152.

Jørgensen, P.R., and Fredericia, J. 1992. Migration of nutrients, pesticides, and heavy metals in fractured clay till. Geotechnique, **42**: 62-77.

Kelln, C.J., Barbour, S.L., and Qualizza, C.V. 2007a. Quantifying contributions to interflow in a reclamation cover using isotope hydrograph separation. *In* 60th Canadian Geotechnical Conference, Ottawa, ON, pp. 1512-1517.

Kelln, C.J., Barbour, S.L., and Qualizza, C.V. 2007b. Preferential flow in a reclamation cover: hydrological and geochemical response. Journal of Geotechnical and Geoenvironmental Engineering, **133**(10): 1277-1289.

Kelln, C.J., Barbour, S.L., and Qualizza, C.V. 2008. Controls on the spatial distribution of soil moisture and salt transport in a sloping reclamation cover. Canadian Geotechnical Journal, **45**: 351-366.

Kelln, C.J., Purdy, B., Barbour, S.L., and Qualizza, C.V. 2007c. Comparison of Tree Growth Statistics with Moisture and Salt Dynamics for Reclamation Soil Covers over Saline-Sodic Overburden. *In* Canadian Land Reclamation Association Conference, Halifax, NS.

Kendall, C., McDonnell, J.J., and Gu, W. 2001. A look inside 'black box' hydrograph separation models: a study at the Hydrohill catchment. Hydrological Processes, **15**(10): 1877-1902.

Kessler, S. 2007. Salinity Profiles in Reconstructed Soils Over Saline-Sodic Waste from the Oil Sands Industry. M.Sc. Thesis, University of Saskatchewan, Saskatoon, SK.

Khire, M.V., Benson, G.H., and Bosscher, P.J. 1997. Water balance modelling of earthen final covers. Journal of Geotechnical and Geoenvironmental Engineering, **123**(8): 744-754.

Khire, M.V., Benson, G.H., and Bosscher, P.J. 2000. Capillary barriers: Design variables and water balance. Journal of Geotechnical and Geoenvironmental Engineering, **126**(8): 695-708.

King, G.J., Acton, D.F., and St Arnaud, R.J. 1983. Soil-landscape analysis relation to soil distribution and mapping at a site within the Weyburn Association. Canadian Journal of Soil Science, **63**(4): 657-670.

Kirkby, M.J. 1978. Hillslope Hydrology. John Wiley, p. 389.

Koehler, G., Wassenaar, L.I., and Hendry, M.J. 2000. An automated technique for measuring δD and $\delta^{18}O$ values of porewater by direct CO_2- and H_2- equilibration. Analytical Chemistry, **72**(22): 5659-5664.

Köhne, J.M., and Gerke, H.H. 2005. Spatial and temporal dynamics of preferential bromide movement towards a tile drain. Vadose Zone Journal, **4**(1): 79-88.

Köhne, J.M., Gerke, H.H., and Köhne, S. 2002. Effective diffusion coefficients of soil aggregates with surface skins. Soil Science Society of America Journal, **66**: 1430-1438.

Komex International Ltd. 2000. Geophysical Characterization of Sodic Soil Dumps, Syncrude Base Mine: A report prepared for Syncrude Canada Ltd., Calgary, AB.

Larsson, M.H., and Jarvis, N.J. 1999. Evaluation of a dual-porosity model to predict field-scale solute transport in a macroporous soil. Journal of Hydrology, **215**: 153-171.

Lauden, H., Seibert, J., Kohler, S., and Bishop, K. 2004. Hydrological flow paths during snowmelt: Congruence between hydrometric measurements and oxygen 18 in meltwater, soil water, and runoff. Water Resources Research, **40**: W03102.

Leskiw, L.A. 1998. Land Capability Classification System for Forest Ecosystems in the Oil Sands Region.

Lim, P.C., Barbour, S.L., and Fredlund, D.G. 1998. The influence of the degree of saturation on the coefficient of aqueous diffusion. Canadian Geotechnical Journal, **35**: 811-827.

Lin, H.S., McInnes, K.J., Wilding, L.P., and Hallmark, C.T. 1996. Effective porosity and flow rate with infiltration at low tensions into a well-structured subsoil. Transactions of the ASAE, **39**(1): 131-135.

Lissey, A. 1971. Depression-focused transient groundwater flow patterns in Manitoba. Geological Association of Canada Special Paper 9: 333-341.

Logan, W.S., and Rudolph, D.L. 1997. Microdepression-focused recharge in a coastal wetland, La Plata, Argentina. Journal of Hydrology, **194**: 221238.

Lutton, R.J., Regan, G.L., and Jones, L.W. 1980. Covers for solid wastes. *In* Protective Barriers for Containment of Toxic Materials. Noyes Data Corporation, New Jersey. pp. 189-198.

Luxmoore, R.J. 1981. Micro-, meso-, and macroporosity of soil. Soil Science Society of America Journal, **45**(3): 671-672.

McConville, Kalin, R., and Flood, D. 1999. Direct equilibration of soil water for O-18 analysis and its application to tracer studies. Rapid Commum. Mass Spectrom, **13**(13): 1339-1345.

McCord, J.T., and Stephens, D.B. 1987. Lateral moisture flow beneath a sandy hillslope without an apparent impeding layer. Hydrological Processes, **1**: 225-238.

McDonnell, J. 2003. Where does water go when it rains? Moving beyond the variable source area concept of rainfall-runoff response. Hydrological Processes, **17**: 1869-1875.

McDonnell, J.J. 1990. A rationale for old water discharge through macropores in a steep, humid catchment. Water Resources Research, **26**(11): 2821-2832.

McDonnell, J.J., Hopp, L., Mazurkiewicz, A., Penna, D., Condon, P., and O'Kane, M. 2007. Assessing cover system performance: A hillslope hydrology approach.

McIntosh, J., McDonnell, J., and Peters, N.E. 1999. Tracer and hydrometric study of preferential flow in large undisturbed soil core from the Georgia Piedmont, USA. Hydrological Processes, **13**: 139-155.

McKay, L.D., and Fredericia, J. 1995. Distribution, origin, and hydraulic influence of fractures in a clay-rich glacial deposit. Canadian Geotechnical Journal, **32**: 957-975.

McKay, L.D., Cherry, J.A., and Gillham, R.W. 1993a. Field experiments in a fractured clay till: 1. Hydraulic conductivity and fracture aperture. Water Resources Research, **29**(4): 1149-1162.

McKay, L.D., Gillharm, R.W., and Cherry, J.A. 1993b. Field experiments in a fractured clay till 2: solute and colloid transport. Water Resources Research, **29**(12): 3897-3890.

McKay, L.D., Stafford, P.L., and Toran, L.E. 1997. EPM Modeling of a field-scale tritium tracer experiment in fractured, weathered shale. Ground Water, **35**(6): 997-1007.

McKeague, J.A. 1978. Manual on sampling and methods of analysis. Canadian Society of Soil Science, Ottawa, ON, p. 212.

McKnight, T.L., and Hess, D. 2005. Physical Geography: A Landscape Appreciation. Pearson Prentice Hall, Upper Saddle River, NJ.

Meiers, G.P., Barbour, S.L., and Meiers, M.K. 2003. The use of field measurements of hydraulic conductivity to characterize the performance of reclamation soil covers with time. *In* 6th International Conference on Acid Rock Drainage, Cairns, Australia.

Meiers, G.P., Barbour, S.L., and Qualizza, C.V. 2006. The use of *in situ* measurements of hydraulic conductivity to provide an understanding of cover system performance over time. *In* 7th International Conference on Acid Rock Drainage, St. Louis, MO.

Melchior, S. 1997. In-situ studies of the performance of landfill caps (compacted soil liners, geomembranes, geosynthetic clay liners, capillary barriers). Land Contamination and Reclamation, **5**(3): 209-213.

Miyazaki, T. 1988. Water flow in unsaturated soil in layered slopes. Journal of Hydrology, **102**: 201-214.

Morris, C.E., and Stormont, J.C. 1997. Capillary barriers and subtitle D covers: estimating equivalency. Journal of Environmental Engineering(January): 3-10.

Newman, B.D., Wilcox, B.P., and Graham, R.C. 2004. Snowmelt-driven macropore flow and soil saturation in a semiarid forest. Hydrological Processes, **18**(5): 1035-1042.

Nichol, C., Kessler, S., Wall, S.N., Barbour, S.L., and Hendry, J. 2006. 30 Dump Instrumented Watersheds Geochemical Analysis: A Report Prepared for Syncrude Canada Ltd., University of Saskatchewan, Saskatoon.

Nicholson, R.V., Gillham, R.W., Cherry, J.A., and Reardon, E.J. 1989. Reduction of acid generation in mine tailings through the use of moisture-retaining cover layers as oxygen barriers. Canadian Geotechnical Journal, **26**: 1-8.

Nyberg, L. 1996. Spatial variability of water content in the covered catchment at Gardsjon, Sweden. Hydrological Processes, **10**: 89-103.

Nyhan, J.W., Hakonson, T.E., and Drennon, B.J. 1990. A water balance study of two landfill cover designs for semiarid regions. Journal of Environmental Quality, **19**(2): 281-288.

Oddie, T.A., and Bailey, A.W. 1988. Subsoil thickness effects on yield and soil water when reclaiming sodic minespoil. Journal of Environmental Quality, **17**(4): 623-627.

Othman, M., and Benson, C. 1993. Effect of freeze-thaw on the hydraulic conductivity and morphology of compacted clay. Canadian Geotechnical Journal, **30**(2): 236-246.

Pal, D.K., Srivastava, P., Durge, S.L., and Bhattacharyya, T. 2003. Role of microtopography in the formation of sodic soils in the semi-arid part of the Indo-Gangetic Plains, India. Catena, **51**: 3-31.

Penman, H.C. 1948. Natural evapotranspiration from open water, bare soil and grass. Proceedings of the Royal Society of London, **A193**: 120-145.

Peters, D.L., Buttle, J.M., Taylor, C.H., and LaZerte, B.D. 1995. Runoff production in a forested, shallow soil, Canadian Shield basin. Water Resources Research, **31**(5): 1291-1304.

Philip, J.R. 1991a. Hillslope infiltration: divergent and convergent slopes. Water Resources Research, **27**(6): 1035-1040.

Philip, J.R. 1991b. Infiltration and downslope unsaturated flows in concave and convex topographies. Water Resources Research, **27**(6): 1041-1048.

Pinder, G.F., and Jones, J.F. 1969. Determination of the groundwater component of peak discharge from the chemistry of total runoff. Water Resources Research, **5**(2): 438-445.

Price, A. 2005. Evaluation of groundwater flow and salt transport within an undrained tailings sand dam. M.Sc. Thesis, University of Alberta, Edmonton, AB.

Qualizza, C., Chapman, D., Barbour, S.L., and Purdy, B. 2004. Reclamation research at Syncrude Canada's Mining Operation in Alberta's Athabasca Oil Sands Region. *In* 16th International Conference, Society for Ecological Restoration, Victoria, Canada.

Reynolds, W.D. 1993. Saturated hydraulic conductivity field measurements. *In* Soil Sampling and Methods of Analysis. pp. 599-605.

Richards, L.A. 1954. Diagnosis and Improvement of Saline and Alkali Soils: Agriculture Handbok 60. United States Department of Agriculture, Washington, p. 159.

Ridolfi, L., Odorico, P.D., Porporato, A., and Rodriguez-Iturbe, I. 2003. Stochastic soil moisture dynamics along a hillslope. Journal of Hydrology, **272**: 264-275.

Rodriguez-Iturbe, I., D'Odorico, P., Porporato, A., and Ridolfi, L. 1999. On the spatial and temporal links between vegetation, climate, and soil moisture. Water Resources Research, **35**(12): 3709-3722.

Ross, B. 1990. The diversion capacity of capillary barriers. Water Resources Research, **26**(10): 2625-2629.

Ruland, W.W., Cherry, J.A., and Feenstra, S. 1991. The depth of fractures and active groundwater flow in a clayey till plain in southwestern Ontario. Ground Water, **29**(3): 405-417.

Rutten, K. 2006. Long-term Controls in a Groundwater Flow System. M.Eng., University of Saskatchewan, Saskatoon, SK.

Sandoval, F.M., and Gould, W.L. 1978. Improvement of saline- and sodium-affected disturbed lands. *In* Reclamation of drastically disturbed lands. American Society of Agronomy, Madison, WI. pp. 485-504.

Schwartz, F.W., and Smith, L. 1988. A continuum approach for modeling mass transport in fractured media. Water Resources Research, **24**(8): 1360-1372.

Sharratt, B.S., and Goldsmith, R.S. 1997. Field study of spatial variability in unsaturated flow beneath and adjacent to playas. Water Resources Research, **33**(10): 2239-2252.

Shaw, J.R., and Hendry, M.J. 1998. Hydrogeology of a thick clay till and Cretaceous clay sequence, Saskatchewan, Canada. Canadian Geotechnical Journal, **35**: 1-12.

Shurniak, R. 2003. Predictive Modeling of Moisture Movement within Soil Cover Systems for Saline/Sodic Overburden Piles. M.Sc. Thesis, University of Saskatchewan, Saskatoon, SK.

Sidle, R.C., Nilsson, B., Hansen, M., and Fredericia, J. 1998. Spatially varying hydraulic and solute transport characteristics of a fractured till determined by field tracer tests, Funen, Denmark. Water Resources Research, **34**(10): 2515-2527.

Simpkins, W.W., and Bradbury, K.W. 1992. Groundwater flow, velocity, and age in a thick, fine-grained till unit in southeastern Wisconsin. Journal of Hydrology, **132**: 283-319.

Šimůnek, J., Jarvis, N.J., van Genuchten, M.T., and Gärdenäs, A. 2003. Review and comparison of models for describing non-equilibrium and preferential flow and transport in the vadose zone. Journal of Hydrology, **272**(1-4): 14-35.

Sivapalan, M. 2003. Process complexity at the hillslope scale, process simplicity at the watershed scale: is there a connection? Hydrological Processes, **17**: 1037-1041.

Sklash, M.G., and Farvolden, R.N. 1979. The role of groundwater in storm runoff. Journal of Hydrology, **43**(1): 45-65.

Smettem, K.R.J., Chittleborough, D.J., Richards, B.G., and Leaney, F.W. 1991. The influence of macropores on runoff generation from a hillslope soil with a contrasting textural class. Journal of Hydrology, **122**: 235-252.

Sollins, P., and Radulovich, R. 1988. Effects of soil physical structure on solute transport in a weathered topical soil. Soil Science Society of America Journal, **52**(4): 1168-1173.

Stadler, D., Fluhler, H., and Jansson, P.-E. 1997a. Modelling vertical and lateral water flow in frozen and sloped forest soil plots. Cold Regions Science and Technology, **26**(3): 181-194.

Stadler, D., Flühler, H., and Jansson, P.-E. 1997b. Modelling vertical and lateral water flow in frozen and sloped forest soil plots. Cold Regions Science and Technology, **26**(3): 181-194.

Stadler, D., Stähli, M., Aeby, P., and Flühler, H. 2000. Dye tracing and image analysis for quantifying water infiltration into frozen soils. Soil Science Society of America Journal, **64**: 505-516.

Stähli, M., Jansson, P.-E., and Lundin, L.-C. 1996. Preferential flow in a frozen soil: a two-domain model approach. Hydrological Processes, **10**(10): 1305-1316.

Stähli, M., Jansson, P.-E., and Lundin, L.-C. 1999. Soil moisture redistribution and infiltration into frozen sandy soils. Water Resources Research, **35**(1): 95-103.

Stolte, W.J., Barbour, S.L., and Boese, C.D. 2000. Reclamation of saline-sodic waste dumps associated with the oilsands industry. *In* Canadian Land Reclamation Conference. Canadian Land Reclamation Association, Edmonton, AB.

Stormont, J.C. 1995. The effect of constant anisotropy on capillary barrier performance. Water Resources Research, **31**(3): 783-785.

Stormont, J.C. 1996. The effectiveness of two capillary barriers on a 10% slope. Geotechnical and Geological Engineering, **14**: 243-267.

Tami, D., Rahardjo, H., Leong, E.-C., and Fredlund, D.G. 2004a. Design of a laboratory verification of a physical model of sloping capillary barrier. Canadian Geotechnical Journal, **41**: 814-830.

Tami, D., Rahardjo, H., Leong, E.-C., and Fredlund, D.G. 2004b. A physical model for sloping capillary barriers. Geotechnical Testing Journal, **27**(2): 173-183.

Tang, D.H., Frind, E.O., and Sudicky, E.A. 1981. Contaminant transport in fractured porous media: Analytical solutions for a single fracture. Water Resources Research, **17**(3): 555-564.

Taylor, S., Feng, X., Williams, M., and McNamara, J. 2002. How isotopic fractionation of snowmelt affects hydrograph separation. *In* 59th Eastern Snow Conference, Stowe, Vermont, USA, pp. 285-293.

Thunholm, B., Lundin, L.-C., and Lindell, S. 1989a. Infiltration into a frozen heavy clay soil. Nordic Hydrology, **20**: 153-166.

Thunholm, B., Lundin, L.-C., and Lindell, S. 1989b. Infiltration into a frozen heavy clay soil. Nordic Hydrology, **20**(3): 153-166.

Tromp van Meerveld, I., and McDonnell, J.J. 2006a. Threshold relations in subsurface stormflow: 1. A 147 storm analysis of the Panola hillslope. Water Resources Research, **42**: W02410, doi:02410.01029/02004WR003778.

Tromp van Meerveld, I., and McDonnell, J.J. 2006b. Threshold relations in subsurface stormflow: 2. The fill and spill hypothesis. Water Resources Research, **42**(W02411): doi:10.1029/2004WR003800.

Tsaparas, I., Rahardjo, H., Toll, D.G., and Leong, E.-C. 2003. Infiltration characteristics of two instrumented residual soil slopes. Canadian Geotechnical Journal, **40**: 1012-1032.

Tsuboyama, Y., Sidle, R.C., Noguchi, S., and Hosoda, I. 1994. Flow and solute transport through the soil matrix and macropores of a hillslope segment. Water Resources Research, **30**(4): 879-890.

Uchida, T., Asano, Y., Mizuyama, T., and McDonnell, J. 2004. Role of upslope soil pore pressure on lateral subsurface storm flow dynamics. Water Resources Research, **40**: W12401.

van der Kamp, G. 1992. Evaluating the effects of fractures on solute transport through fractured clayey aquitards. *In* International Association of Hydrogeologists Conference, Hamilton, Ontario, Canada.

van Genuchten, M.T. 1980. A Closed-form equation for predicting the hydraulic conductivity of unsaturated soils. Soil Science Society of America Journal, **44**: 892-898.

Villholth, K.G., and Jensen, K.H. 1998a. Flow and transport processes in a macroporous subsurface-drained glacial till soil I. Field Investigations. Journal of Hydrology, **207**: 98-120.

Villholth, K.G., and Jensen, K.H. 1998b. Flow and transport processes in a macroporous subsurface-drained glacial till soil II. Model analysis. Journal of Hydrology, **207**: 121-135.

Waduwawatte, B., and Si, B.C. 2004. Near-saturated surface soil hydraulic properties under different land uses in the St. Denis National Wildlife Area, Saskatchewan, Canada. Hydrological Processes, **18**(15): 2835-2850.

Waduwawatte, B., Si, B.C., and Xiao, C. 2004. New method for determining water-conducting macro- and mesoporosity from tension infiltrometer. Soil Science Society of America Journal, **68**: 760-769.

Wall, S.N. 2005. Characterizing the geochemical reactions in an overburden waste pile: Syncrude mine site, Fort McMurray, Alberta, Canada. M.Sc. Thesis, University of Saskatchewan, Saskatoon.

Watson, K.W., and Luxmoore, R.J. 1986. Estimating macroporosity in a forest watershed by use of a tension infiltrometer. Soil Science Society of America Journal, **50**(3): 578-582.

Weeks, B., and Wilson, W.G. 2004. The impact of slope and aspect on evaporation from soils in three dimensions. *In* 57th Canadian Geotechnical Conference. Quebec City, Canada.

Weiler, M., and McDonnell, J.J. 2006. Testing nutrient flushing hypotheses at the hillslope scale: A virtual experiment approach. Journal of Hydrology, **319**: 339-356.

Wels, C., Cornett, R.J., and LaZerte, B.D. 1991. Hydrograph separation: A comparison of geochemical and isotopic tracers. Journal of Hydrology, **122**(1-4): 253-274.

Western, A.W., Zhou, S.-L., Grayson, R.B., McMahon, T.A., Bloschl, G., and Wilson, D.J. 2004. Spatial correlation of soil moisture in small catchments and its relationship to dominant spatial hydrological processes. Journal of Hydrology, **286**: 113-134.

Weyman, D.R. 1973. Measurements of the downslope flow of water in a soil. Journal of Hydrology, **20**: 267-288.

Wieler, M., and Naef, F. 2003. An experimental tracer study of the role of macropores in infiltration in grassland soils. Hydrological Processes, **17**(2): 477-493.

Wilson, G.V., and Luxmoore, R.J. 1988. Infiltration, macroporosity and mesoporosity distributions in two forested watersheds. Soil Science Society of America Journal, **52**(2): 329-335.

Yanful, E.K. 1993. Oxygen diffusion through soil covers on sulphidic mine tailings. Journal of Geotechnical Engineering, **119**(8): 1207-1229.

Yanful, E.K., Riley, M.D., Woyshner, M.R., and Duncan, J. 1993. Construction and monitoring of a composite soil cover on an experimental waste-rock pile near Newcastle, New Brunswick, Canada. Canadian Geotechnical Journal, **30**: 588-599.

Yeh, T.-C., Gelhar, L.W., and Gutjahr, A.L. 1985a. Stochastic analysis of unsaturated flow in heterogeneous soils, I. Statistically isotropic media. Water Resources Research, **24**(4): 447-457.

Yeh, T.-C., Gelhar, L.W., and Gutjahr, A.L. 1985b. Stochastic analysis of unsaturated flow in heterogeneous soil, 3. Observations and applications. Water Resources Research, **21**(4): 465-471.

Yeh, T.-C., Gelhar, L.W., and Gutjahr, A.L. 1985c. Stochastic analysis of unsaturated flow in heterogeneous soil, 2. Statistically isotropic media with variable α. Water Resources Research, **21**(4): 457-465.

Zaslavsky, D., and Sinai, G. 1981a. Surface hydrology III. Causes of lateral flow. Journal of the Hydraulics Division, **107**.

Zaslavsky, D., and Sinai, G. 1981b. Surface hydrology I. Explanation of phenomena. Journal of the Hydraulics Division, **107**.

Zaslavsky, D., and Sinai, G. 1981c. Surface hydrology IV. Flow in sloping, layered soil. Journal of the Hydraulics Division, **107**.

Zaslavsky, D., and Sinai, G. 1981d. Surface hydrology V. In-surface transient flow. Journal of the Hydraulics Division, **107**.

Appendix A - Comparison of Tree Growth Statistics with Moisture and Salt Dynamics

Abstract

Tree-growth rates were compared to the spatial distribution of soil moisture and pore water salt concentrations in three 7 year old reclamation covers of varying thickness (35, 50, and 100 cm) placed over saline-sodic overburden from oil sands mining. The objective of this comparison was to determine the primary eco-physical factors controlling re-vegetation efforts. Soil moisture availability likely imposes the greatest control on tree-growth as the height and diameter of trembling aspen trees were statistically smaller for the thinnest cover. The thinnest cover had the least available water holding capacity and therefore approached wilting point conditions each year over the monitoring period. Foliar nutrient levels were similar from cover to cover and are not considered to be a limiting factor. The data suggests a correlation between topographic location and tree growth for the two thickest covers. Specifically, lower-slope positions exhibited slightly better growth rates than middle and upper-slope locations. This correlation was in part attributed to the spatial distribution of soil moisture, as middle and upper-slope positions are drier due to down-slope moisture translocation along with a lack of upslope contributing area for surface run-off. Salt ingress may play a role in limiting plant development at lower slope positions in the thinnest cover due to the proximity of the plant root zone to high salinity pore water near the cover-waste interface.

Reference: Kelln, C.J., Barbour, S.L., and Qualizza, C.V., 2007. Comparison of Tree Growth Statistics with Moisture and Salt Dynamics for Reclamation Covers over Saline-

Introduction

Successful reclamation of mine landscapes in the oil sands region of north-central Canada will ultimately be determined by the health, diversity, and sustainability of the re-established ecosystem. Government legislation (Alberta Environmental Protection 1994) requires oil sands operators to return the disturbed areas to an equivalent land capability (ELC). An ELC implies that the land will be able to support various land uses after reclamation that are similar, but not identical, to the ability that existed prior to disturbance. For mine operators located in northern Alberta, silviculture will play an integral component of land reclamation as the mines are located in the Mid-Boreal Upland (MBU) eco-region of North America. The MBU contains an abundance of plant species, but trees are the most prominent vegetation (Beckingham et al. 1996) and their growth will likely be the ultimate gauge of cover performance.

The health and sustainability of any forest stand on reclaimed land will depend on a variety of complex and inter-related biotic and abiotic factors. Edaphic factors (i.e. moisture and nutrients) will likely impose the greatest control on tree growth and govern the diversity and types of species that successfully re-establish during reclamation (Purdy et al. 2005). The soil moisture regime of a site is a composite function of many factors such as topographic position, soil texture, and slope angle and aspect. The geochemistry of the underlying waste may also impact the long-term performance of vegetation. This is particularly pertinent to the oil sands region, where hundreds of square kilometres of saline saline-sodic shale overburden will eventually be reclaimed.

The objective of this study was to determine the dominant spatial controls on tree-growth for three reclamation covers overlying saline-sodic shale overburden. Soil moisture was monitored in each cover over a seven-year period. In-situ profiles of Na+ pore-water concentrations were determined at a number of locations to investigate the spatial variability of salt ingress into the covers. The height and diameter of two different tree species on the covers were measured and compared to the spatial distribution of soil

moisture and salt ingress to evaluate the relationship between the ecological and physical response of the covers.

Background

The study was conducted at the SW30 Overburden Research Site (57°2' N, 111°33' W), located in north-central Canada at the Syncrude Canada Ltd. mine site. The climate of the region is classified as semi-arid to sub-humid with a mean annual air temperature of 1.5 °C and a mean annual precipitation of 442 mm (1945-1995). Monthly mean air temperatures range from 18 °C in July to -20.7 °C in January. Potential evapotranspiration (PET), as estimated by Penman (1948), typically exceeds 500 mm per year with daily maximums (~ 7 mm/day) occurring during July and August.

An instrumented watershed was commissioned in 1999 on a 2 km2 saline-sodic shale overburden dump (Boese 2003). The shale overburden is excavated during open-pit mining to gain access to the underlying oil-rich sand. It is then deposited in large waste dumps and re-contoured to resemble a natural landscape. The shale is of marine origin (Cretaceous age) and naturally contains high pore water concentrations of dissolved salts (Wall 2005). Reclamation was achieved by placing a clay-rich cover over the shale, which functions to provide sufficient moisture and nutrients for the re-establishment of vegetation.

Three alternative prototype test covers of varying thickness (35, 50, and 100 cm) were constructed on a north-facing 11° slope to determine the optimal cover design for reclamation. Each cover had an area of 50 by 200 m and drained into a single swale ditch located at the toe of the slope, which connected into the overall drainage system for the hill. The design alternatives were: 15cm of peat-mineral mix (PM) overlying 20 cm of clay-rich glacial soil (35 cm cover); 20 cm of PM overlying 30 cm of clay-rich soil (50 cm cover); and 20 cm of PM over 80 cm of clay-rich glacial soil (100 cm cover). Each cover was planted in the fall of 1999 with alternating rows of trembling aspen (Populus tremuloides) and white spruce (Picea glauca) trees spaced approximately 5 m apart (~ 2000 stems/ha total).

Materials and Methods

A soil instrumentation station was installed in the centre of each cover in 1999 to monitor volumetric water content, matric suction, and ground temperature throughout the cover profile and into the shale. All of the sensors were laboratory-calibrated and connected to a data acquisition system. The monitored water content profiles (2000-2005) for the covers were plotted and the envelopes of 'minimum' and 'maximum' water contents were established for each of the cover soils. The minimum and maximum moisture content envelopes were assumed to coincide with wilting (WP) point and field capacity (FC), respectively. The available water holding capacity (AWHC) for each cover was determined as the difference between FC and WP integrated over the depth of the cover. Soil moisture was also monitored in neutron and capacitance probe access tubes at various locations traversing the entire watershed.

Detailed profiles of in situ pore water chemistry were used to study the spatial variability of salt transport into the reclamation covers. Soil samples were collected from the cover and shale in 10-20 cm depth intervals from over thirty locations using a hand auger (Kessler 2007). The samples were placed in sealed plastic bags and stored in a temperature and humidity controlled room until the analysis was performed. High-speed centrifugation and the saturated paste techniques were used to extract pore water from over 100 samples. Chemical analysis for major ion chemistry (Na+, Ca2+, K+, Mg2+, SO42-, Cl-, HCO3-, CO32-) was performed using ion chromatography.

A survey of the trembling aspen and white spruce trees on all three covers was conducted in the summer of 2005. Tree height was measured using a telescoping survey rod while the root collar diameter was measured using calipers. The topographic position (i.e., lower, middle, or upper slope) of each tree was recorded according to Beckingham (1996). Notes on tree health were recorded including indications of tree stress, missing trees, dead trees, or lost leaders. The UTM coordinate of each tree was determined by GPS survey. Tree-growth statistics were compiled according to cover thickness and slope position within each cover. The data were checked for normality using

Kolmogorov-Smirnov tests while statistical differences were analysed using Student's t-tests.

Results

Soil Moisture

Figure 1 presents the volume of water stored in each cover between 1999 and 2005. Data collected between November 1 and May 15 of each year were removed because the ground is frozen during this time. The measured FC of the clay-rich cover soil and peat-mineral mix was 0.35 and 0.53, respectively. The measured WP was 0.21 and 0.25, respectively. Using these values and the corresponding cover layer thickness yields an AWHC of 63, 88, and 196 mm for the 35, 50, and 100 cm covers, respectively.

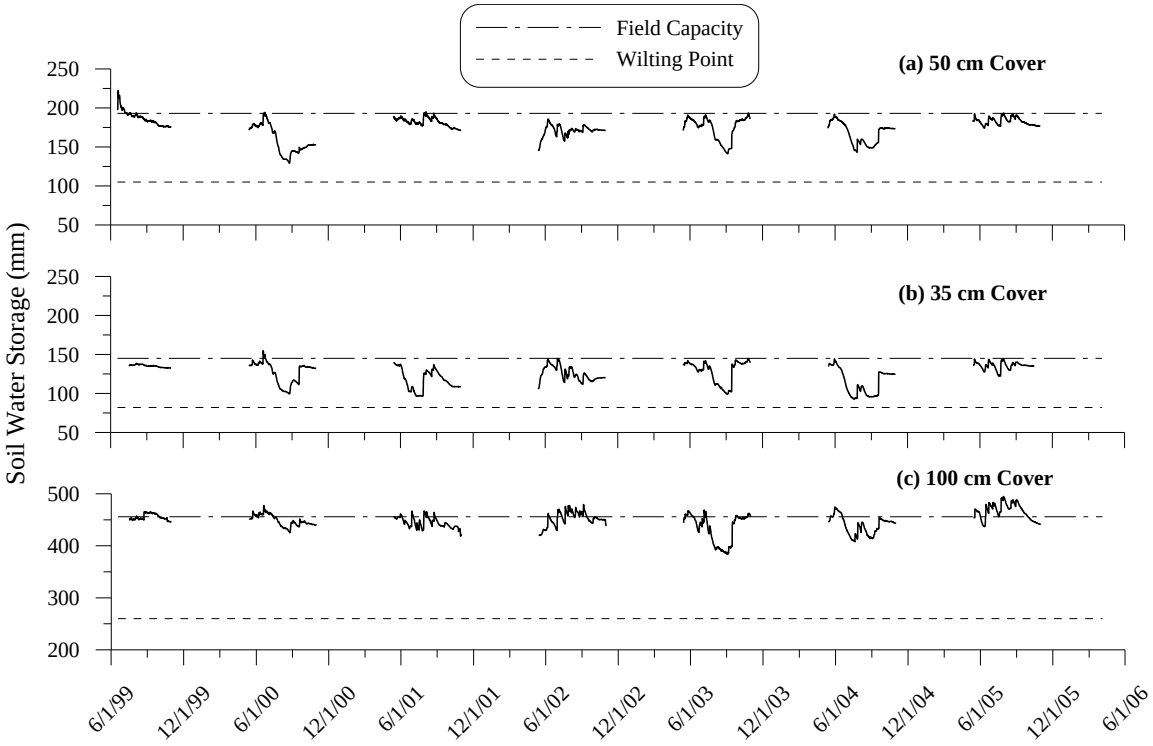

Figure 1. Soil water storage in the 35, 50, and 100 cm covers.

The soil water storage in each cover approaches FC during the spring, when surface run-off rates are high due to snow melt, and net infiltration is greater due to spring rain

and low evapotranspiration rates. The covers also reach FC periodically throughout the summer and autumn months due to heavy rainfalls. Wilting point conditions did not develop through the full depth of the 35 cm cover each year although the average water storage volumes did approach WP during most years due its lower AWHC. Soil water storage in the 50 and 100 cm remains significantly above WP conditions, even in the driest years, due to the higher AWHC of these covers. A review of individual sensor data (not presented) indicated that the 100 cm cover exhibits excess moisture (i.e. above FC) near the cover-shale interface, which suggests that plant moisture uptake is limited to the upper 80 cm of the cover profile. Coupled soil-atmosphere modelling demonstrated that the thicker covers have sufficient soil moisture to accommodate drought years (Shurniak 2003).

Salt Ingress

In-situ profiles of pore water solute concentration determined on 2:1 saturated paste extracts (data not presented) revealed that: (1) salt ingress is ubiquitous across the watershed; and, (2) the extent of salt ingress varies from cover to cover and is also a function of location within each cover (i.e. spatial variability). On average, salt ingress has occurred 15 to 30 cm above the cover-shale interface in the 35 and 50 cm thick covers, and about 40 cm above the interface in the 100 cm cover. The increased salt ingress in the 100 cm cover is attributed to excess moisture conditions at the base of the cover, which increase the coefficient of diffusion (Conca and Wright 1990; Lim et al. 1998) and therefore solute transport via diffusion. Although salt ingress has occurred to a greater extent in the thickest cover, the thinner covers have the greatest potential for salt impact over time due to a loss of the entire soil profile to salinization.

Figure 2 presents twelve pore water Na+ profiles at lower and upper-slope positions for the 100 cm cover. The profiles demonstrate that salt ingress has occurred to a greater extent in lower-slope positions. The average Na+ concentration at 20 cm above the cover-shale interface ranges from about 750 to 1750 mg/l in the lower-slope positions. In the upper-slope positions, the average concentration at the same height is about 500 mg/l. Furthermore, the shape of the profile at upper-slope locations is much sharper, indicating

that upward salt ingress has been attenuated. The difference in salt ingress between the upper and lower slope locations is attributed to spatial variability in the soil moisture regime. Lower-slope positions are typically wetter due to down-slope moisture translocation and the accumulation of surface-runoff at down-slope positions which will result in increased water contents and increased rates of upward diffusive salt transport.

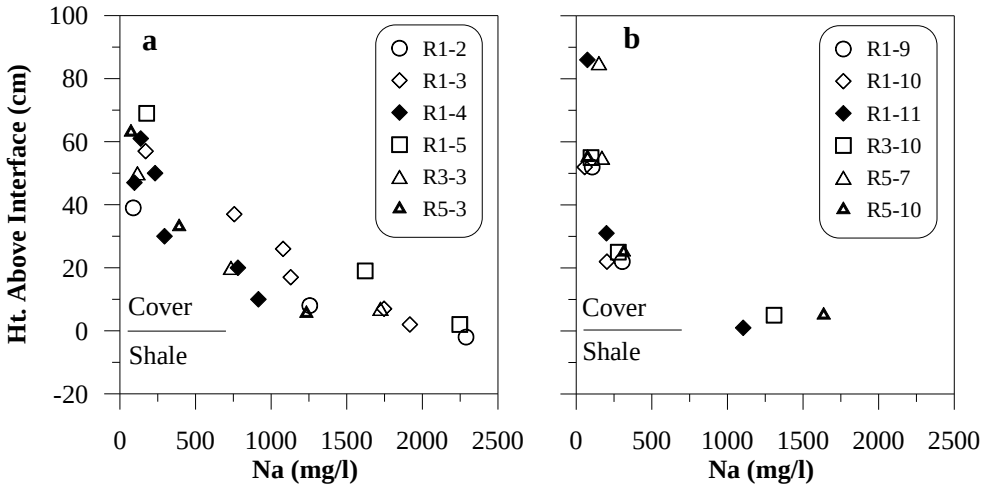

Figure 2. In-situ depth profiles of pore-water sodium concentration. (a) Lower slope positions. (b) Upper slope positions.

Tree Survey

Table 3 presents the results from the 2005 tree survey including the average diameter and height of both the trembling aspen and white spruce trees on all three covers, along with the total number of trees surveyed. The largest average height (222 cm) of aspen was observed on the 100 cm cover, while the smallest average height (195 cm) was measured on the 35 cm cover. A Student's t-test of the 100 cm/35 cm Aspen data yielded a $p < 0.0005$ and $p = 0.013$ for tree height and diameter, respectively, suggesting that the datasets are statistically different based on a 5% level of significance. In contrast, the height and diameter of trembling aspen for the 100 cm/50 cm covers were not statistically different ($p = 0.162$; 0.183 respectively). Overall, the trembling aspen has performed better on both the 100 and 50 cm covers versus the thinner 35 cm cover.

Table 3. Average height and diameter of Aspen and Spruce trees on the 35, 50, and 100 cm covers.

	Aspen			**Spruce**		
Cover	**Mean Diameter (cm)**	**Mean Height (cm)**	**# of Trees**	**Mean Diameter (cm)**	**Mean Height (cm)**	**# of Trees**
50 cm	28.9 ± 7.55	216 ± 58.1	234	20.8 ± 5.35	94.7 ± 25.5	259
35 cm	26.4 ± 7.04	195 ± 56.1	207	20.2 ± 5.26	89.1 ± 25.2	236
100 cm	28.0 ± 8.79	222 ± 61.6	206	18.2 ± 5.00	88.2 ± 24.4	213

The average height and diameter of white spruce trees on the three covers were very similar (Table 3). The largest mean height (94.7 cm) was measured on the 50 cm cover, while the smallest mean height (88.2 cm) was measured on the 100 cm cover. Similarly, the largest and smallest mean diameters were measured on the 50 and 100 cm covers, respectively. The data appears to suggest that the white spruce performed best on the 50 cm cover. The 50 cm cover white spruce trees were taller ($p = 0.002$) and had greater root collar diameter ($p < 0.0005$) than those from the 100 cm cover. The 50 cm cover

white spruce were taller (p = 0.007) than those from the 35 cm cover but had similar root collar diameters.

Table 4 presents the average trembling aspen tree height and diameter as a function of topographic location. On the 100 cm cover, the tree heights at the lower and mid-slope locations were similar (~225 cm) and greater than the overall average of 222 cm for the cover. Trees located at upper slope positions were markedly smaller (210 cm). Tree heights on the 50 cm cover were also greatest at the bottom and smallest at the upper-slope locations; but the average height at mid-slope locations was similar to top-slope locations. In contrast to the 50 and 100 cm covers, the thinnest cover exhibited slower growth rates at lower and mid-slope locations (~190 cm), while the largest average tree height (207 cm) was measured at upper-slope locations. The latter value is considerably larger than the average trembling aspen height of 195 cm for the entire cover. The average tree diameters were typically within 3 cm across all mesotopographic locations.

Table 4. Average height and diameter grouped by slope position.

Cover	Height/Diameter (cm)		
	Lower	**Middle**	**Upper**
50 cm	228/30.5 (n = 65)	212/28.3 (n = 127)	213/28.1 (n = 42)
35 cm	187/26.8 (n = 32)	192/26.1 (n = 129)	207/27.0 (n = 45)
100 cm	226/29.4 (n = 79)	225/27.5 (n = 83)	210/27.0 (n = 42)

Discussion

The trembling aspen data demonstrate that tree growth rates are greatest on the thicker covers (50 and 100 cm). This observation is keeping with previous vegetation studies that have shown a greater number of species establishing on the thickest covers. These covers have also remained more amenable sites for germination and establishment than the thin cover (Purdy, unpublished data). To date, improved tree-growth on the thicker covers is likely attributed to water availability differences between the covers. Foliar nutrient levels in all three covers were mostly within ranges considered acceptable and non-limiting in trembling aspen and white spruce based on comparisons of measured and literature values (Purdy, unpublished data). The soil moisture data clearly demonstrates that the thinnest cover has a lower AWHC, in addition to a shallower rooting depth and the proximity of high pore water Na+ concentrations to the root zone. It is also noted that lower transpiration rates have been measured on the thinnest cover (Purdy, unpublished data), which is consistent with the lower AWHC.

In general, the tree survey data also indicated that the white spruce is not a good metric for cover performance after only six years of growth. The white spruce tree data did not reveal a difference in growth rates among the three cover treatments. The similarity in the white spruce among the covers is attributed to slower growth rates compared to trembling aspen. Furthermore, the white spruce species has a shallower rooting depth than the trembling aspen, which minimizes the effects of soil moisture and/or salt ingress on the overall growth rate.

It is difficult to make inferences on the relationship between topographic location and tree-growth rates based on the limited data; however, the data may suggest that there is some correlation that warrants further investigation. In general, tree growth rates on the 50 and 100 cm covers are greatest in lower-slope positions and smallest at upper-slope locations. The 35 cm cover exhibits the opposite trend with greater growth rates at upper-slope positions. This discrepancy may be explained by the spatial variability in soil moisture and salt dynamics within each cover. In-situ profiles of pore water Na+ concentration demonstrated that salt ingress is more substantial in lower slope positions due to elevated soil moisture conditions. In the thicker covers, the vegetation appears to

be 'capitalizing' on increased moisture conditions in lower-slope positions, which would increase transpiration rates, nutrient up-take, and therefore growth rates. The additional cover thickness provides a safeguard between the high salinity pore water near the interface and the root uptake zone. In contrast, the 35 cm cover has less thickness to buffer the impacts of salt ingress. Consequently, plant growth on the thinnest cover would be limited by high salinity in lower-slope positions and would therefore perform better at upper-slope locations, despite the reduced soil moisture.

Conclusions

Tree-growth rates on three reclamation covers overlying saline-sodic shale overburden were a function of soil moisture, pore water salinity, and possibly topographic position. The largest average height and diameter of trembling aspen was measured on the two thickest covers (50 and 100 cm). Both of these covers had sufficient soil moisture storage to accommodate dry climatic conditions because of a greater available water holding capacity. Correspondingly, transpiration rates were greatest on the thickest covers. In contrast, the thinnest cover (35 cm) approached wilting point conditions during the summer months and therefore had a smaller average tree height and diameter. Foliar nutrient levels were comparable on all three covers and not considered to be a limiting factor.

Topographic position also appears to impose some control on tree growth. Tree-growth rates were greater at lower-slope positions for the 50 and 100 cm, likely as a result of increased moisture availability at these locations. In contrast, the 35 cm cover exhibited the opposite trend, with smaller tree growth at the lower-slope positions and greater growth at upper-slope positions. Although further investigation is warranted, the smaller tree-growth in lower-slope positions is likely a result of the reduced cover thickness, which places the root zone in close proximity to the higher pore water salt concentrations near the cover-shale interface. This study suggests that a cover thickness greater than 50 cm is the optimal design in terms of tree growth because (1) it provides sufficient moisture for plant-growth and (2) it creates a safeguard between high salinity pore water near the cover-shale interface and the root zone.

References

Alberta Environmental Protection. (1994). "A Guide for Oil Production Sites, Pursuant to the Environmental Protection and Enhancement Act and Regulations." L. R. D. Alberta Environmental Protection, ed., Queen's Printer.

Beckingham, J. D., Nielsen, D. G., and Futoransky, V. A. (1996). "Field Guide to Ecosites of the Mid-Boreal Ecoregions of Saskatchewan: Special Report 6." Natural Resources Canada.

Boese, C. D. (2003). "The Design and Installation of a Field Instrumentation Program for the Evaluation of Soil-Atmosphere Water Fluxes in a Vegetated Cover over Saline/Sodic Shale Overburden," M.Sc. Thesis, University of Saskatchewan, Saskatoon, Canada.

Conca, J. L., and Wright, J. (1990). "Diffusion coefficients in gravel under unsaturated conditions." Water Resources Research, 26(5), 1055-1066.

Kessler, S. (2007). "Salinity Profiles in Reconstructed Soils Over Saline-Sodic Waste from the Oil Sands Industry," M.Sc. Thesis, University of Saskatchewan, Saskatoon, SK.

Lim, P. C., Barbour, S. L., and Fredlund, D. G. (1998). "The influence of the degree of saturation on the coefficient of aqueous diffusion." Canadian Geotechnical Journal, 35, 811-827.

Penman, H. C. (1948). "Natural evapotranspiration from open water, bare soil and grass." Proceedings of the Royal Society of London, A193, 120-145.

Purdy, B. G., Macdonald, S. E., and Lieffers, V. J. (2005). "Naturally saline boreal communities as models for reclamation of saline oil sand tailings." Restoration Ecology, 13, 667-677.

Shurniak, R. (2003). "Predictive Modeling of Moisture Movement within Soil Cover Systems for Saline/Sodic Overburden Piles," M.Sc., University of Saskatchewan, Saskatoon, SK.

Wall, S. N. (2005). "Characterizing the geochemical reactions in an overburden waste pile: Syncrude mine site, Fort McMurray, Alberta, Canada," M.Sc., University of Saskatchewan, Saskatoon.

Appendix B -
Data and Modelling Results

All of data collected during this study and used in the preparation of the manuscripts is included on the enclosed CD. The finite element (FE) simulations and associated spreadsheets are also included. The file structure is shown in the figure below. The 'Syncrude SW30' directory contains twelve sub-directories for the various categories of data.